



WPI

Project ID: JMC-2103

A Fluidics Bioreactor for Streamlined *In Vitro* Modeling of Neuroblastoma Tumors

A Major Qualifying Project Report submitted to the faculty of
WORCESTER POLYTECHNIC INSTITUTE
in partial fulfillment of the requirements for the degree of Bachelor of Science

Submitted by:

Sarah Boermeester

Elizabeth Inger

Coulter Ralston

May 6th, 2021

Professor Jeannine Coburn, Ph.D., Advisor
Department of Biomedical Engineering

This report represents the work of one or more WPI undergraduate students submitted to the faculty as evidence of completion of a degree requirement. WPI routinely publishes these reports on the web without editorial or peer review.

Table of Contents

Acknowledgements	v
Abstract	vi
Table of Figures	vii
Table of Tables.....	ix
CHAPTER 1—INTRODUCTION	1
CHAPTER 2 – LITERATURE REVIEW	3
2.1 Neuroblastoma.....	3
2.1.1 Statistics	3
2.1.2 Pathophysiology	3
2.1.3 Tumor Microenvironment	4
2.1.4 Treatment	6
2.2 Tumor Models	7
2.2.1 Two-Dimensional	7
2.2.2 Cell Aggregates	8
2.2.3 Hydrogels.....	8
2.2.4 Scaffolds	9
2.3 Silk Fibroin as a Biomaterial.....	10
2.3.1 Fabrication Strategies	10
2.3.2 Silk Fibroin Applications.....	10
2.3.3 Silk Fibroin for Tumor Modelling	11
2.4 Fluidic Systems and Media Management	11
2.4.1 Mathematical Modeling for Fluid Dynamics	12
2.4.2 Fabrication Processes.....	13
2.4.3 Methods for Facilitating Fluid Flow	14
2.5 Materials and Properties	14
CHAPTER 3 – PROJECT STRATEGY.....	16
3.1 Initial Client Statement.....	16
3.2 Design Requirements	16
3.2.1 Objectives	16
3.2.2 Functions.....	16
3.2.3 Specifications.....	16

3.3 Standards and Lab-Specific Protocols	17
3.3.1 Medical Device Quality	17
3.3.2 Cell Culture.....	18
3.3.3 Scaffold Fabrication and Seeding.....	18
3.4 Revised Client Statement	19
3.5 Management Approach	19
3.5.1 Gantt Chart.....	19
3.5.2. Budget.....	21
CHAPTER 4 – DESIGN PROCESS	22
4.1 Needs Analysis	22
4.1.1 Design Criteria.....	22
4.1.2 Pairwise Analysis.....	24
4.2 Concept Functions and Means	26
4.2.1 Function Means Analysis	26
4.2.1 Concept Map.....	26
4.3 Prototyping	27
4.3.1 Conceptual Designs	27
4.3.2 Mathematical Geometric Analysis.....	29
4.4 Modeling for Virtual Simulation	31
4.5 Design Selection.....	33
CHAPTER 5 – DESIGN VERIFICATION.....	38
5.1 Verification of Fluid Flow Device	38
5.2 Cytotoxicity of Device Materials	38
5.3 Leak Testing	40
5.3.1 Syringe Pump Testing.....	41
5.3.2 Peristaltic Pump Testing.....	43
5.4 Longevity Testing.....	43
5.5 Surface Chemistry Analysis of PEGylated Glass Slides.....	44
CHAPTER 6 – FINAL DESIGN AND VALIDATION.....	46
6.1 Final Design	46
6.2 Tumor Modeling Potential for Design Validation	47
6.2.1 Virtual Simulation with COMSOL.....	47
6.2.2 DNA Quantification for Assessing Cell Sustainability	49

6.2.3 Cell Sustainability Histology	50
6.3 Industry Standards	51
6.4 Project Impact.....	51
6.4.1 Economic Impact	51
6.4.2 Environmental Impact	52
6.4.3 Societal Influence	52
6.4.4 Political Ramifications.....	52
6.4.5 Ethical Concerns	52
6.4.6 Health and Safety Concerns.....	52
6.4.7 Manufacturability	53
6.4.8 Sustainability	53
CHAPTER 7 – DISCUSSION	54
7.1 Device Functionality	54
7.2 Modeling Capabilities	55
CHAPTER 8 – CONCLUSIONS AND RECOMMENDATIONS	57
8.1 Conclusions	57
8.2 Recommendations	57
REFERENCES.....	59
APPENDIX.....	65
Appendix A: PEGylation Protocol	65
Appendix B: Resazurin Assay Protocol	66
Appendix C: Plasma Bonding Protocol.....	69
Appendix D: XPS Analysis.....	70
Appendix E: Sterilization Techniques.....	71
Appendix F: Device User Manual.....	72
Appendix G: COMSOL User Manual.....	81
Appendix H: PicoGreen Protocol.....	85
Appendix I: H&E Staining Protocol	88
Appendix J: Machining	89

Authorship

Chapter	Primary Author
Chapter 1 – Introduction	Sarah Boormeester
Chapter 2 – Literature Review 2.1 Neuroblastoma 2.2 Tumor Models 2.3 Silk Fibroin as a Biomaterial 2.4 Fluidic Systems and Media Management 2.5 Materials and Properties	Elizabeth Inger Coulter Ralston & Sarah Boormeester Coulter Ralston Sarah Boormeester Elizabeth Inger
Chapter 3 – Project Strategy 3.1 Initial Client Statement 3.2 Design Requirements 3.3 Standards and Lab Specific Protocols 3.4 Revised Client Statement 3.5 Management Approach	All All Elizabeth Inger & Coulter Ralston All All
Chapter 4 – Design Process 4.1 Needs Analysis 4.2 Concept Functions and Means 4.3 Prototyping 4.4 Modeling for Virtual Simulation 4.5 Design Selection	Coulter Ralston Sarah Boormeester Sarah Boormeester & Coulter Ralston Coulter Ralston Sarah Boormeester
Chapter 5 – Design Verification 5.1 Verification of Fluid Flow Device 5.2 Cytotoxicity of Device Materials 5.3 Leak Testing 5.4 Longevity Testing 5.5 Surface Chemistry Analysis of PEGylated Glass Slides	Coulter Ralston All Elizabeth Inger Elizabeth Inger Sarah Boormeester
Chapter 6 – Final Design and Validation 6.1 Final Design 6.2 Tumor Modeling Potential for Design Validation 6.3 Industry Standards 6.4 Project Impact	Coulter Ralston Coulter Ralston Elizabeth Inger Elizabeth Inger
Chapter 7 – Discussion 7.1 Device Functionality 7.2 Modeling Capabilities	Sarah Boormeester Coulter Ralston & Elizabeth Inger Coulter Ralston
Chapter 8 – Conclusions and Recommendations 8.1 Conclusions 8.2 Recommendations	Sarah Boormeester Elizabeth Inger
Appendices Appendix A – PEGylation Protocol Appendix B – Resazurin Protocol Appendix C – Plasma Bonding Protocol Appendix D – XPS Analysis Appendix E – Sterilization Techniques Appendix F – Device User Manual Appendix G – COMSOL User Manual Appendix H – PICO Green Protocol Appendix I – H&E Staining Protocol Appendix J – Machining	Sarah Boormeester Coulter Ralston Elizabeth Inger Sarah Boormeester Sarah Boormeester Sarah Boormeester Coulter Ralston Coulter Ralston Coulter Ralston Elizabeth Inger

Acknowledgements

The project team would like to acknowledge and thank all of following people for their unwavering support throughout the year. This project would not have been possible without their knowledge, time and generosity.

Dr. Jeannine Coburn and **Katelyn Mistretta** for advising the project over the course of the year and assisting with lab access, obtaining resources, and revising deliverables. Your guidance has made us better engineers and more thoughtful problem solvers.

Alycia Abbott for her assistance with obtaining silk scaffolds and material sterilization.

Lisa Wall for her incredible work with obtaining the necessary materials for our device with short notice.

Tom Partington for the fabrication of the flow chamber prototype as well as insight to simplify both manufacturability and use of the device.

Dr. Adriana Hera for her help with COMSOL modeling and the tools necessary for accurately conducting virtual simulations.

Jakob Sperry for the 3D printing of our PLA molds.

Dr. Ronald Grimm and **Julia Martin** for explaining concepts and helping the team with everything related to XPS, and for their lab resources of piranha solution.

James Loiselle and **Robert Peralta** for their help with ESPRIT files and machining the device components. Their patience and expertise helped us learn valuable skills that we would not have otherwise learned outside of this project.

Abstract

Neuroblastoma is the most common extracranial malignant tumor in pediatrics. Patients with the disease have a 40-50% survival rate over 5 years [1]. Neuroblastoma has heterogeneous presentations, meaning there is significant variation in genotypic and phenotypic properties of the disease among patients. To improve patient outcomes, better drug testing strategies are crucial, but also challenging. The unique presentation of the cancer necessitates the development of *in vitro* neuroblastoma tumor models that can be used to test individualized treatment options [2]. To better understand this disease, the Coburn Lab at WPI models neuroblastoma by culturing cells in silk fibroin scaffolds and stacking them in multiple layers, mimicking a solid tumor. The team aimed to improve upon this tumor modeling system. To accomplish this, the group created a fluidic bioreactor that integrates fluid flow, conserves resources, reduces contamination risk, and increases ease of use. The device consists of a flow chamber, a modified chip to secure the scaffolds, and a circulatory perfusion system. Through verification and validation testing, the team determined that the new bioreactor better addressed the client's need for an improved drug efficacy testing system.

Table of Figures

Figure 1. Gantt Chart for A-Term	20
Figure 2. Gantt Chart for B-Term	20
Figure 3. Gantt Chart for C-Term	20
Figure 4. Gantt Chart for D-Term	20
Figure 5. Concept Map for Final Design Considerations	27
Figure 6. Sectioned View of Flow Chamber Design #1	27
Figure 7. Closed Flow Chamber Design #1	28
Figure 8. Sectioned View of Flow Chamber Design #2	28
Figure 9. Closed Flow Chamber Design #2	29
Figure 10. Sectioned Drawing of Flow Chamber Design #3	29
Figure 11. Fluid Flow on Both Sides for Design #1	31
Figure 12. Fluid Flow on One Side for Design #2	32
Figure 13. Fluid Flow through Scaffold for Design #3	32
Figure 14. Expanded Assembly of Final Design	33
Figure 15. Closed Assembly of Final Design	34
Figure 16. Chip for Full Assembly	35
Figure 17. Flow Chamber Cross Section	36
Figure 18. Syringe Pump System Overview	37
Figure 19. Peristaltic Pump System Overview	37
Figure 20. SK-N-AS Cell Culture with Device Materials to Visualize Cytotoxicity	39
Figure 21. Metabolic Activity After 48 Hours of Culturing with Materials	40
Figure 22. Non-bonded PDMS and Glass with Scaffolds Before (A) and After (B) Flow	41
Figure 23. Bonded PDMS and Glass Before (A) and After (B) 3 Days of Flow using a Peristaltic Pump	44
Figure 24. Photoelectron Counts to Determine the Presence of PEG on the Glass Surface Using XPS	45
Figure 25. Fabrication Process for Internal Chip	46
Figure 26. Labeled Final System	47
Figure 27. Oxygen Concentration Profile for the Design Validation Study	48
Figure 28. Oxygen Concentration Profile with the Stacks of 3 (A) and Stacks of 4 (B)	49
Figure 29. Oxygen Concentration Profile with 3 Stacks (A) and 4 Stacks (B)	49
Figure 30. DNA Quantification Between Stacked Tumor Models	50

Figure 31. H&E Visualization Our Stacked Model (A) and the Coburn Lab Stacked Model (B).
Enlarged Images for Each Stack are Seen in (C) and (D) Respectively51

Table of Tables

Table 1. Team Budget and Spending	21
Table 2. Cost per Device	21
Table 3. Design Requirements and Value.....	23
Table 4. Pairwise Analysis for Prioritization	25
Table 5. Function Means Analysis.....	26
Table 6. Mathematical Analysis for Flow Chamber Design.....	30
Table 7. Syringe Pump Testing Comments and Observations.....	42
Table 8. Peristaltic Pump Testing Comments and Observations	43
Table 9. Total Peak Area Rations for XPS Analysis	45

CHAPTER 1—INTRODUCTION

Accurately modeling cancer for the use of drug testing is a tough feat, especially given the clinical needs. One of the most prevalent pediatric cancers is neuroblastoma, which is a malignant cancer that develops from undifferentiated or mis-migrated neuroblasts.

Neuroblastoma accounts for the most solid tumor occurrences in infancy and the second most extracranial malignant tumors in childhood [1]. In addition to impacting children, the disease is notoriously difficult to study and model in the lab. It is heterogenous, meaning it presents differently across each patient. This indicates the importance and need for developing neuroblastoma tumor models, as there is much more to learn when investigating treatment methods [2].

In the United States, costs for an oncology drug development through research and development, clinical trials, and finally getting to the market exceed \$650 million dollars [3]. Even with the substantial investments, many drugs have difficulty reaching clinical trials, with even fewer progressing to the market. This can be attributed to the limited translatability of cancer models in each stage of progression. Tumor models generally start out in 2D, where cells are grown on plates. The next general step is animal models, typically mice. This presents problems with ethics and accuracy. The pain and discomfort of animals in clinical studies, as well as the fact that mice immune response to tumor cells and targeted drugs is vastly different than in humans brings light to the need for new tumor models [4]. 3D tumor models offer an *in vitro* option that can be more physiologically accurate and more ethical compared to *in vivo* animal studies.

The Coburn Lab at Worcester Polytechnic Institute developed a novel 3D tumor model using silk fibroin scaffolds. This model allows for a closer representation of the *in vivo* tumor microenvironment, can simulate the effects of hypoxia normally seen in patient tumors, and allows for drug testing. Individual silk scaffolds are 200 μm thick and are stacked in layers in order to visualize exact sections of the tumor [5, 6]. The current method of culture includes using a device that requires hands on manipulation, small components, and manual media changes [7]. These factors increase the risk of contamination through human error and hinder the ability to run reproducible, high-throughput experiments for drug efficacy.

To reduce these risks the team set out to create a bioreactor device that secures, and cultures scaffolded neuroblastoma models. An ideal device supports fluid flow, conserves resources, allows for multiple replicate studies, reduces contamination risk, and increases ease of system use. The team selected an appropriate flow geometry for the inside of the device using COMSOL modeling on three design iterations. The design with continuous laminar flow was selected.

Since the design was set, the team then worked to find device materials. Through literature and cytotoxicity testing using a resazurin assay, the chosen materials were deemed biocompatible and appropriate for the design. This was followed by using SOLIDWORKS to create models of the device and working with a WPI machinist to create a working prototype.

Once the prototype was created, the team needed to validate its functionality and select a perfusion system to circulate media. Based on leak testing and versatility, a suitable pump was chosen. The pump needed to allow for the recirculation of media, which saves resources, and have options to mitigate surface tension in the device that could affect the scaffolds.

When the device was fully validated the team could then verify that it met the ideal criteria. COMSOL modeling showed the nutrient and oxygen diffusion through the stacked scaffolds. This was used to indicate whether there was hypoxia in the tumor stacks to mimic *in vivo* conditions. The final verification consisted of running a full-length cell study. The stacked neuroblastoma models were evaluated experimentally by comparing the previous method and the team's new bioreactor. Harris hematoxylin and eosin (H&E) staining was used to visualize the cells throughout the scaffolds. A Quant-iT™ PicoGreen™ dsDNA assay was used for DNA quantification of the scaffolded cells.

This project presents a fluidic bioreactor that can hold and culture scaffolded neuroblastoma models while improving upon current lab methods. This could be used to scale-up drug efficacy testing on neuroblastoma tumors with conserved resources, ease of use, and reduced contamination risk.

CHAPTER 2 – LITERATURE REVIEW

2.1 Neuroblastoma

Neuroblastoma is a form of malignant cancer from undifferentiated or mis-migrated neuroblasts, which usually originating in the adrenal gland. It is the most common form of infant cancer. Neuroblasts are stem cells that typically develop into nerve cells; however, it is believed that a genetic defect causes the cells to grow uncontrollably, thus forming the solid tumors. While genetic abnormalities can be attributed to most cases, there are dozens of genes that could play a role in the abnormality, and few cases are hereditary. Even though it is possible for the tumor to diminish on its own, treatment is usually required in the form of surgery, chemotherapy, radiation, immunotherapy, or stem cell treatments; often a combination of these methods is used [1].

2.1.1 Statistics

Neuroblastoma is a pediatric cancer. It is the most common solid tumor of infancy and the second most common extracranial malignant tumor during childhood. The prognosis varies with the severity of the diagnosis. While 9% of all deaths from childhood cancer are attributed to neuroblastoma, neuroblastoma accounts for pediatric cancer diagnoses about 5% of the time [1, 8]. Patients are classified into one of 16 broad risk groups designated according to the International Neuroblastoma Risk Group (INRG). The highest risk group has a 40-50% survival rate due to bone marrow metastasis, while the lowest risk group has over a 95% chance of survival. Alternatively, one group, the 4S group, typically develops in patients less than one year of age and spontaneously regresses, resulting in successful outcomes 90% of the time [9]. Between the years 1975 – 1995, neuroblastoma and ganglioneuroblastoma accounted for 14% of cancer diagnoses under the age of 5, 2.6% of cancer diagnoses from ages 5 – 9, 0.8% of cases diagnosed from ages 10 – 14, and .3% of cancer diagnoses from ages 15 – 19 inclusive of both sexes and all races [10]. Diagnoses have been shown to vary slightly between ethnicities and geographical location. While it is possible that the discrepancies are a result of genetic predisposition, it is also possible that the low rates of childhood cancer in developing countries could be a result of under reporting [11].

2.1.2 Pathophysiology

Neuroblastoma tumors develop anywhere in the sympathetic nervous system. The distribution of tumors can be found in the neck, chest, pelvis, or abdomen, with most tumors located in the adrenal medulla [12]. The disease originates from sympathoadrenal progenitor cells derived from the neural crest [2, 12]. After primary tumor formation, the heterogeneity of the disease can lead to patient discrepancies in pathophysiology. About 40% of the patients presenting with neuroblastoma have localized tumors, while about half of the entire patient population experiences hematogenous metastasis [12]. Patients are classified to be in critical condition in cases where hematogenous metastasis is observed, and tumors may have formed in other locations including cortical bone, bone marrow, liver, and lymph nodes [12].

Neuroblastoma is known for its heterogeneity, meaning it has a wide range of phenotypes presenting in patients with the disease. Due to neuroblastoma having embryonic origins and its

high degree of heterogeneity, it serves as a fitting model for research pertaining to solid tumors [2]. With a variety of tumor responses and interactions to analyze, *in vitro* models of neuroblastoma would allow for informative therapeutic studies.

2.1.3 Tumor Microenvironment

Each form of cancer has its own tumor microenvironment which controls the biological processes involved in cancer progression. These hallmarks of cancer presentation include invasion or metastasis, replicative immortality, angiogenesis, immune destruction evasion, deregulated cellular metabolism, growth suppression, resistance to cell death, and sustainment of proliferative signals [13]. The tumor microenvironment consists of nourishment to the tumor from surrounding cells, blood vessels, and other molecules creating a delicate *in vivo* balance, which promotes tumor growth and expansion. Tumor-derived signals are involved in downregulating anti-tumor functions as the immune effector B cells, or short-lived immune cells, are recruited to the tumor site. These effector cells, sometimes called plasma cells, secrete antibodies and carry out cell-mediated responses with the help of activated T-cells.

An important signaling pathway utilized is the NF- κ B pathway, which is formed from a gene that controls DNA transcription and production of cytokines, lending to cell survival [14]. However, this prolonged activity in the NF- κ B pathway within the environment of the tumor appears to support survival of the tumor as well and prevent the activation of immune cells resulting in tumor escape from the host immune system. Progression of the tumor is likely associated with chronic inflammation of the tumor site which is linked to the NF- κ B pathway [15]. As a result, pro-inflammation cytokines are produced to promote tumor survival. The growth of the tumor is supported by leukocyte functionality, where they receive a signal from the NF- κ B pathway to infiltrate the cell [16].

While only around 2% of neuroblastoma cases are hereditary, 80% of those cases present two mutated genes: ALK, which normally prevents tumor growth, and PHOX2B which normally helps to regulate neuroblast stem cell formation [17]. For neuroblastoma cells to proliferate, they are regulated by multiple growth factors that interact with non-receptor tyrosine kinases as well as receptor tyrosine kinases. Researchers are most familiar with neurotrophin receptors that bind with cognate ligands, which include nerve growth factor, neurotrophin-3, and brain-derived neurotrophic factor [18]. As a result of these growth factors, autocrine mechanisms activate, and cell proliferation begins. However, in neuroblastoma cells, the large quantity of nerve growth factor and neurotrophin may result in both amplified and non-amplified MYCN genes leading to spontaneous regression or differentiation into other cancers such as ganglioneuroblastoma [19]. The MYCN gene is a cellular proto-oncogene and has been highly correlated to be a strong predictor of the severity of neuroblastoma, and, when detected, usually indicates a poor prognosis for the patient [20].

The extracellular matrix is also partially responsible for the microenvironment necessary for neuroblastoma to thrive. While neuroblastoma is not typically found in epithelial cells, some neuroblastoma cell lines contain layers of cancer cells with epithelial phenotypes. Cancer cells within this epithelial phenotype layer tend to be stiff due to the consistent growth of dense fibrous tissues that leads to scar tissue, which is a normal bodily reaction to certain tumor types [21]. The microenvironment of neuroblastoma is designed to evade growth suppressors, the most

prevalent one in this disease state being Tumor Protein 53 (TP53). Interestingly, at tumor diagnosis or recurrence, the frequency of TP53 mutations remains low [22]. There is available research to suggest that the IL-6 pathway can help to upregulate MDM2 in cells that are both transformed and non-transformed, although this fact is not specific to neuroblastoma. MDM2 is an inhibitor of TP53 that promotes TP53 degradation [23]. One common genetic mutation in cancer is the over production of telomerase, which prevents the shortening of telomeres. In normal cell division, the telomeres get shorter with each generation until the telomeres can no longer protect the chromosome and the cell undergoes apoptosis. With the over production of telomerase, the telomeres do not shorten, and the cell is able to uncontrollably divide. High levels of telomerase are expressed in neuroblastoma (consistent with most other cancers), which may be correlated to amplification of the MYCN gene as well[24]. As evidence suggests, telomerase activity in neuroblastoma may be controlled by the tumor microenvironment and its inflammatory monocytes and macrophages [25]. It is thought that through monocytes and macrophages, the resulting inflammation helps dictate the microenvironment.

The tumor environment of neuroblastoma is conducive to cell invasion and metastasis, most commonly in the bone, liver, and bone marrow. Investigations conducted with cell lines from patients with high-risk neuroblastoma express CXCR4 and CXCR7 receptors for CXCL12 (a chemokine) [26]. Increased presence of these receptors is correlated to metastasis within the bone and bone marrow. When the cancer within the bone has metastasized, it is a result of activated osteoclasts, which are supported by the tumor microenvironment to secrete IL-6 which in turn degrades bone [27].

Due to the tumor microenvironment of neuroblastoma, the cells are able to thrive due to the increased availability of nutrients as a result of both vasculogenesis and angiogenesis. These processes both effectively promote tumor vascularization [27]. Angiogenesis is driven in part by the secretion of angiogenic factors such as the vascular endothelial cell growth factor (VEGF), platelet derived cell growth factor (PDCGF) and fibroblast cell growth factor (FCGF) [27]. Angiogenesis is also advanced by the hypoxia that occurs in tumors and the need to overcome the lack of oxygen and nutrients due to the rapid metabolism of the cancer. The hypoxia often triggers the release of VEGF and PDCGF to encourage vascularization and in turn deliver the missing nutrients to the tumor.

Unlike healthy cells, where a protein called caspase-8 works to force the cell into apoptosis, in neuroblastoma cells caspase-8 expression is limited, resulting in the cancer evading cell death [28]. correlation to MYCN amplification and aggressiveness of the tumor [29]. There is also research that supports the regulatory role of MYCN in the immune system, inhibiting mechanisms that would normally detect and attack abnormal cells. Neuroblastoma can go undetected in the immune system due to advanced mechanisms such as low presentations of HLA class I molecules that impair the recognition of target peptides by cytotoxic T cells [30].

Further, the tumor microenvironment in neuroblastoma is complicated by the fact that it maintains its energy through a glycolytic pathway. This contrasts most other cells which are dependent on oxidative phosphorylation as the process, which is significantly more efficient for cells. The process of oxidative phosphorylation is known as the Warburg Effect. This phenomenon overall aids in the development of ATP (energy for cells). *In vitro* evidence suggests that there are dietary restrictions that may play a role in low glucose concentrations

necessitating the need for the cells to find alternative nutrient sources [13, 31]. It is believed that this process in cancer cell proliferation works to facilitate the uptake and incorporation of specific nutrients such as lipids, nucleotides, and amino acids. Mutations specifically associated with cancer cells acquire and metabolize nutrients in a way that does not likely allow for efficient ATP production but rather encourages rapid cell proliferation [32].

2.1.4 Treatment

Medical advancements have made it so that patients receive individualized treatment plans. When patients are classified as having low and intermediate risk neuroblastoma, the prognosis is excellent. In the low-risk Children's Oncology Group (COG) P9641 clinical trial, 915 patients with stage 2a or 2b tumors had surgery alone for their localized tumors and experienced about a 96% success rate in observational studies [33]. Similar results were seen with patients in stage 1 or stage 4s neuroblastoma as well. COG A3961, a different clinical trial with 479 intermediate risk patients, was a study that saw survival rates in the mid 90% range by developing a treatment plan based on the patient's disease state [34]. Individual treatments allowed for smaller amounts of chemotherapy to be administered and reduced the length of time patients were on medications. This strategy indicates that individualized treatment is comparable to the standard of care treatment [35].

Treatment becomes more complicated when treating neuroblastoma patients who are in critical condition, as most of these patients have high-risk neuroblastoma. There are three phases of treatment that include induction (primary tumor resection and chemotherapy), tumor consolidation (radiotherapy and high-dose chemotherapy with stem cell infusion), and post-consolidation phase (immunotherapy and cytokines). During the induction phase, treatment usually begins with surgery or chemotherapy in the form of cisplatin, cyclophosphamide, doxorubicin, etoposide, topotecan, and vincristine. In the tumor consolidation phase, myeloablative regimens are used including a variety of the listed chemotherapeutic combinations [35].

If possible, surgery is usually the first step in successful treatment. Depending on the size, location, or complexity of the tumor, surgeons may be able to remove or resect most of it. This becomes challenging and risky if the tumor is attached to a vital organ such as the spinal cord, lymph nodes, bone marrow, or the liver. Surgery may be an option after efforts have been made to consolidate the tumor making removal or resection easier. Chemotherapy may be used before surgery to help consolidate the tumor, but it may also be used after surgery to help control tumor growth. While these treatments can effectively kill cancer cells, they come with many side effects that may harm healthy cells as well. Radiation therapy is used as part of the second treatment phase to destroy cancer cells. This too, can be dangerous if not dosed correctly. Bone marrow transplants, or stem cell transplants, may be used to revive healthy blood cells in the body by removing them before chemotherapy and then injecting them into the patient afterwards. Immunotherapies are used in the last phase of neuroblastoma treatment and are used to trigger the immune system of the patient to kill existing neuroblastoma cells [35, 36].

Metaiodobenzylguanine (MIBG) therapy is an increasingly used option as it is combined with radioactive iodine to deliver targeted radiation therapy in the last treatment phase of post consolidation of the tumor, helping with disease stabilization [35, 37].

2.2 Tumor Models

In vitro modeling is different than *in vivo* modeling. In drug testing, *in vitro* modeling is when the drug of interest is tested outside of the organism, (i.e., in a lab). *In vivo* modeling is when the drug is inserted directly into a non-human model such as mice or rats to offered insight into the drug's functionality and adverse effects. *In vitro* modeling can use complex models as a cost-effective alternative to animal testing, but *in vivo* models still allow more comprehensive testing of drug dosing and efficacy than simple *in vitro* testing.

2.2.1 Two-Dimensional

Two-dimensional (2D) cultures typically consist of a monolayer of cells cultured on plastic surfaces [38]. 2D cultures are beneficial for simple and inexpensive testing. However, they lack many features that affect cell behavior *in vivo*. The lack of natural structures found in 2D cultures result in cellular behavior and morphologies that can be drastically different than the physiological tumor microenvironment. The altered cell morphology in 2D cultures affects the function, signaling, and organization of intracellular components. Cells grown in a monolayer culture are exposed to nutrients and diffused gases at a much higher levels than *in vivo* conditions. The *in vivo* microenvironment would consist of different concentration profiles and diffusion rates, which affect gene expression and cell behavior [38].

When modeling tumor cells to test therapeutic efficacy, monolayer cultures are the most commonly utilized 2D cultures [39]. 2D cultures can still be employed to assess how specific pathways affect therapeutic efficacy by methods such as gene transfection, gene transduction, and CRISPR technologies [39]. Genes that mediate pathways of interest can be studied through knockdown, overexpression, or targeting them directly with pathway inhibitors. This allows for high throughput screening of specific pathways to determine which ones have the most therapeutic potential [39].

Although therapeutic screening potential is effective in 2D cultures, there are still many *in vivo* factors that could further affect therapeutic efficacy that are neglected in these initial studies. To add an additional level of complexity, monolayer co-culture models offer insight to how cell-cell interactions affect cell behavior and drug resistance. Monolayer co-culture combines multiple cell types in a single culture to better model the cellular interactions that occur in physiological tumor microenvironments. In the case of a neuroblastoma tumor microenvironment, many other cell types influence the behavior and phenotypes of neuroblastoma cells [39]. These cell types include macrophages, natural killer (NK) cells, T-cells, and fibroblasts [39]. One study conducted by Hashimoto et al. examined how proliferation rate changes when tumor cells and healthy human cell types are cultured together. They co-cultured an aggressive neuroblastoma phenotype with fibroblasts and determined that proliferation rates of the neuroblastoma cells increased in co-culture [40]. Other studies use co-culture of neuroblastoma cells with NK cells to examine the therapeutic efficacy of immunotherapies as opposed to chemotherapies. These 2D models are able to analyze the specific relationship between NK cells and neuroblastoma cells in the presence of antibodies [41]. These studies require verification in animal models to ensure that they are effective, and one minor oversight may result in the failure of the treatment. In order to provide a more complete model, factors such as mechanical properties and diffusion

characteristics of solutes and gases must be accounted for in terms of mimicking physiologically accurate conditions. Three-dimensional (3D) models are able to provide these more accurate systems by manifesting themselves in many different forms such as aggregates, hydrogels, and scaffolds.

2.2.2 Cell Aggregates

Cell aggregates, also known as spheroids, are organizations of cells that form a 3D structure, which better mimic *in vivo* conditions than 2D culturing. The 3D clustering of cells offers a platform that models a clinical phenotype of tumor cells more accurately for application in therapeutic efficacy studies [39]. Spheroids are typically formed through centrifugation in a nonadherent microplate [42]. This production process is high throughput, making it ideal for rapid testing of therapeutics. Additionally, spheroid cultures of neuroblastoma cells were proven to better model *in vivo* condition in comparison to 2D culture through proteome analysis [43]. Proteins in spheroids associated with structure, signal transduction, transportation, stress response, and glycolysis all matched *in vivo* conditions better than monolayer cultures [43]. Spheroids are critical to therapeutic efficacy studies because microenvironment changes in 3D cultures result in different cell responses that may be linked to therapeutic resistance. Cells that have less exposure to nutrients, such as oxygen, experience hypoxia, which then alters the tumor microenvironment to become more resistant to therapeutic strategies [44]. This change in tumor microenvironment behavior is eminent when the distance away from a nutrient source is greater than 100 μm .

There is no question that spheroids offer an increased level of complexity that 2D cultures lack. The scalability and minimal need for additional materials allow for them to be standard preclinical testing models. Although spheroids are much more accurate models, they still have limitations [39]. Spheroids of a single cell type lack the heterogeneous environment needed to accurately mimic *in vivo* behaviors. Size and shape also limit the capabilities of spheroids. Heterogeneity among generated spheroids lead to different diffusion characteristics, which may lead to inconsistent experimental data [39]. Larger spheroids also tend to develop a necrotic core as a result of low nutrient exposure. This behavior is typically avoided *in vivo* by the release of angiogenic growth factors by hypoxic cancer cells. Additional limitations in spheroids include a lack of additional cells in co-culture and nonuniform spheroid geometries that contribute to variable experimental results [39].

2.2.3 Hydrogels

Another method to model solid tumors is with hydrogels, which are crosslinked polymeric networks that hold large quantities of water resembling the *in vivo* environment. These swollen networks can be fabricated using both synthetic and natural polymers, and this provides the ability to customize and fine tune almost all of the hydrogel's properties to best suit the application. This shows potential for the material to mimic the extracellular matrix found *in vivo* and better promotes the extended maturation of tumors compared to a 2D culture. The inherent 3D complexity of hydrogels can allow for cell infiltration and proliferation, which is an issue often seen with other models that have tightly packed materials or limited customizability [45, 46]. Additionally, they can be altered for specific mechanical properties, degradability, cell

adhesion properties. In addition to the aforementioned properties, its biocompatibility makes hydrogels a desirable model [47].

A common shape for hydrogels used in modeling neuroblastoma is a 3D sphere. These spheres can be fabricated via 3D bioprinting, casting the 3D gels, or with hydrophobic cell culture plate coatings [48]. The hydrogel allows for a more reproducible shape when growing the tumor models, which is critical for drug screening studies. It also allows for effective nutrient and oxygen diffusion throughout the tumor microenvironment, while still allowing for replication of some critical *in vivo* conditions such as cell organization and phenotype [49]. Marrella et al. noted that the use of models such as cell laden alginate spheres has the potential to be standardized, and with the preserved neuroblastoma physiology and immunophenotype it offers the rare combination of reproducibility and *in vivo* conditions [49].

While hydrogels have many possibilities for drug testing, they still have some limiting factors. Many desired materials are animal derived, which can make reproducibility difficult. There can be considerable differences between lots, and they even have the potential to alter the biomechanical properties of the hydrogel [49]. This limits the scope of use for hydrogels, but they are still a viable option.

2.2.4 Scaffolds

In addition to hydrogels, scaffolds offer the ability to mimic the extracellular matrix of tumors, while also offering a platform for cell adhesion, growth, and proliferation. Scaffolds are typically porous or fibrous in configuration, and they can have custom degradation characteristics based on the material used. Scaffolds have been employed as a viable option for tumor modeling. However, they have not been widely used to model neuroblastoma [39]. One scaffold model for neuroblastoma uses graphene nanofibers as the material of choice. Neuroblastoma cells in this scaffold system appear to have different morphologies and gene expression when compared to monolayer neuroblastoma cultures [50]. The expression of more physiologically realistic genes and accurate cell morphologies allow for better therapeutic efficacy studies to be administered. Another pediatric cancer model uses a poly(lactide-co-glycolide) (PLGA) scaffold specifically to evaluate chemotherapeutic efficacy against retinoblastoma. The outcome of the experiment revealed that there was lower efficacy in scaffolded cultures than in monolayer cultures [51]. The difference between models can be attributed the different diffusion rates caused by the extracellular matrix serving as a barrier in scaffolded cultures and not in 2D systems.

Fabrication of scaffolds can vary widely including electrospinning or lyophilizing polymer formulations in order to achieve the proper sizes and geometries of the material [39]. In addition to the various types of fabrication methods, there are also different types of cell seeding methods for scaffolds. For tumor models, it is ideal to have a consistent cell density throughout the entirety of the scaffold. One method involves the direct seeding of cells within scaffold. A highly concentrated solution of cells can be directly pipetted in the scaffold with agarose gels coating the bottom to ensure that cells only adhere to the scaffold [52]. Other methods rely on a more diluted but higher volume of cells to introduce a moving cell suspension to allow for attachment throughout the scaffold. These systems include rotating vessels, spinner flasks, and perfusion devices.

The complexity of scaffolds can be further enhanced for therapeutic efficacy by incorporating co-culture into the model. Co-culture with scaffolds would allow for a much more advanced model that incorporates physiologically accurate cellular interactions, mechanical properties, and nutrient diffusion, the complexity of these models would ensure a valid platform for *in vitro* therapeutic studies. Although the theory of this is compelling, the complexity of the system may also be its downfall. 3D tumor models in general are not widely used due to a lack of reproducibility and their low throughput [53]. Microfluidic devices have been developed, but scaffolds have proven to be difficult to incorporate into such systems [53]. With the increased throughput of scaffold systems, *in vitro* therapeutic efficacy studies can become much more streamlined and ultimately increase the rate of drug development.

2.3 Silk Fibroin as a Biomaterial

Silk fibroin is a natural polymer with favorable biocompatibility. Additionally, silk fibroin consists of proteins aligned in β -sheet structures, which are highly crystalline [54]. The structure of silk fibroin results in strong material properties and a slow degradation rate, which is favorable for a wide variety of biomedical applications [54].

2.3.1 Fabrication Strategies

Silk fibroin has proven to be a valuable biomaterial, and one of its key features is its versatility. Once silk fibroin is extracted, a solution of silk in water can be manipulated into a variety of different constructs for various applications. The solution can be fabricated into films, hydrogels, fibers, and sponges [55]. Films can easily be produced by taking an aqueous silk solution and casting it over clean surface to let dry [55]. Hydrogels can be a bit more complex to form as opposed to films, but they can be fabricated rapidly. Hydrogels of silk can be formed by several methods including sonication, vortexing, heating, photo-crosslinking, and enzymatic crosslinking [55].

Aside from films and gels, fibers and sponges can also easily be produced with various fabrication methods. Silk fibroin fibers can be formed by wet-spinning, dry jet spinning, and electrospinning [56]. Electrospinning is unique in the fact that it can produce fibers with diameters on the nano level with the ability to incorporate molecules also on the nano scale into them [56]. Finally, silk fibroin sponges are porous structures that can be created through salt leaching, gas foaming, or freeze drying [55]. Sponges are synonymous with scaffolds and the porous architecture of silk sponges results in tunable porosity, mechanical strength, and degradation rates for a variety of different applications [56].

2.3.2 Silk Fibroin Applications

With each different silk fibroin fabrication method, different applications follow. Silk films have applications in wound dressing, drug delivery, and artificial skin grafts [55]. The nanostructure and the β -sheets content of the films are responsible for altering drug release, while the mechanical properties and permeability of the films allow for it to be an effective wound dressing [55]. Silk hydrogels are typically used for drug delivery systems. One study that uses ultrasonication as a fabrication method yields a silk hydrogel that has higher gelation rate of the construct, which consists of a hydrophobic material with stability coming from the β -sheet structures [57].

The first application of silk as a biomaterial was as in a fiber form as a suture material centuries ago [55]. Now with more advanced techniques, electrospun silk fibers can be later manipulated into nano and micro particles for drug delivery or scaffolds for tissue regeneration and wound healing applications [56]. Silk sponges have been used for tissue engineering, implantable devices, and disease models due to their previously described characteristics [56]. The porosity of the sponges allows for cell penetration in a 3D system that also allows for nutrient exchange. Since the material demonstrates biocompatibility, it is logical that cell seeded silk scaffolds can be used independently or in conjunction with other materials as superior implants or models [55].

2.3.3 Silk Fibroin for Tumor Modelling

The sponges, also described as scaffolds, in this specific application can be used specifically as tumor models. One specific example can be seen in a previously reported model for breast cancer. The model was able to incorporate three-dimensional co-culture of fibroblasts and breast cancer cells on silk scaffolds [58]. Studies ultimately concluded that the silk scaffold models proved to be the most effective for drug efficacy testing [58]. The increased biomimicry of the silk model allows for a therapeutic testing platform that is more indicative of *in vivo* drug response when compared to monolayer culture. The capacity of silk scaffolds as a tumor model are not limited to breast cancer. In fact, they can be applied to any solid tumor cell line.

In our specific case, previous advances in neuroblastoma modeling also relied on the mechanical properties and porosity of silk scaffolds to reproduce the heterogeneity of a physiological neuroblastoma tumor [5]. Gene expression and histology proved that cells were distributed throughout the silk scaffolds while expressing genes that are indicative of *in vivo* conditions [5]. Drug efficacy testing is also possible in these models, but one major limitation is the thickness of the scaffolds. If scaffolds are fabricated any thicker than 200 μm , then uneven cell distribution is observed. Quantitatively, scaffolds with a thickness of 600 μm reported equivalent or reduced DNA content when compared to 200 μm thick scaffolds after three days of culture, suggesting that the scaffold thickness is limited to a thickness of 200 μm . To combat this, scaffolds had been seeded independently with a 200 μm thickness and then stacked in different quantities to increase the tumor model thickness and observe a wider range of nutrient diffusion characteristics [7].

2.4 Fluidic Systems and Media Management

With all the possibilities regarding the material and formation of the tumor model, it is important to consider the system that keeps the cells alive. Some of the most common forms of media handling include microfluidics, macrofluidics, and automated media changes. Microfluidic systems are systems that allow for the manipulation and control of small amounts of fluid, often through channels custom designed for their application. These have the potential to model entire laboratory operations on a device the size of a chip and offer a high throughput of experiments and controlled environments. Microfluidic systems are of interest for modeling neuroblastoma because of their customizability, accuracy, creation of *in vivo*-like microenvironments, and size [59]. Macrofluidics are very similar to their microfluidic counterparts in terms of function, but as the name suggests, are larger in size. These systems often use large bore tubing and carry

volumes higher than microliters [46]. While similar, macrofluidics have their comparative advantages and disadvantages. A larger system is easier to manipulate by the user but requires more resources to run. These are important to consider when deciding how to manage media in a system. Next is automated media changes. This technique is more common on larger scales of production for a system. There are multiple forms of automated media changes, the first being equipment made specifically for media changes, for example a perfusion bioreactor. Next would be using various forms of automation basics to use laboratory equipment as the means of media change. PLC (Programmable Logic Controllers) can be used to manipulate equipment such as peristaltic pumps to change media. This requires access to the equipment's program and knowledge on how to integrate systems. Purchasing media change equipment can be a large investment, and using PLC to automate systems requires investing in controllers and a niche knowledge base of integrating systems. Therefore, it is mostly seen at a larger scale compared to research endeavors. Microfluidics and macrofluidics are likely the methods of media management the group will consider, based on how large the actual device needs to be to operate.

2.4.1 Mathematical Modeling for Fluid Dynamics

There are many governing equations that will be used to help make assumptions regarding the behavior of the fluid flow in this system. One of those assumptions is that the system will utilize laminar flow to distribute the media in smooth, consistent layers. Laminar flow is flow that is fully developed and contains little to no mixing between the cross-sectional layers. The other types of flow include turbulent, where a significant amount of mixing between layers occurs within the flow path, and transitional flow, which is a scale between laminar and turbulent with varying amounts of mixing. Reynold's number is a ratio between the kinetic forces and viscous forces of a fluid, can be used to quantify and describe these types of flow:

$$Re = \frac{Dv\rho}{\mu} \quad (1)$$

where Re = Reynold's Number, D = diameter, v = velocity, ρ = density, and μ = viscosity. If the value of the Reynold's number is less than 2300, the flow is laminar. If the number is between 2300 and 4000, the flow is transitional. Lastly, if the number is greater than 4000, the flow is classified as turbulent.

As fluid moves throughout a system, changes in geometry can cause laminar flow to shift to transitional or even turbulent. Fluid requires a certain amount of space to again become fully developed after a change in geometry, which is often the entrance to a system. The entrance length, X_e , equation is used to calculate the distance required in a system for flow to return to a laminar state:

$$X_e = 0.06(Re)(D) \quad (2)$$

Bernoulli's equation is a widely accepted principle describing flow due to a pressure source. The principle states that when there is horizontal fluid flow, there will be more pressure in points of lower fluid speed than points of higher fluid speed. This suggests that in areas where there is a change of diameter, there will be a change of pressure. The equation relates the pressure, speed,

and height of any two points with the fluid density of ρ . The equation is similar to that of kinetic and potential energy because the equation is using the energy conservation equation and applying it to fluid flow [60]:

$$P_1 + \frac{\rho v_1^2}{2} + \rho g h_1 = P_2 + \frac{\rho v_2^2}{2} + \rho g h_2 \quad (3)$$

where P = pressure, ρ = density, v = velocity, g = gravitational constant, and h = height of elevation at positions 1 and 2 within the flow path. When using this equation, it's assumed an incompressible fluid, the system runs at steady state, inviscid fluid, no shaft work within the system, and an isothermic system.

Hagen-Poiseuille Law is a fluidic law used to calculate the flow pressure drop across a cylindrical pipe, or in the case of this project, the device flow chamber. This law is applicable to fluids with laminar flow that are at steady state [61]:

$$\Delta P = \frac{8Q\mu L}{\pi r^4} \quad (4)$$

where ΔP = change in pressure, Q = volumetric flow rate, μ = viscosity, L = length of the chamber, and r = radius. For using this law, it is assumed that the flowing medium is an incompressible, Newtonian fluid.

2.4.2 Fabrication Processes

The fabrication of lab-on-a-chip models vary greatly depending on the materials used and applications. The most common forms of fabrication related to the group's model of interest include photolithography and laser micromachining, as they offer the most accuracy and are compatible with materials used in tumor modeling and cell culture.

The process of photolithography can be broken down into design, mold creation, and finally microfluidic fabrication. First, a design made from external software is either printed in UV-resistant ink on plastic or etched in chromium on glass. Next, resin is layered with the design and exposed to UV light, where the areas surrounding the design are cured and crosslinked, leaving the design areas alone creating a mold for the microfluidic channels. This mold is then combined with the material of interest, something like PDMS, where the cured material will have etched and accurate microfluidics [62-64]. This method is used to etch fine details on a film that can act as a stamp or mold and is highly popular for their applications in microelectromechanical systems. However, in a microfluidics device, major drawbacks include the inability to achieve consistent depth while printing on the film. Another major drawback is the inability to reuse the materials, creating a significant amount of waste over time. The drawbacks of this method outweighs the potential benefit, therefore the team will not proceed with this method [65].

Laser micromachining is a process that is more widely used in adjacent industries, but its availability, rapid prototyping time, and cost effectiveness make it a desirable method for microfluidics. With this method, a laser's power, speed, and focal distance are all adjusted to control the depth, width, and geometry of a channel [66]. This allows for accurate channels with limited cost to a user, which is a valuable asset in product development. The downsides to this technique severely limit its applications. The process of laser ablation causes an increased

surface roughness and an increase in pores along the channels, which should be avoided when dealing with cell culture. Matellan et al. notes that various surface treatments such as acetone vapor can help to address these issues, and there have been many strides to further improve the potential for laser cut devices [66].

2.4.3 Methods for Facilitating Fluid Flow

Another important parameter to consider with microfluidics is the type of fluid flow that is required. The design of a system varies greatly based on how fluid enters and exits the chip as well as the desired flow rate. The most common types of fluid flow systems for these applications include batch, versions of perfusion, and continuous flow.

Batch fluid systems are not as common in microfluidics but are often the base type of system used in many benchtop scale operations. This is when a media or fluid is fed to a system, and the fluid is not removed from the system until the laboratory process is complete. This is not always ideal for scale up, because the media components (nutrients and gases) are depleted over time, metabolic waste products accumulate over time, and it does not allow for a high throughput process. Perfusion is one of the most common types of flow seen in microfluidics, as it is associated with the varied flow in highly customized channels [64]. Perfusion is characterized by the addition of media when needed and the removal of waste and unwanted substrates from the system. This approach is beneficial because it still supplies nutrients but can do so with relatively slow flow rates and limited shear stress on the system. Lastly are continuous flow systems, where a fluid or media is constantly circulated throughout the system. This type of flow is common within membrane and tangential flow systems, as it supplies a constant feed of nutrients. This approach can assist in closed loop designs where the recirculation of a fluid is necessary. A limitation of this approach is that it has the potential to apply shear stress on the system depending on flow rate and cellular requirements.

2.5 Materials and Properties

Polydimethylsiloxane (PDMS) is a widely utilized material for biomedical applications most notably for its low cost, ease of fabrication, oxygen permeability, and ease of sterilization. Additionally, PDMS is a good option for membranes and microfluidic channels due to its high elasticity. Its qualities contribute to a device that is easy to replicate since combining the elastomer and curing agents of PDMS is a reliable process. A downside of PDMS is that leaching additives is a risk when using the material, such as plastics, however, this is not of concern for the project. PDMS has a high absorption rate of small hydrophobic molecules that are present throughout the fabrication process, which has the potential to alter drug toxicity and efficacy. While PDMS is gas permeable, it is not compatible with organic solvents, and due to the inconsistency of PDMS, there is a high likelihood of variations in the osmolarity of the material, random bubbles, and anoxic behavior.

Thermoplastics, such as polycarbonate or polytetrafluoroethylene (PTFE), are also excellent options in the design of biomedical devices. They have many of the same positive attributes as PDMS such as high manufacturability and low shear. While not as flexible, their processability precision allows for high throughput, and have desirable mechanical strength. It is advantageous because it is durable, rigid, and is easy to fabricate. A disadvantage of polycarbonate though is

its potential absorbance in UV and the high temperature of thermal bonding. Thermoplastics tend to be less sought out in microscale designs. For example, polycarbonate absorbs a low percentage of water and has low hydrophobicity making it challenging to sustain cell growth. Alternatively, polylactic acid (PLA) has properties very similar to polycarbonate and can be rapidly prototyped, however it usually is an ineffective choice in biomedical applications because it must be chemically modified in order to be suitable for cell culture.

Elastomers such as cis-polyisoprene are also a cheap alternative with adaptive mechanical properties. Thermoplastic elastomers are a nice alternative as they are entangled polymer chains that are flexible, re-processable, have a low absorption, and have simple yet fast bonding. When combined with inert materials, the advantageous properties of these materials become enhanced. A recent study using tetrafluoroethylene-propylene (FEPM) detailed how a microfluidic device could be created using two layers as microchannels with a collagen membrane between them to show how the epithelial and endothelial layers interact for fluid flow and the accompanying mechanical strain. Even though they have many promising features and maintenance of mechanical integrity, hydrogels are difficult to use due to sterility issues. They are often used in stereolithography printing and are most effective when combined with another material [67].

In creating microfluidic devices, one of the biggest challenges is to create a device that allows for gradients of media as well as other nutrients such as oxygen, which are necessary to the livelihood of cell culture. There is evidence of a successful microfluidic device that used a polydimethylsiloxane-polycarbonate (PDMS-PC) hybrid device to maintain cell cultures using various chemical and oxygen gradient combinations. The device was built using two layers of PDMS with a channel pattern embedded and separated with a thin membrane of PDMS. The top half of the device contains a PC film and a channel made out of serpentine to limit the directionality of the oxygen flow. The bottom layer also contains arrangements of channels constructed of serpentine as well. In order to characterize the dispersion of chemicals and cytotoxicity were tested using fluorescein solution, an oxygen sensitive dye, migration assay. The results indicated positive cell compatibility and control of a gradient [68].

PEGylation is frequently used in the pharmaceutical industry to stabilize therapeutic agents by attaching polyethylene glycol (PEG), a biocompatible polymer, to other molecules through covalent conjugation. PEGylation changes surface and material properties, most notably the hydrophobicity being reduced on the surface it is placed on. This is common when working with microfluidic devices to prevent the adhesion of cellular material to the surface. *In vivo*, PEGylation increases stability and time a drug remains in the blood. This is beneficial in reducing the frequency in which the drug is delivered. Other factors that are impacted include the number of linking chains, the site of the molecular PEG attachment, and the mass. When used in conjunction with drugs, it improves the solubility while decreasing the likelihood of an adverse immunogenic effect [69]. While the surface of glass is different from that of human plasma fibronectin, the PEGylated surface is still expected to allow for amino acids and polypeptides to be broken down by proteins. Overall, a PEGylated surface can effectively reduce cell adhesion and cell interactions with a system [70].

CHAPTER 3 – PROJECT STRATEGY

3.1 Initial Client Statement

The initial statement regarding the project was provided by Professor Jeannine Coburn, where the team must develop a silk scaffolded tumor on a chip model.

3.2 Design Requirements

3.2.1 Objectives

The goal of this project is to develop a high throughput, high complexity device for therapeutic efficacy studies. The device should limit human interactions for loading the scaffold as well as limit the maintenance and upkeep required during use. Lastly, the device should conserve resources to keep costs down and allow for scalability in the future. A device like this would allow for more efficient testing of potential neuroblastoma treatments.

3.2.2 Functions

To accomplish the indicated objectives, there are functional needs to take into consideration with the design. The scaffold, which contains various layers of 200 μm thick lyophilized silk fibroin, must be held in place securely. The device must also utilize a material that is not only easily processable, but biocompatible as well. This will allow for consistency between experiments and prevent negative interaction between the tumor and the device. Additionally, the device must have physiologically accurate fluid dynamics, which mimic the *in vivo* environment, provided by a flow pressure source. Next, the device must be made from a sterilizable material, which would ensure its reuse and conservation of resources. Lastly, the device must allow for analyte capture so that the microenvironment of the model can be monitored when needed.

3.2.3 Specifications

There are general parameters that coincide with many of the functions of the device. Regarding fluid dynamics the parameters include having laminar and consistent flow within the device, as well preventing bubbles within the flow path. This not only mimics normal flow within the body, but also ensures there will not be interruptions in flow that could dislodge the scaffolds. The flow characteristics must also avoid harm to the cells by controlling the shear stress on the culturing surface. Cell viability decreases at a shear of 10 dynes/cm² for neuroblastoma cell lines [71]. To accommodate a safety factor of two, we will ensure that the maximum shear stress 5 dynes/cm². Parameters such as easy assembly, no leaks, and autoclavable components allow for a closed system that can be sterilized and prevent contaminants throughout the process. The entire system must maintain a constant flow rate that accommodates the previously stated fluid characteristics while maintaining a tight seal for at least 3 days. These will be incorporated in the design process to better accomplish the overall project objectives.

The acceptance criteria will be two successful trials of both the syringe and peristaltic pump as well as one successful trial of the three-day longevity study. Furthermore, the acceptance criteria for the material biocompatibility testing are no statistically significant differences between untreated cells and cells culturing with the materials.

3.3 Standards and Lab-Specific Protocols

The International Organization for Standardization (ISO) is an important regulatory body that works to ensure industries are working with standards that encourage high levels of safety to maximize product efficacy. ISO standards are widely accepted internationally among companies, regulatory agencies, and other organizations to determine best practices and criteria to safely operate equipment and prevent illness or injury. ISO standards are not developed by any governmental body, but rather industry experts who aggregate technical knowledge, soft skills, experience, and business outcomes. While the industry experts are not identified, they are chosen to represent the industry and as such are tasked with ensuring they have a complete understanding of the stakeholder needs as well as how the standard is applicable to the target audience of users [72].

3.3.1 Medical Device Quality

The ISO standards described here outline protocols for medical devices and products used in health care. While the group's device is not intended for use *in vivo*, there are still some considerations the team took in order to mitigate risks of contamination while using the device in drug efficacy studies. Even though the device is not interacting with patients, the team decided the standards would still be applicable, as the device works to mimic the body's reaction when in contact with the same drugs. The application is different, but it is important to ensure that the device is clean, risks are mitigated, and that the efficacy of the system is consistently evaluated.

ISO 11737-2:2009 is a standard that addresses the sterilization of medical devices. The second clause of the standard addresses testing for sterility used for validation of testing. The purpose of this standard is to make sure best practices are maintained while describing, validating, or upholding a process for sterilization [73]. This standard is often used in parallel with ISO 14937:2009 which describes the use of sterilization in environments utilizing microorganisms that must be cleaned following process development, manufacturing, and medical device creation. The standard upholds quality features necessary for the proper sterilization agents, routine monitoring and control of the process [74].

ISO standard 10993-1:2018 addresses proper evaluation and testing using a risk management process when medical devices are evaluated with use of biological specimens. It also describes the use of medical devices that are used primarily while in contact of the human body, risk analysis of said medical device and any gaps within the testing, the need for other data sets to help aid the completion of available data sets, and understanding the overall safety of the medical device [75]. As per Section 201(h) of the Food, Drug, and Cosmetic Act, a medical device is an "instrument, apparatus, implement, machine contrivance, implant, *in vitro* reagent, or other similar or related article, including a component part, or accessory" which is recognized by the United States to diagnose, treat, prevent, manage a disease and does not rely primarily on chemical reactions to work [76].

Furthermore, ISO 13485 is used to ensure the organization that makes a given medical device is meeting the needs of the customer as well as appropriate regulatory requirements. This evaluates the lifecycle of the product to make sure there is adequate technical support to maintain the

lifecycle of the product [77]. When the medical device also utilizes drug delivery systems, it is important that ISO 20069:2019 is followed. The standards are applicable from the moment the system enters clinical studies until the end of life. Examples of systems covered within the standard are when the system maintains the same route of administration, changes in the design of the system, changes of the drug product (e.g. consistency or size of particles), changes to how the system is produced/handled, changes to sourced materials or software, changes to user interactions (such as packaging), or changes in instructions for use [78].

3.3.2 Cell Culture

When cells are used, it is important that ISO 13408-1:2008 is understood to maintain aseptic processing of health care products to prevent contamination. In addition to outlining best practices for development, validation, and routine control of the processes, this standard also documents the importance of each practice as it relates to filtration, lyophilization, clean-in-place technology, sterilization-in-place technology and isolator systems [79]. When conducting cell culture, contamination can be prevented through the proper use of equipment such as Petri dishes that are designed for single use. This standard, which is not inclusive of dishes with pre-loaded microbiological media, is described in ISO 24998:2008 [80]. ISO 20391-2:2019 helps to regulate cell counting techniques to ensure the statistical analysis and experimental design is valid (applicable mostly to eukaryotic cells). It is used to ensure the method is replicable and the frequency in which the results align with ideal data [81]. While this device is not a health care product, following these high standards helps to ensure the bioreactor, which does come in contact with many cells in order to model drug delivery systems, is handled in a similar fashion. Furthermore, many of the team's tests are dependent on a specific cell count, which makes accuracy important for the verification of the device.

3.3.3 Scaffold Fabrication and Seeding

To produce 3D porous scaffolds, the first step is to extract silk fibroin from *Bombyx mori* silkworm cocoons. The cocoon consists of two proteins known as fibroin and sericin. Fibroin is a block copolymer responsible for robust mechanical properties, while sericin is a group of glycoproteins that coat the surface of silk fibroin. Sericin is known to cause an immune response, which compromises biocompatibility [82]. Due to this, the first step in silk fibroin scaffold is the purification of silk fibroin. Silk cocoons are first cut and boiled in a 0.02 M solution of sodium carbonate (Na_2CO_3) for thirty minutes. The silk remnants then undergo three 20-minute rinses before the water is squeezed out and dried overnight. Next, the fibers are dissolved in 9.3 M lithium bromide (LiBr) by incubating the mixture at 60°C for 4 hours. Once the mixture is fully dissolved, it is dispensed into dialysis tubing and dialyzed in deionized water for 48 hours. After dialysis, the silk solution in water is centrifuged, filtered, adjusted to a concentration of 5% (w/v) and stored at 4°C [5, 82].

Once a silk fibroin solution is obtained at the desired concentration, scaffold fabrication commences. The silk fibroin solution is placed in cylindrical molds and lyophilized with an initial temperature of 20°C for 30 minutes followed by a controlled freezing with a step of -0.5°C/minute until the temperature is -45°C where the temperature is held for two hours. Then, the vacuum is initiated at a value of 220 mTorr as the temperature increases at a rate of 0.5°C/minute until -25°C where the first drying stage will occur for 30 hours. A 1°C/minute

ramp follows until the temperature of -4°C is reached where the second drying stage begins and lasts for 2 hours until finally ramping up by $1^{\circ}\text{C}/\text{minute}$ again to a final temperature of 20°C . Samples are then removed, steam-treated to result in insoluble 3D porous scaffolds, vibratome sectioned to $200\ \mu\text{m}$, and biopsy punched to 6 mm in diameter. Scaffolds are biopsy punched to 6 mm in diameter to avoid edge effects from lyophilization, and the thickness of the scaffolds are $200\ \mu\text{m}$ so that cell distribution is consistent throughout the entire scaffold [5].

Once 3D porous scaffolds are produced and sterilized via autoclaving, cell seeding onto scaffolds must be performed. Prior to cell seeding, scaffolds must be soaked in culture medium overnight. The following day, a stock solution of cells at 1×10^8 cells/mL is prepared, and $5\ \mu\text{L}$ of the stock is directly applied with a pipette to the surface of the scaffolds. The scaffolds sit for 10 minutes, and then they are all flipped for an additional $5\ \mu\text{L}$ application to the other surface of the scaffolds. The seeded scaffolds incubate for 4 hours at 37°C , 5% CO_2 , and 21% O_2 before they are distributed into well plates with culture medium and a bottom layer of 1.5% agarose to avoid cell adhesion to the tissue culture plastic [5].

3.4 Revised Client Statement

Based on the client's functional needs and industry standards, the final client statement is to develop a device that secures, and cultures scaffolded neuroblastoma models. The device needs to support fluid flow, conserve resources, allow for multiple replicate studies, reduce contamination risk, and increase ease of system use. This will be used to conduct therapeutic efficacy studies in a complex 3D model.

3.5 Management Approach

3.5.1 Gantt Chart

In order to design and create the device, the group broke down the project into major milestones and goals according to each week and term. **Figure 1** indicates the work structure for A term. This term mainly focuses on topics such as background research regarding neuroblastoma, current best devices and models, and potential solutions. It also includes topics such as planning the project timeline, and conceptual design.

For B term, shown in **Figure 2**, more technical aspects were to be incorporated into the project. This starts off with learning and using COMSOL to model the environments created within the preliminary designs and using the software to find the best version of the design. B term focuses on design edits, concept evaluation, prototyping, and biocompatibility testing. This allows for the design to be optimized before fully running and testing the device and overall system.

For C term, shown in **Figure 3**, the bulk of the validation and testing was completed. The integrity of the device was investigated, and the chip component was created with a fully PEGylated glass slide that was plasma bonded to PDMS. The original CAD files for the device were converted to ESPRIT files so the team can machine new ones. Lastly, longevity studies to look for full system leaks was completed.

In D-Term, the team finished the validation testing including a virtual simulation and a cell study lasting about a week. The data analysis of the cell study was completed the week after.

3.5.2. Budget

The team allocated their funds to the items listed in **Table 1**. The cost for a single device can be seen in **Table 2**. As of the end of C-term, the team spent money on supplies for the device and did not list consumable supplies necessary for verification and validation testing.

Table 1. Team Budget and Spending

Item	Cost	Total Spent
Model System		
PTFE	\$360.32	\$360.32
Glass Slides	\$14.65	Available Resource
MPEG 5000 Siloxane	\$100.00	Available Resource
Silicone Sheet	\$48.08	\$48.08
PDMS	\$96.30	Available Resource
Hex Button Screws and Flat Washers	\$63.74	Available Resource
Luer-Locks (Different Types)	\$32.50	\$32.50
Tubing	\$114.00	Available Resource
Aluminum	\$25.96	\$25.96
PLA	\$3.66	\$3.66
5 mm Disposable Biopsy Punch	\$32.00	\$32.00
Budget: \$750 Total	\$891.21	\$454.44

Table 2. Cost per Device

Item	Cost	Total Spent
Model System		
PTFE	\$90.08	\$90.08
Glass Slide	\$0.62	Available Resource
MPEG 5000 Siloxane	\$1.00	Available Resource
Silicone Sheet	\$1.51	\$1.51
PDMS	\$0.92	Available Resource
Screws and Washers	\$15.94	Available Resource
Luer-Locks (Different Types)	\$3.25	\$3.25
Tubing	\$19.00	\$19.00
Budget: \$750 Total	\$132.32	\$113.84

CHAPTER 4 – DESIGN PROCESS

4.1 Needs Analysis

Existing disease models face the issue of balancing the complexity of the *in vivo* pathophysiological conditions while also maintaining relatively high throughput for expedited testing. In the case of therapeutic testing, high throughput is a virtue that may be prioritized over the complexity of a model especially for *in vitro* testing. An existing neuroblastoma model developed using silk scaffolds was proven to be effective to mimic aspects of the natural tumor microenvironment [5, 7]. Although these models have been used for chemotherapeutic efficacy studies, the models rely on devices that do not support consistent fluid flow in addition to repeatability issues. Therefore, there is a need to develop a device that maintains a consistent fluid flow for high throughput therapeutic efficacy studies.

4.1.1 Design Criteria

The design requirements are listed in **Table 3**. The design requirements were split into three main sections. The first section was a re-evaluation of the current model to confirm that the cell type and scaffold material were optimal for the design's desired outcomes. The next section addresses the criteria needed for the fluidic chip device materials to ensure that there are no cytotoxic effects and that materials are reusable. The final section refers to the requirements that the fluid flow system must maintain to host a complex *in vitro* model with high throughput.

Table 3. Design Requirements and Value

Design Requirements	Value or Attribute
Scaffold Material	
Cell Type	Cell type must be adherent and have similar gene expression to clinical neuroblastoma
Processible	Easy to fabricate and reproduce
Biocompatible	Reduces the interaction and influence of the material on the cells and media
Bio-functional	Surface topography and orientation allows for behavior of adhered cells to mimic that of <i>in vivo</i>
Chip Material	
Biocompatibility	Reduces the interaction and influence of the material on the cells and media
Sterilizable	Eliminates possible areas for contamination through the system (autoclavable)
Nondegradable	Reduces the risk of product degradation and degradation byproducts on the cells over time
Processable	Easy to fabricate and reproduce
Restricted Cell Attachment	Resists cell attachment to confine the cells within the scaffold
Oxygen Diffusivity and Permeability	The material allows for modelling and calculations of oxygen exposure to the tumor models
Inexpensive	Allows for multiple trials and for budget allocation elsewhere
Fluidics System	
Control of Flow	Allows for precise and accurate flow rates
Quantitative and Qualitative Assessments	Offers the ability for the analysis of multiple parameters to better characterize the system
Shear Rate	Affects the growth of the cells and the stress on the scaffold
Channel Geometry	This can affect the shear rate, stress, and fabrication of the chip and scaffold system
Nutrient Diffusion	Allow for equitable distribution of nutrients across the scaffold
Limited Maintenance	Easy to fix and supplies are easy to acquire while also reducing risk of possible cell contamination
Conserves Resources	Limited amount of media consumption
High Throughput	Increase the output of results for a complex tumor model to rapidly test therapeutic efficacy <i>in vitro</i>

The scaffold material currently used is silk fibroin, which was addressed in Section 2.3.3. Scaffolds must have a thickness of no greater than 200 μm . If scaffolds were thicker, then there would be an uneven distribution of cells within the scaffold because they cells must be no farther than 100 μm away from a nutrient source [5]. To achieve models with larger thicknesses, scaffolds can be stacked after initial cell seeding and an incubation period of three days [7]. It is also important to ensure that the scaffold material can be sterilized by available methods such as autoclave steam sterilization. Finally, the microstructure of the scaffold material must support the adhesion and proliferation of cells integrated into the system. The desired seeding density for the model is 1.0×10^6 cells per scaffold, which was determined by previous studies conducted in the Coburn Lab to account for about half of the cells not adhering during the cell seeding process [5].

The fluid flow device materials also must be analyzed to ensure that there are no cytotoxic or other undesirable effects. Much like the scaffold material, these systems must also have the ability to be easily sterilized to alleviate the risk of contamination. The materials must be simple to machine or easily obtained at a relatively cheap price to abide by our budget, which was defined in an earlier section. Additionally, the material in which the cell-seeded scaffold is in direct contact with must support no cell adhesion in order to confine cell proliferation and growth only within the scaffolds. Finally, to ensure that oxygen diffusivity can be accurately modeled, the materials that enclose the system must not be oxygen permeable. Materials that are permeable to oxygen could cause the model to be inaccurate and not achieve well-defined oxygen diffusion for modeling hypoxia.

The fluidics system is essential to combining complexity with high throughput to achieve our project goal. The first requirement is a source that can induce a precise flow rate for medium through the system. The source must be able to support a slow flow rate with a limited amount of cell culture medium to conserve resources. The flow rate needed can be achieved based on the shear rate specifications. According to research for modeling neuroblastoma, cell viability begins to decrease at a shear of 10 dynes/cm² [71]. For a safety factor of two, we will ensure that our system does not exceed a shear force any greater than 5 dynes/cm². In addition to the shear stress requirements, the geometry of the flow chamber must be modified to ensure that the flow is laminar, fully developed, and less than the maximum shear to accommodate the flow rate. The entire system also must form a tight seal to ensure a sterile environment with no leaks.

4.1.2 Pairwise Analysis

After consolidating the design criteria, we compared the essential design criteria for the flow system and the scaffold model. Our team compared each design parameter and marked a “1” if the row took priority over the column, a “0” if the column took priority over the row, and a “0.5” if both the row and column were of equal importance. **Table 4** shows a pairwise analysis to prioritize which features the design should focus on accomplishing. We aim to fulfill all these criteria, but we may have to sacrifice certain parameters such as inexpensive materials to ensure that the system is biocompatible

Table 4. Pairwise Analysis for Prioritization

	Cell Type	Cell Adherence	Bio-functionality	Processability	Biocompatibility	Sterilizability	Non Degradable	No Cell Attachment	Inexpensive	Reproducibility	Nutrient Diffusion	Flow Control	Quantitative and Qualitative Results	Limited Interaction	Resource Conservation	High Throughput	Total
Scaffold																	
Cell Type	—	0	1	1	0	0	1	0	1	0	1	1	1	0	1	0	8
Cell Adherence	1	—	0.5	1	0	0	1	0.5	1	0	1	1	1	0	1	0	9
Bio-functionality	0	0.5	—	0	0	0	1	0	1	0	1	1	1	0	1	0	6.5
Fluidics System																	
Processability	0	0	1	—	0	0	0.5	0	1	0	0	0	1	0	1	0	4
Biocompatibility	1	1	1	1	—	0.5	1	1	1	1	1	1	1	1	1	0.5	14
Sterilizability	1	1	1	1	0.5	—	1	1	1	1	1	1	1	1	1	0.5	14
Non Degradable	0	0	0	0.5	0	0	—	0	0	0	0	0	0	0	0	0	0.5
No Cell Attachment	1	0.5	1	1	0	0	1	—	1	0.5	1	1	1	1	1	0.5	11.5
Inexpensive	0	0	0	0	0	0	1	0	—	0	0	0	0	0	0.5	0	1.5
Reproducibility	1	1	1	1	0	0	1	0.5	1	—	1	1	1	1	1	1	12.5
Nutrient Diffusion	0	0	0	1	0	0	1	0	1	0	—	0.5	1	1	1	0	6.5
Flow Control	0	0	0	1	0	0	1	0	1	0	0.5	—	0.5	1	1	0	6
Quantitative and Qualitative Results	0	0	0	0	0	0	1	0	1	0	0	0.5	—	1	1	0	4.5
Limited Interaction	1	1	1	1	0	0	1	0	1	0	0	0	0	—	1	0	7
Resource Conservation	0	0	0	0	0	0	1	0	0.5	0	0	0	0	0	—	0	1.5
High Throughput	1	1	1	1	0.5	0.5	1	0.5	1	0	1	1	1	1	1	—	12.5

The analysis of the various design criteria revealed that the most important aspects of our design are biocompatible and sterilizable materials, repeatability, and a system that offers high throughput. Criteria that are of the lowest priority are resource conservation and materials that are nondegradable and inexpensive.

4.2 Concept Functions and Means

After the prioritization of design criteria were established. We first focused on the key functions that the device must accomplish, and how we could accomplish those functions by various means. We also developed a general concept map to visualize the different aspects of our device and how these aspects can individually be accomplished to achieve a successful fluidic model to evaluate chemotherapeutics with high throughput.

4.2.1 Function Means Analysis

The functions that our device should accomplish first begins with securing scaffolds in place so that they can be stacked. We also discussed other options for silk fibroin for the tumor model material. After the tumor model functions were determined, the chip device material must be biocompatible, offer physiologically accurate flow, and a way for capturing analyte for possible cytokine secretion analysis. Additionally, a source must be determined to provide a constant flow rate through the system. A breakdown of these functions and possible means to accomplish these functions are displayed in **Table 5**. Some functions may only require one mean to accomplish the specific task, but other functions may rely on several means working together to achieve the desired outcome.

Table 5. Function Means Analysis

Feature of Function	Means					
Holds Scaffold in Place	Microfluidics	Flow Channel	Scaffold Holder			
Processible Model Material	Silk Fibroin Scaffold	Collagen I Gel	Matrigel	Collagen I Scaffolds	Synthetic Scaffolds	Spheroids
Biocompatible Chip Device	PDMS	PTFE	Glass	Silicon	Other Polymers	
Physiologically Accurate Fluid Dynamics	Pore Channel Geometry	Perfusion through Scaffold	Media flow across surface			
Flow Pressure Source	Peristaltic pump	Syringe				
Analyte Capture	Holding tank	Continuous flow (sample at periodic time points)				

4.2.1 Concept Map

In order to segment the design process, a concept map can be seen in **Figure 5**. The first step in the design process focused on confirming the previously used silk fibroin scaffolds as our tumor model material. Next, the focus shifts to the flow chamber design and geometries. Different placements of the model system were explored to develop the best design to avoid harmful stresses while also keeping the model as simple as possible. The investigation of the flow chamber's geometry goes further to ensure that fully developed laminar flow is possible at physiologically accurate flow rate conditions. The material(s) needed to fabricate a fluidics

device were researched and integrated into a model that is biocompatible, sterile, and simple to machine. Finally, a pump system was selected that provided consistent flow rates through several devices at once.

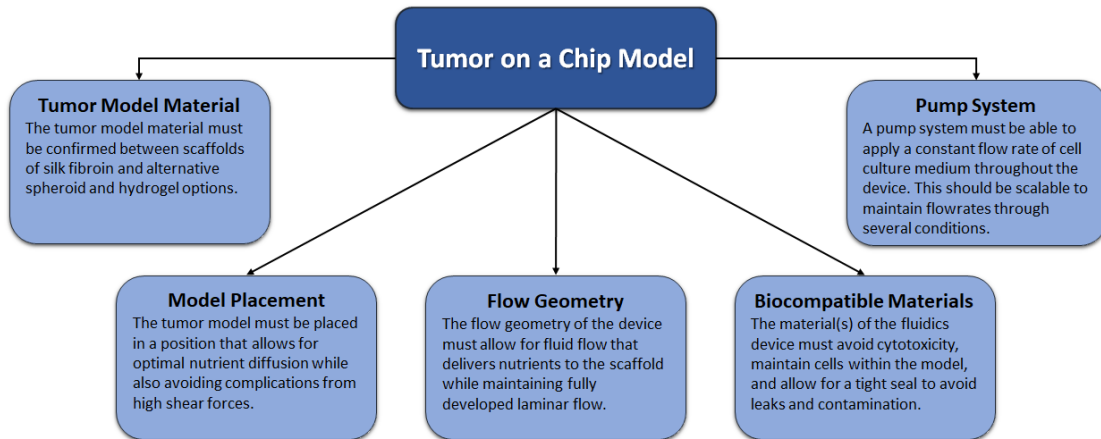


Figure 5. Concept Map for Final Design Considerations

4.3 Prototyping

4.3.1 Conceptual Designs

Based on the needs analysis and function means, the team formed three preliminary designs. Each version provided different flow paths and stresses on the scaffold, showing flow over both sides, over one side, and through the scaffold, respectively.

The first design indicated in **Figures 6 and 7** show a device that provides flow over both the top and bottom of the scaffold. A chip holding the scaffolds would sit in the indent, leaving room underneath and above the chip for fluid flow and nutrient diffusion from both sides of the scaffold. The device would be two pieces, secured by four screws, and the flow path is completely horizontal across the device.

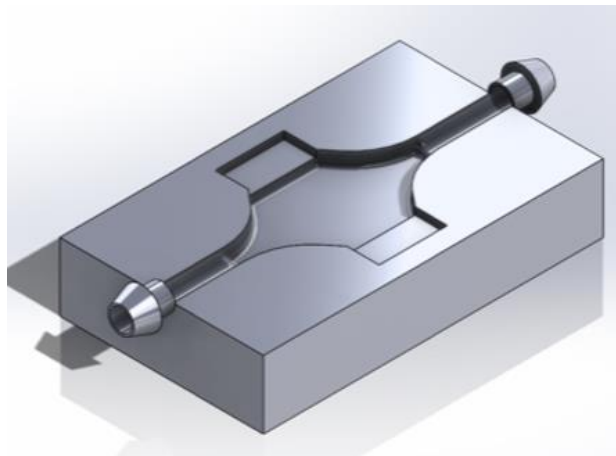


Figure 6. Sectioned View of Flow Chamber Design #1

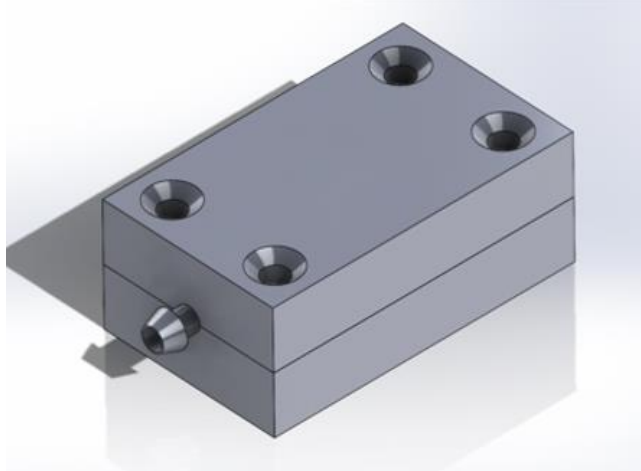


Figure 7. Closed Flow Chamber Design #1

The second design option shown in **Figures 8** and **9** is a model that has flow over one side of the scaffold. This allows for the scaffold to be laid across the top, permitting shear flow above and nutrient diffusion from one side. The flow comes in from the top before taking on a horizontal flow path across the actual scaffold and exiting out of the top of the device, as seen in the cross section of **Figure 8**.

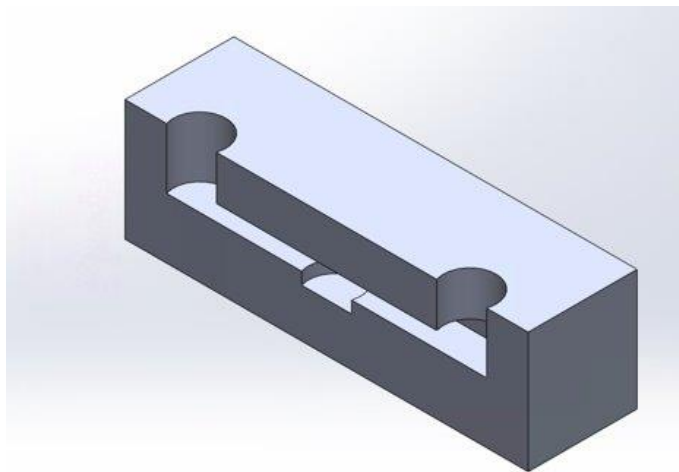


Figure 8. Sectioned View of Flow Chamber Design #2

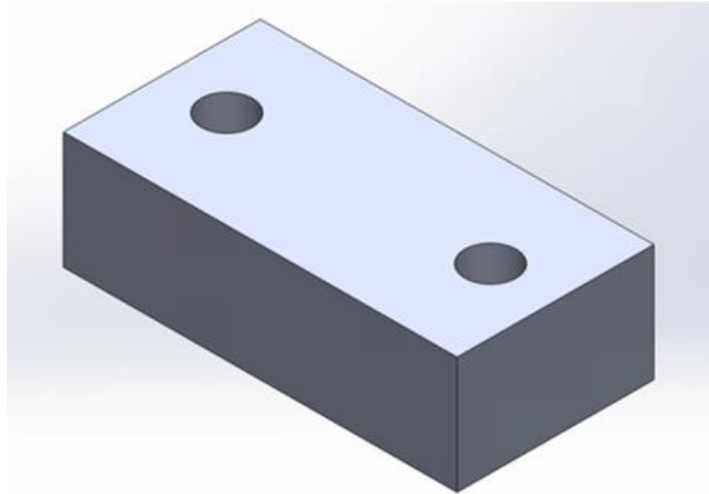


Figure 9. Closed Flow Chamber Design #2

The last conceptual design in **Figure 10** shows flow through the scaffold, where a chip holds the scaffold in place and flow goes through one side of the scaffold and out of the other. This ensures that nutrient diffusion would occur throughout the entire scaffold.

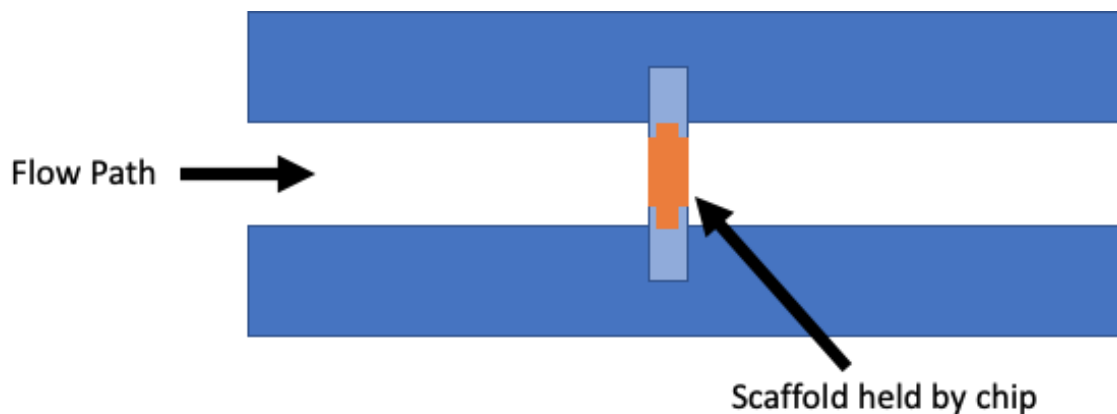


Figure 10. Sectioned Drawing of Flow Chamber Design #3

4.3.2 Mathematical Geometric Analysis

The flow chamber must offer laminar and fully developed flow at the point just before the fluid passes over or through the scaffold. Fully developed laminar flow is needed for several calculations including analysis of shear forces at the scaffold interface. A key design parameter was ensuring that the flow rate does not induce high amounts of shear stresses that could possibly harm the cells. The maximum shear stress our model can have is 5 dynes/cm². Our system must rely on a constant flow rate that does not exceed the previously established shear specifications.

An analysis relating key design parameters to a set flow rate can be seen in **Table 6**. The table has fixed geometric values and constants that apply to our system in purple. The width and height refer to the horizontal and vertical axes respectively of a rectangular flow chamber. These

dimensions were the primary values that were altered to determine a flow rate that best fits our system. All other values are constants that cannot be changed in our current model. The viscosity of standard cell culture medium supplemented with 10% FBS was found to be about 9.4×10^4 Pa*s [83]. The density of the same medium was found to be about 1007 kg/m^3 [84]. The Re contains the pipe diameter assuming a cylindrical pipe. For our system, the “pipe” is a rectangular duct, and the diameter for the Re calculation can be approximated using an equation for the hydraulic diameter, D_h .

$$D_h = \frac{4A}{p} \quad (5)$$

where A is the cross-sectional area and p is the perimeter. Since the pumps typically control the flow rate based on volumetric flow rates, the velocity can be calculated from the pre-defined volumetric flow rates as:

$$v = \frac{Q}{A} \quad (6)$$

where A is the cross-sectional area and Q is the volumetric flow rate. The velocity of the flow chamber can then be applied to equations to determine the both the Reynolds Number and entrance length from Equation 1 and Equation 2, respectively.

$$D_h = \frac{4A}{p} v = \frac{Q}{A}$$

Once the Reynolds number confirms laminar flow and the entrance length is determined, we can calculate the shear stress, τ , that each volumetric flow rate would result via [85]:

$$\tau = \frac{6Q\mu}{wh^2} \quad (7)$$

The variables used in the equation to define shear are Q = flow rate, μ = viscosity, w = width, and h = height.

Table 6. Mathematical Analysis for Flow Chamber Design

Flow Rates Needed for Shear Stresses				
Constants				
Width (mm)	Height (mm)	Viscosity (Pa*s)	Density (kg/m ³)	Hydraulic Diameter (mm)
25	1.84	0.00094	1007	3.427719821
Flow Rate (mL/min)	Velocity (m/s)	Reynolds Number	Entrance Length (mm)	Shear (dyne/cm ²)
0.002	0.00000072	0.0027	0.00055	0.000022
0.05	0.00001812	0.0665	0.01368	0.000555
0.1	0.00003623	0.1330	0.02736	0.001111
0.5	0.00018116	0.6652	0.13681	0.005553
1	0.00036232	1.3304	0.27362	0.011106
5	0.00181159	6.6522	1.36812	0.055529
10	0.00362319	13.3045	2.73624	0.111059
50	0.01811594	66.5224	13.68121	0.555293
100	0.03623188	133.0448	27.36241	1.110586
500	0.18115942	665.2239	136.81207	5.552930
1000	0.36231884	1330.4478	273.62414	11.105860
2000	0.72463768	2660.8957	547.24829	22.211720

4.4 Modeling for Virtual Simulation

COMSOL modeling was used to visualize the velocity profiles of the three potential device designs. All three models used water as a model fluid and an inlet velocity of 5 m/s for fluid flow. Although this flow rate is much faster than our final system, this velocity value is an arbitrary value used to analyze the velocity profile of the three models. The first model can be seen in **Figure 11** where the flow diverges to the top and the bottom of the scaffold, so that the scaffold sits between a nutrient source on both sides. The second model simplifies the first model a bit by only providing a media source on one side of the scaffold. The velocity profile can be seen in **Figure 12**. The final model demonstrates fluid flow through a scaffold material. The scaffold material was modeled with a porous piece of human skin to mimic fluid flow through small pores. The results of this model can be seen in **Figure 13**.

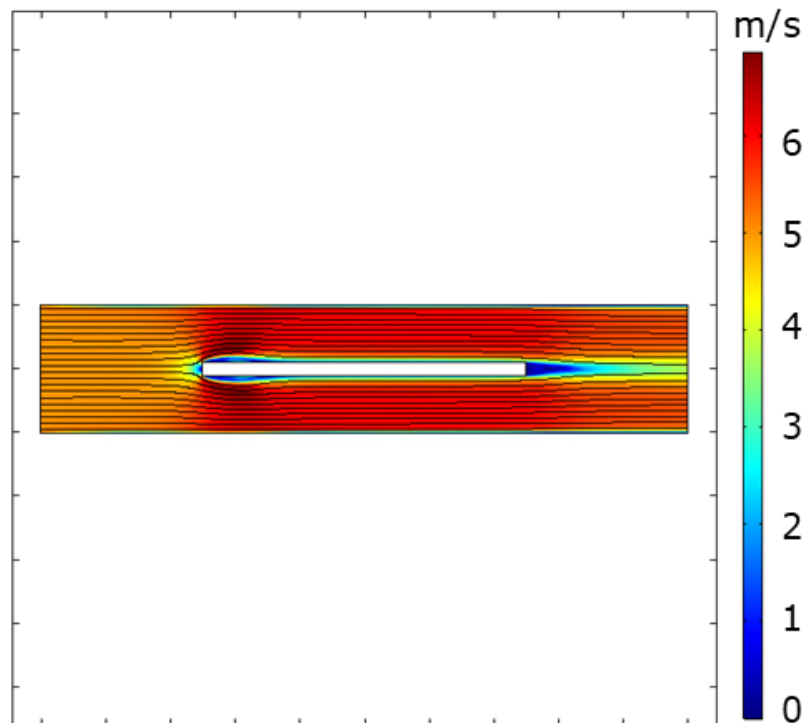


Figure 11. Fluid Flow on Both Sides for Design #1

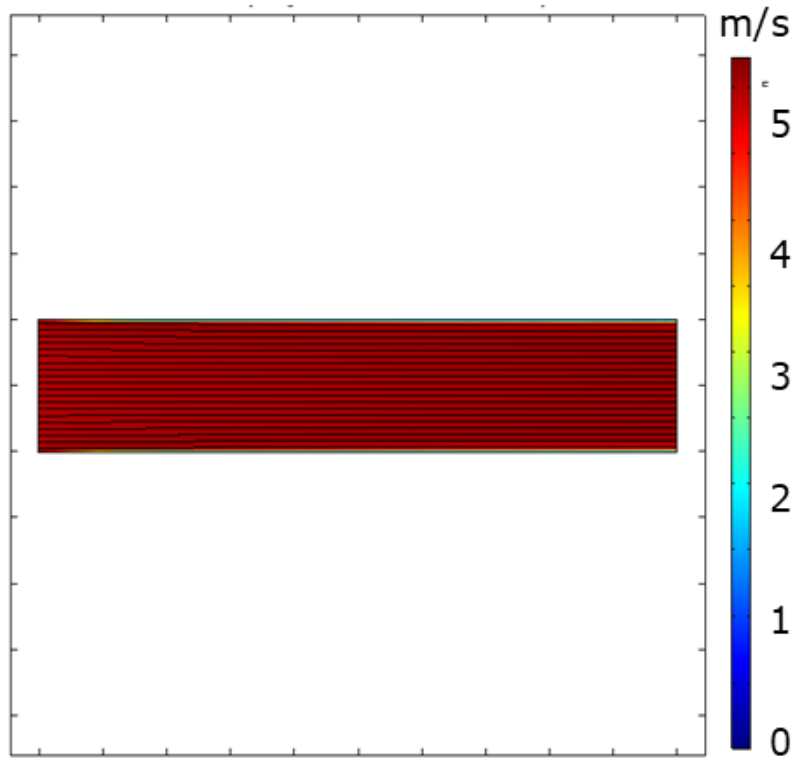


Figure 12. Fluid Flow on One Side for Design #2

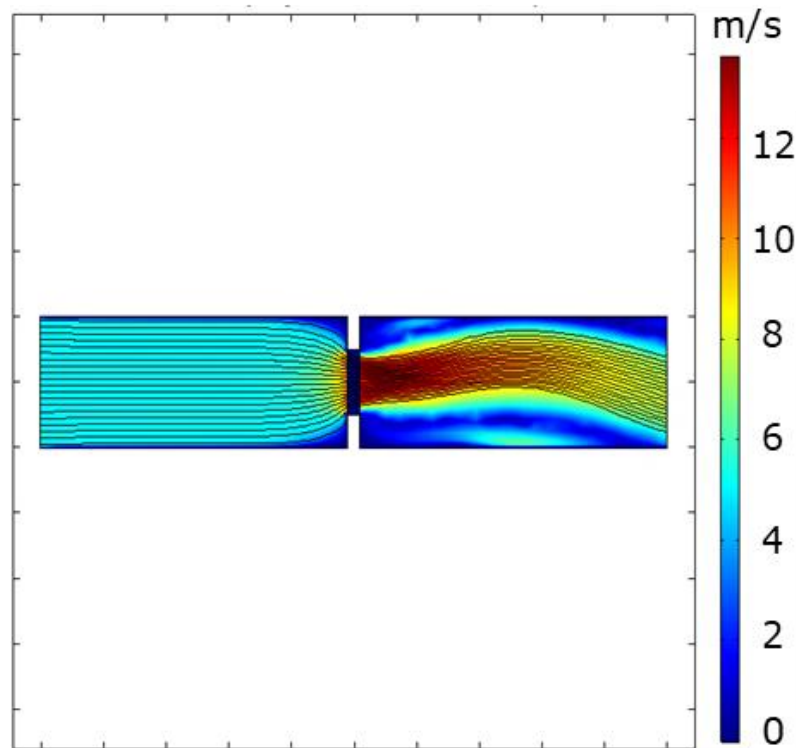


Figure 13. Fluid Flow through Scaffold for Design #3

Upon comparison of the three models, the fluid flow through the scaffold was eliminated. A major concern with this model is the increase in velocity through the scaffold. This complication makes it more difficult to model diffusion of nutrients while also posing a much greater risk in harming the cells. The shear stress on the attached cells can be modified to ensure that the force will not harm the cells, but the forces may still be strong enough to cause cells to detach from the scaffold. Both options with fluid flow over both sides and one side of the scaffold showed a promising velocity profile. We ultimately decided to refine our design to the flow over just one side of the scaffold. The rationale behind this decision is that there are more materials needed to secure the scaffold between two flow paths in comparison to flow over just the top of the scaffold. Additionally, calculations made from **Table 6** are more relevant in the flow over just the top, which makes it much simpler to determine the proper flow rate for our model's desired characteristics.

4.5 Design Selection

The final device is comprised of three main parts: the scaffold, the chip, and the flow chamber. **Figures 14** and **15** shows the full assembly in expanded form and together. SolidWorks 2020 was the software utilized to create the parts and the assembly, which allowed the team the option to 3D-print rapid prototypes as well as machine parts. A silicone layer that is 1 mm thick is in between the two halves of the flow chamber in order to prevent leaks and maintain sterility. There are six screw holes that are placed around the flow path. The varying locations ensure an even closure of the device and equal distribution of the screws. The scaffold, while not shown in the image, fits within the chip and is inserted before assembling the rest of the device.

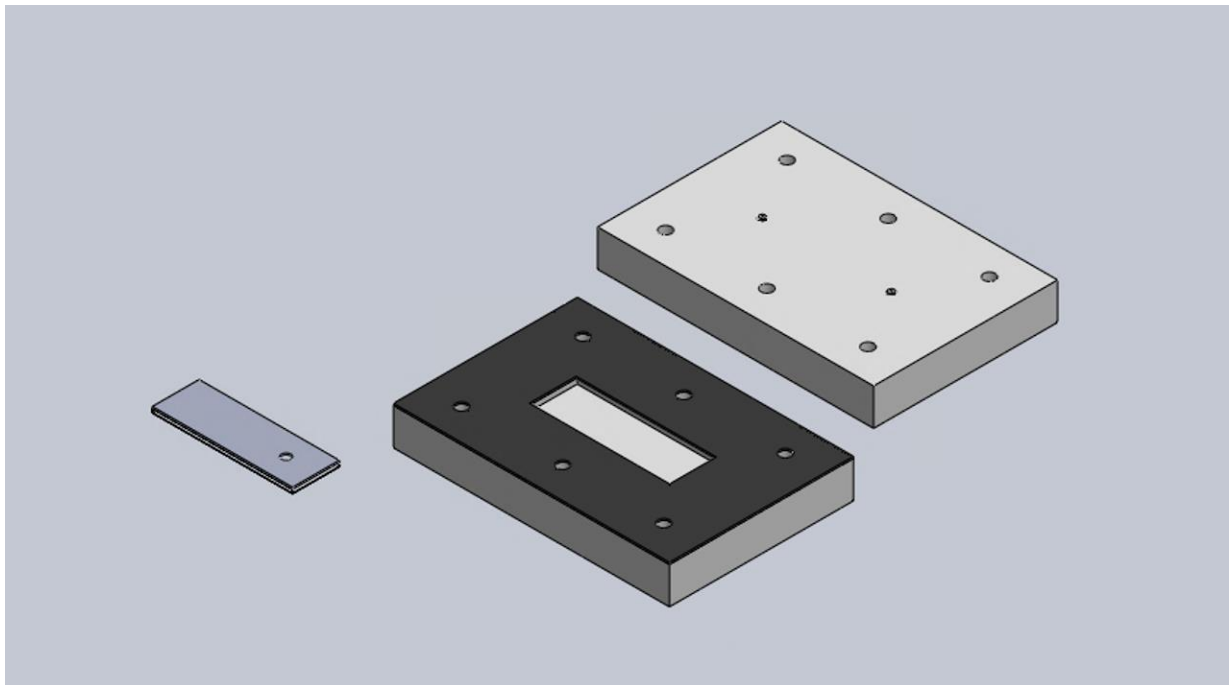


Figure 14. Expanded Assembly of Final Design

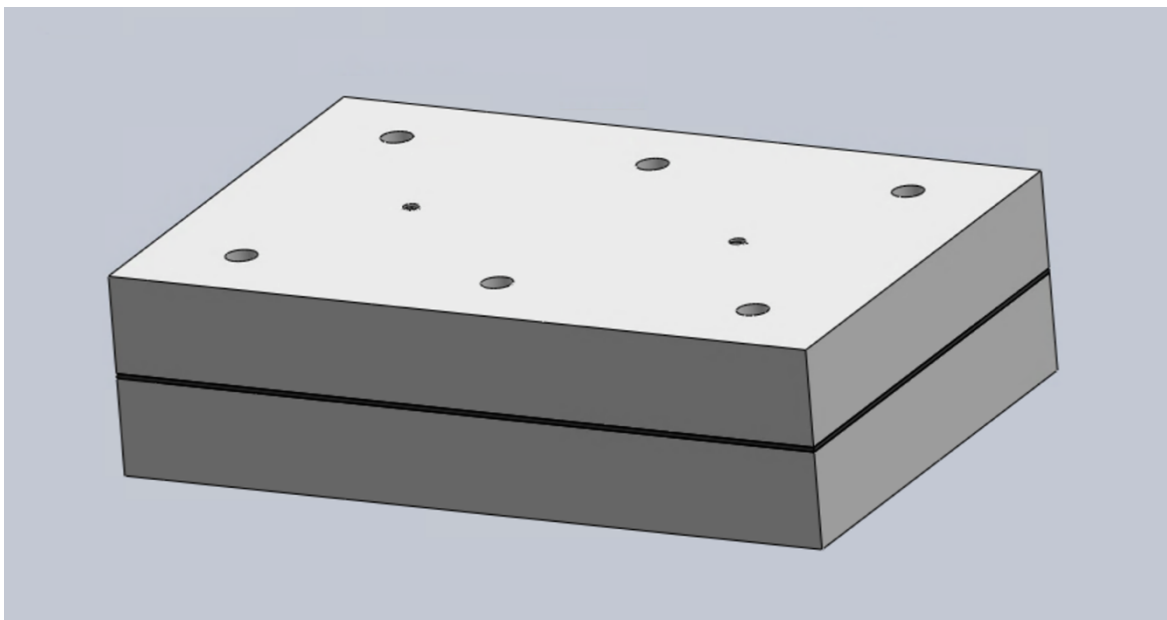


Figure 15. Closed Assembly of Final Design

The chip contains a PEGylated glass slide, and a layer of PDMS with a cutout of the same diameter of the silk scaffolds on top, which will allow for a press fit of the scaffolds when they two halves of the chip are combined (**Figure 16**). This chip fits into the bottom portion of the flow chamber. The PEG was coated onto the glass to ensure the cells would only interact with the scaffold while in use. The PEGylation process is explained in more detail in **Appendix A**. The top part was chosen to be PDMS because it is an autoclavable material that is easy to mold and create the specific geometries the device required. The two are plasma bonded together to prevent leaks in between the layers.

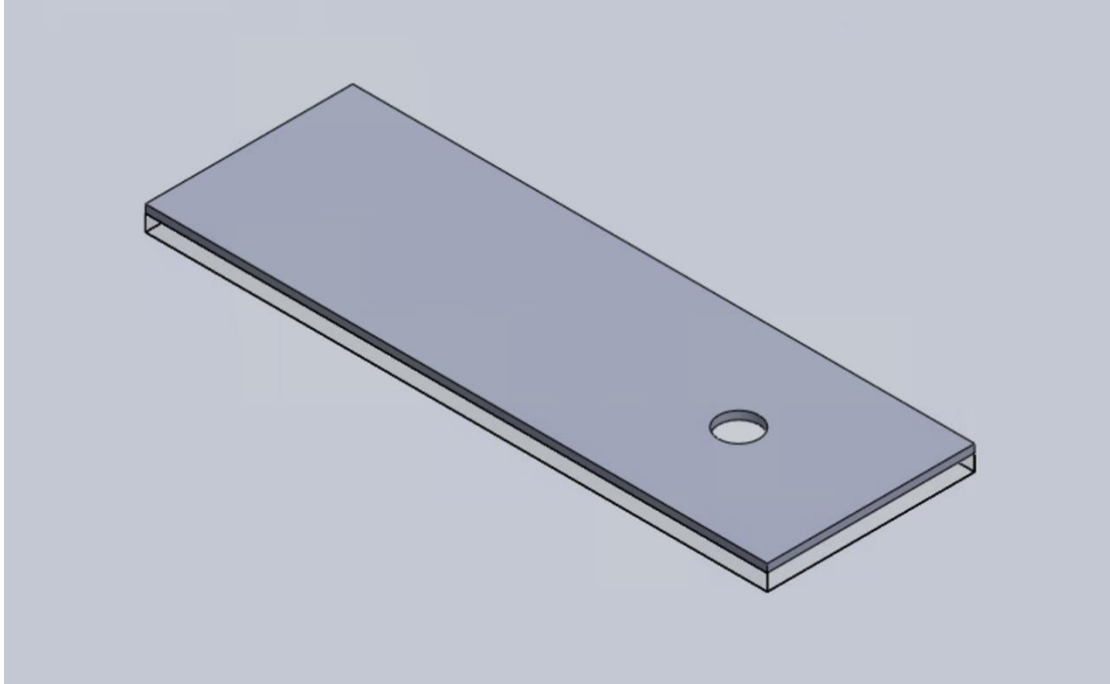


Figure 16. Chip for Full Assembly

Figure 17 is a cross sectional view of the flow chamber. The flow chamber is comprised on the top part of the device. Threaded holes allow for luer locks to be sealed on the entrance and exit of the device, and the headspace and silicone layer allow for an overall headspace of 2 mm. The flow path was designed to gradually fan out in order to accommodate the machining capabilities the team had available. It also provides a more gradual transition of flow profile, meaning the flow can reach laminar status faster within the device. The location of the scaffold on the chip ensures a long enough entrance length so that the fully developed laminar flow passes over the scaffold. The material of the device and flow chamber is Teflon, or PTFE. This material was chosen based on its machinability and ability to be autoclaved.

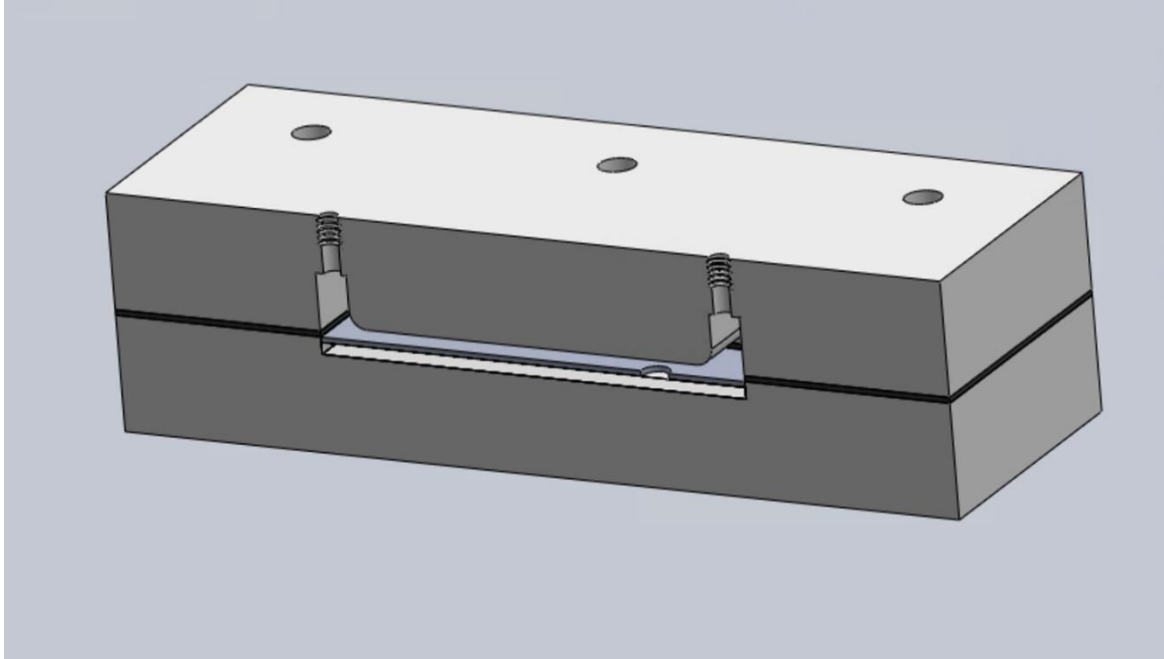


Figure 17. Flow Chamber Cross Section

The overall system will contain more than just the device. Since the entrance and exit will have a luer lock secured onto them, tubing can be attached to form a closed system. The closed system will rely on a pumping mechanism to apply a constant flow rate through the device. Integrating a pump in the system allows for fresh media to constantly be supplied to the scaffolds, which better mimics the *in vivo* tumor microenvironment and allows for better modeling capabilities for drug efficacy testing.

Media circulation systems are a necessity for constantly supplying nutrients to scaffolds in the device. Both peristaltic pumps and syringe pumps are candidates for recirculating media throughout our system. Both induce constant volumetric flow rates throughout the system, but the syringe pump is limited by its throughput. Only one syringe pump can operate at a time for each device, while many different channels can be employed in a single peristaltic pump that operates at the same flow rate. Although peristaltic pumps allow for higher throughput testing, the one available to the team presents challenges associated with the requirement of ethylene-oxide treatment for sterilization of the tubing, as well as large quantities of medium in reservoirs added to the system for large medium supply to ensure proper nourishment to the cell culture. Both pumping systems could prove useful, with syringe pumps being useful for quick functional testing and peristaltic pumps being more useful for multiday, high throughput cellular studies. The syringe pump and peristaltic pump schematics are outlined in **Figure 18** and **Figure 19** respectively.

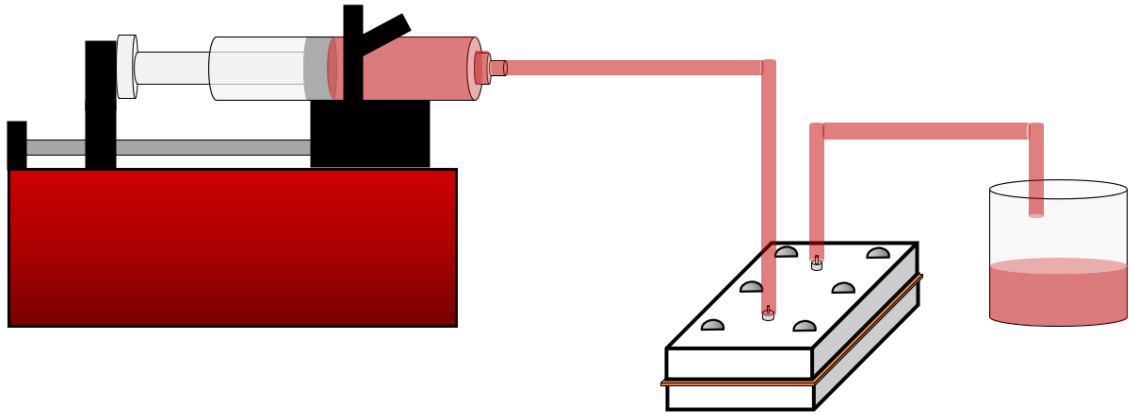


Figure 18. Syringe Pump System Overview

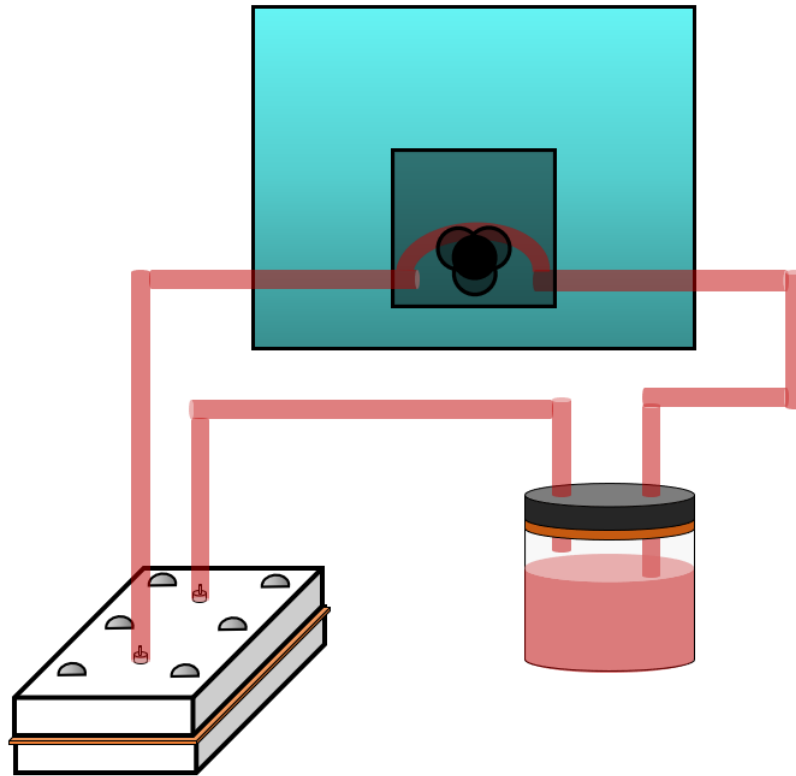


Figure 19. Peristaltic Pump System Overview

CHAPTER 5 – DESIGN VERIFICATION

5.1 Verification of Fluid Flow Device

Before testing our device's modeling capabilities, we first verified the function of device. Cytotoxicity testing was used to confirm that the materials did not cause any harm to cells. Additionally, the fluid chamber was evaluated to ensure that there was no leaking during flow, the scaffolds remained in their stacked formations, and the system sustained function for at least 3 days. Finally, the surface chemistry of the glass chip was assessed to confirm the presence of PEG. If PEG was present on the surface of the glass, then risk of cells attaching to the glass surface during culture would be attenuated.

5.2 Cytotoxicity of Device Materials

Cytotoxicity testing was used to assess the biocompatibility of the device materials. Cytotoxicity was evaluated with a resazurin assay to quantify and compare metabolic activity. Twelve-well plates were prepared with 5.0×10^4 cells seeded per well and 2 mL of culture medium in each well. Materials that were exempt from cytotoxicity studies were glass slides, and PTFE. PDMS and glass slides have been used to create microfluidic devices to evaluate cytotoxicity, which confirms that they have no cytotoxic effect [86]. PTFE also has been used in the past as a material to stack silk scaffold neuroblastoma models, which confirms that it also has no cytotoxic effect [7]. The controls in this experiment were wells with no materials added and wells with latex gloves. The latex glove condition was a positive control for cytotoxicity and the condition with no added materials were the negative control. The experimental groups in this case were PDMS that was casted in a polylactic acid mold, PDMS that was cured by standard processes, samples of polylactic acid, and silicone. All materials were either steam sterilized or soaked in ethanol prior to exposing to the cells.

There were three replicates of each material in this study for a sample to be collected after 24 hours and 48 hours of culture with a material; this resulted in a total of 36 total wells. Cells were cultured for 24 hours prior to treatment. The day of treatment is denoted as day 0. Day 1 and day 2 were for 24 and 48 hours of cells culturing with the material, respectively. Images were taken on day 0, day 1, and day 2, and they can be seen at **Figure 20**.

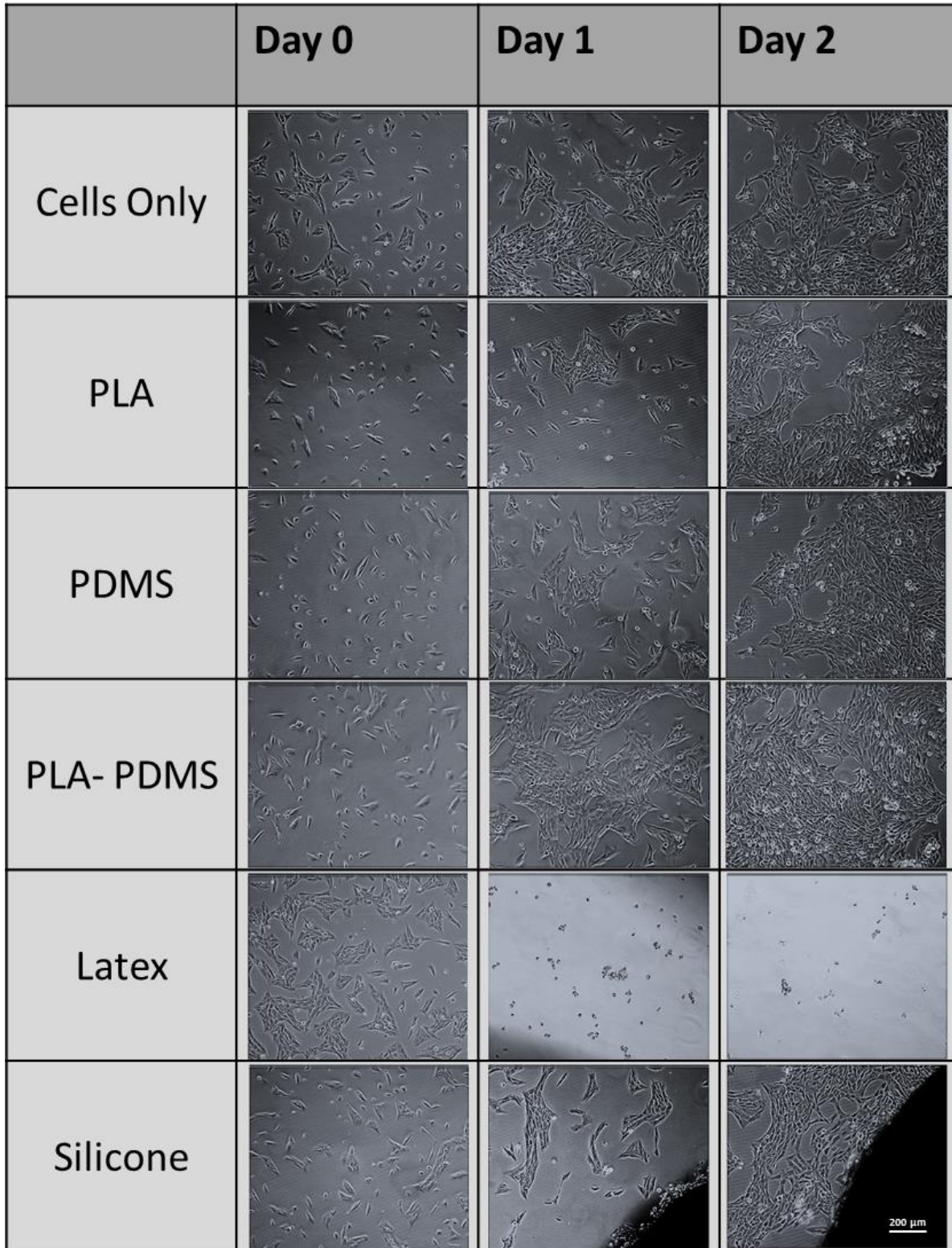


Figure 20. SK-N-AS Cell Culture with Device Materials to Visualize Cytotoxicity

The resazurin assay was conducted on Day 1 and Day 2. The complete assay protocol can be seen in **Appendix B**. The assay increases in fluorescence as metabolic activity increases. This allows for quantification and comparison of metabolic activity between groups. The fluorescence comparison among groups can be seen in **Figure 21**. Statistical significance was evaluated with a two-sample, two-tailed, unpaired t-test for comparison of each experimental mean to the untreated cells.

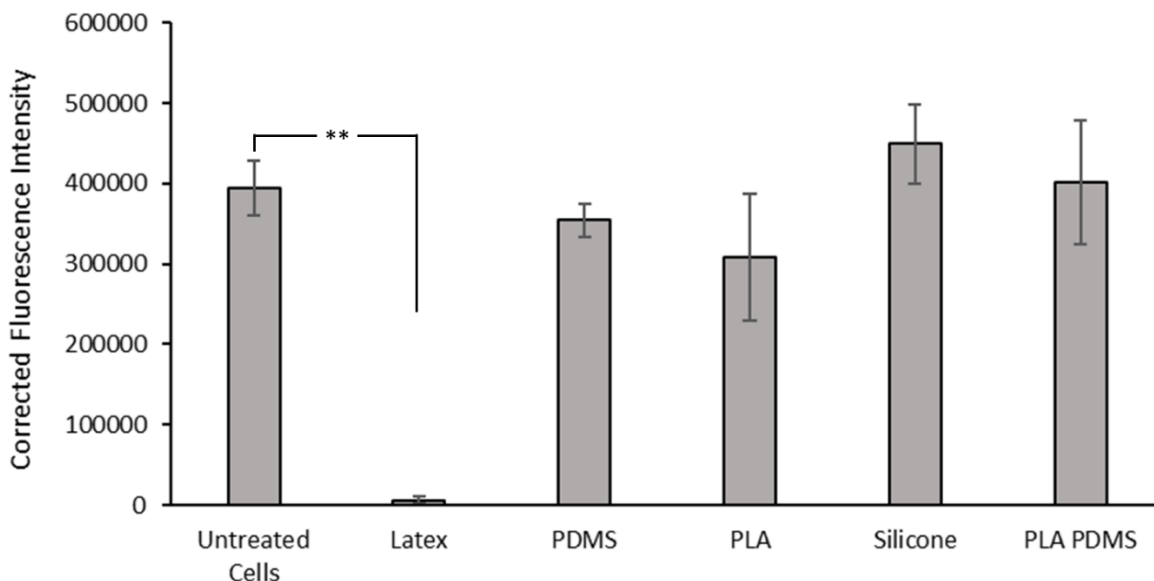


Figure 21. Metabolic Activity After 48 Hours of Culturing with Materials
p<0.01 ()**

5.3 Leak Testing

The fluidic system was tested using 5 mm biopsy punched PDMS press fitted with a glass slide within the device. This functional prototype was used the proper materials, dimensions, and pumping system and was tested in a nonsterile environment. The system used water with red dye to visualize the flow, and a syringe pump with a 50 mL syringe was used to supply specific flow rates to the system. Some initial leaks were observed at 5 mL/min and 3 mL/min, but tightening the luer lock fittings and screws alleviated this issue.

Since no leaks or bubbles were observed, the team proceed with analyzing the stability of silk scaffolds in the system. Scaffolds were dyed with blue food coloring for visualization. Four scaffolds were sandwiched as a stack between PDMS with a 5 mm biopsy punched hole and a glass slide. Under a flow rate of 3 mL/min, the scaffolds remained in their initial location, and some mixing was observed. However, there was liquid found between the layer of PDMS and glass, resulting in undesirable nutrient exposure for our system. This result can be seen in **Figure 22**.

After running multiple trials, the team discovered the best way to set up the system such that leaking did not occur. While no formal sterility testing was conducted, the team believes that a closed system that does not leak would be devoid of contamination and thus could be considered sterile if set up using aseptic techniques.

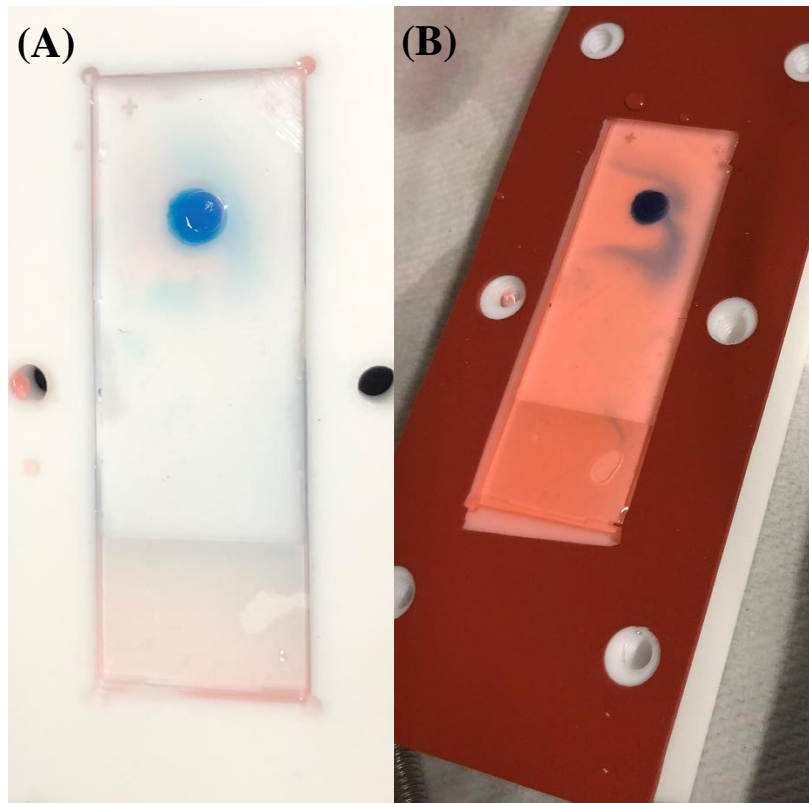


Figure 22. Non-bonded PDMS and Glass with Scaffolds Before (A) and After (B) Flow

5.3.1 Syringe Pump Testing

Further testing with a syringe pump was used to evaluate scaffold placement with varying diameters and stack iterations. To ensure liquid was only maintained across the top surface of the chip, plasma bonding between the glass was plasma bonded to PDMS by the process outlined in **Appendix C**.

Testing notes with the different conditions can be seen in **Table 7**. The tests were conducted similar to the previous trials with scaffolds dyed blue and the water dyed red using food coloring. The team used a 50 ml BD syringe that has a rubber plunger and 1/32" tubing with luer locks (female to male). All of the trials were tested at flow rates between 1.5 mL/min to 3.0 mL/min.

Table 7. Syringe Pump Testing Comments and Observations

Trial	Number of Scaffolds	Comments and Observations
1	2 scaffolds in 1 x 5 mm	Scaffolds did not fit; the team did not proceed with testing
2	2 scaffolds in 1 x 7 mm	Fill time =2 min 49 s (=8.45 mL). Noticed some leaking from both luer locks at around 14 min. When device was opened, the gap caused the scaffold to float away (found one in the center and the other on top of a screw hole), which the team believes was dislodged when raising the device.
3	2 scaffolds in 1 x 6 mm	Leaking around 10 min in from the top of the luer/ tubing connection (team noticed a tear/rip in the tubing). No leaking from luer to device connection. Scaffolds stayed in place.
4	2 scaffolds in each 4 x 6 mm	At about 11 min in, team noticed some leaking at luer to base of device. When opened, all but one hole had (bottom right by exit) had the scaffolds out of place.
5	2 scaffolds in each 4 x 6 mm	No leaking. Some scaffolds had floated away. Observed that no scaffolds were getting stuck in the tubing, so the floating is likely occurring when lifting the device.
6	2 scaffolds in 1 x 6 mm	One stayed in place. One floated away. Used 15 mL of fluid.
7	2 scaffolds in 1 x 6 mm	Both scaffolds stayed in place. Used 15 mL of fluid.
8	2 scaffolds in each 4 x 6 mm	One scaffold remained in each of the two leftmost holes. On the bottom right there was one scaffold. In top right there were two scaffolds. Used 15 mL of fluid.
9	2 scaffolds in each 4 x 6 mm	Noticed some leaking around one of the screws, corrected when tightened. The syringe was placed on the same surface height as the device and the remaining fluid from the tubing came out (in the direction opposite of the device). While the scaffolds had floated away, team could feel seal breaking when device was separated and noticeable pressure release. There was still fluid in the system. About 22 mL of fluid was used
10	2 scaffolds in each 4 x 6 mm	After the syringe emptied (~20 mL of fluid was used), it was lowered to the same height as the device to prevent any impact from potential energy. The syringe was then filled with ~40 ml of air and connected back to the tube until. The syringe pump was on until there was no water coming out of the exit tube of the pump. The device was rotated slowly to help allow the fluid to move. When the device was opened, there still seemed to be a small seal that was broken. While the entrance side had no fluid, there seemed to be some pooling at the exit. Some scaffolds floated away.

5.3.2 Peristaltic Pump Testing

The system was set up according to the instructions provided by the Watson Marlow 323 device. Considering 10 rotations per minute (rpm) was equivalent to 0.069 mL/s or 4.14 mL/min, the team used a flow rate of 5 rpm to achieve a flow rate of 2.07 mL/min. Similar to the syringe pump, it took 2:23 min for the device to fill up (equivalent to 9.06 mL). The comments and observations from testing are observed in **Table 8**.

Table 8. Peristaltic Pump Testing Comments and Observations

Trial	Number of Scaffolds	Comments and Observations
1	1 x 6 mm	Ran device for 5 minutes. Removed tubing from reservoir and ran pump until 30 seconds after team had seen last bubble deposited into reservoir. When device was separated, the scaffolds had floated away, and some fluid was present near the exit of the device.
2	1 x 6 mm	Ran device for 12 minutes. Removed exit tubing from reservoir and set pump to reverse. After no bubbles were visible and tubes were emptied, the device was separated. Fluid pooled on entrance side, but all scaffolds remained in place.
3	1 x 6 mm	Ran device for 10 minutes. Removed exit tubing from reservoir and set pump to reverse. After no bubbles were visible and tubes were emptied, the device was separated. Fluid pooled on entrance side, but all eight scaffolds remained in place.

5.4 Longevity Testing

The model's capability of sustaining a constant flow rate for 3 days was evaluated to ensure that there are no issues overtime when conducting experiments with cells. The desired outcomes were ensuring that the scaffold stayed in place, no bubbles formed, no leakage occurred, and the flow rate remained consistent. Every 24 hours, the team qualitatively assessed the function of the device. The system sustained a constant flow rate with no leaks during each observation.

After 72 hours, the team removed the device from the system and attempted to unscrew and separate the top and bottom pieces. The device was notably difficult to separate as a result of a strong seal. **Figure 23** shows the result of separating the seal with a high force requirement. The image on the left shows the outcome of the internal chamber after separation, and the image on the right shows the desired outcome after system separation. The scaffolds changed color from a dark blue to the color of the water used for testing.

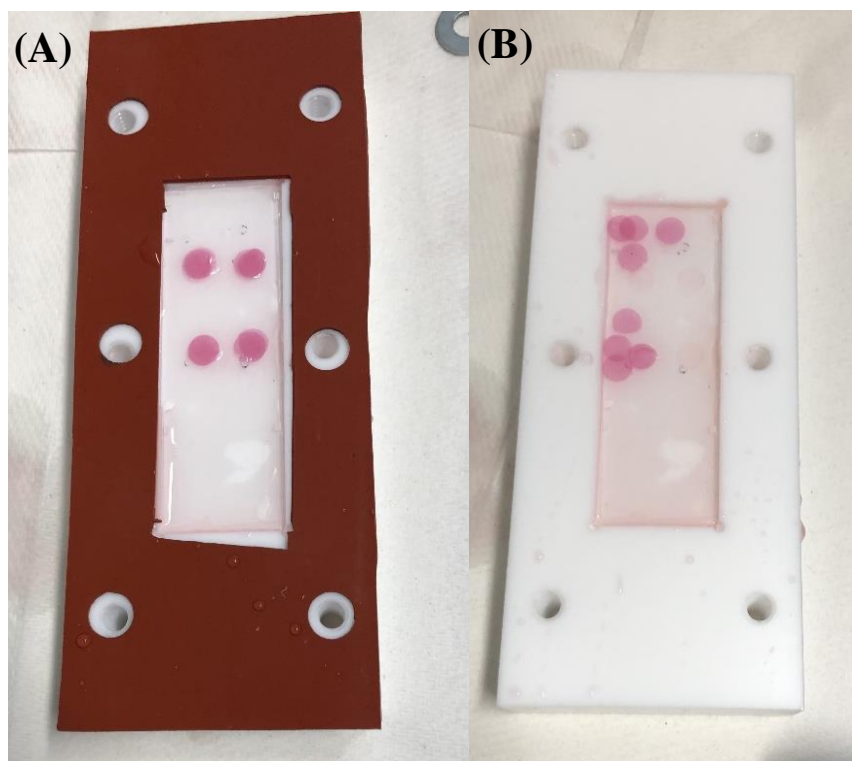


Figure 23. Bonded PDMS and Glass Before (A) and After (B) 3 Days of Flow using a Peristaltic Pump

5.5 Surface Chemistry Analysis of PEGylated Glass Slides

X-ray photoelectron spectroscopy (XPS) was used to evaluate the surface chemistry of PEGylated glass slides. XPS uses concentrated photoelectrons that excite the electrons on the surface of a material, these electrons then leave the material and kinetic energy data is collected. The kinetic energy is used to calculate the binding energy, which can be translated to what material, element, and what orbital the electron came from. This is relevant to the PEGylated glass slides because we can tell what types of elements are on the surface of the glass compared to untreated glass, which can confirm or deny that there is the monolayer of PEG on the surface. The team worked with the Grimm Laboratory, where we started by conducting two wide resolution surveys. This utilizes 1486 electron volts (eV), which would excite almost any element that may be present on the surface. This data then informed the group where to conduct high resolution multiplex scans, which ended up being around the peaks of oxygen, carbon, and silicon. Information and resources regarding the protocol for PEGylating the glass slides can be found in **Appendix A**.

The results of the low and high resolutions scans are shown in **Figure 24**. Using CasaXPS software, the peak area ratios between the untreated glass and the experimental glass were calculated, which included the use of baseline and peak fitting. The peak area ratios are indicated in **Table 9**. Peak ratios are calculated by comparing the difference between the peak height of one element to another that is constant between experimental runs. The difference in peak ratios can be used to compare the relative amounts of an element. In the group's case, primary carbon (not oxidized or bonded to other groups) was constant between experimental groups. The higher

the peak ratio the more silicon or oxidized carbon that was present in the sample. Protocols and data analysis and resources for XPS can be found in **Appendix D**.

Table 9. Total Peak Area Ratios for XPS Analysis

	Untreated Glass	PEGylated Glass
Total Si: Primary Carbon	1.45	0.04
Oxidized Carbon: Primary Carbon	0.11	0.24

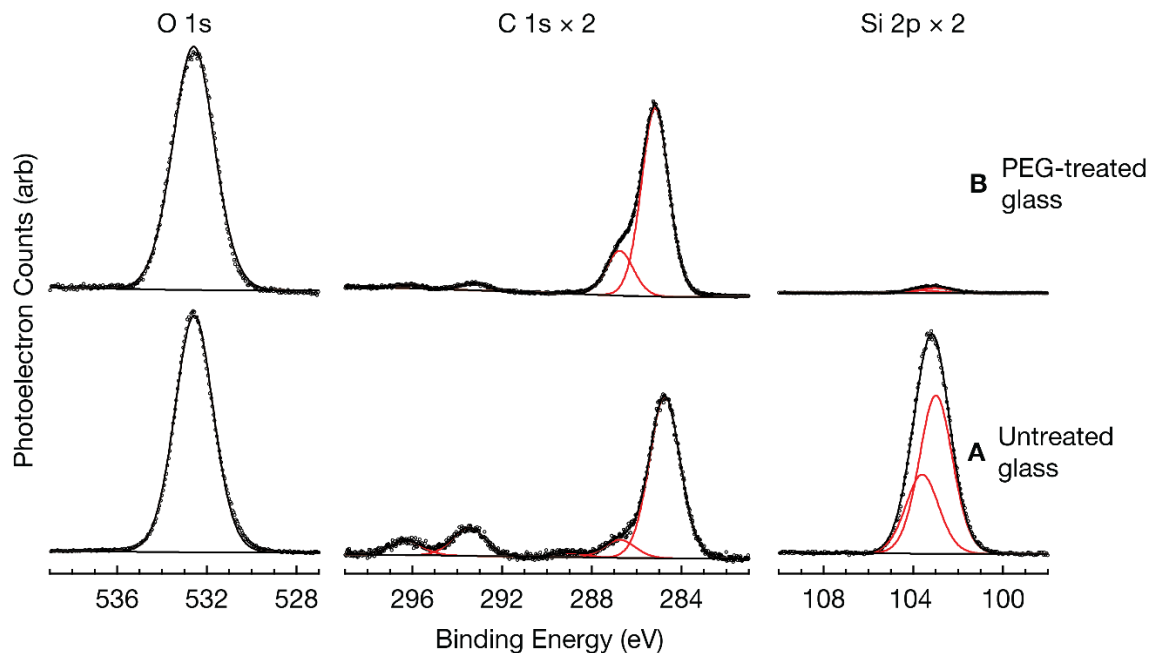


Figure 24. Photoelectron Counts to Determine the Presence of PEG on the Glass Surface Using XPS

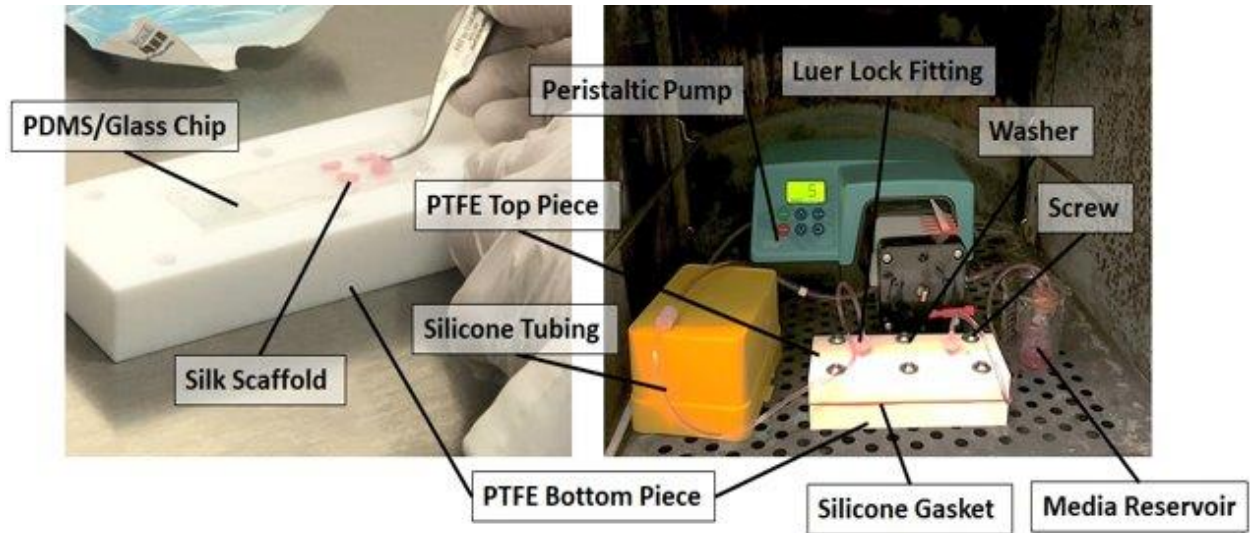


Figure 26. Labeled Final System

6.2 Tumor Modeling Potential for Design Validation

Design validation is ensuring the system meets the needs of the client. For this project, the team confirmed that all goals outlined in the client statement are addressed through testing. These metrics measured the functionality of the device both qualitatively and quantitatively.

6.2.1 Virtual Simulation with COMSOL

A two-dimensional model was created to analyze the oxygen gradients throughout stacked scaffolds when secured in the fluidics device. The multiphysics analysis combined the physics of a transport of diluted species module and a laminar flow module to model the oxygen transport induced by cell-seeded scaffolds in the system.

Oxygen gradients were modeled using Michaelis–Menten kinetics with a transported diluted species physics module. The model uses the rate of oxygen consumption equation as well as the transport of diluted species equation to model the oxygen gradients in the system. These equations are represented in *Equation 8* and *Equation 9*, respectively.

$$R = -\frac{OCR \times C}{MM+C} \quad (8)$$

$$R = \frac{dc}{dt} + \nabla(-D\nabla c) \quad (9)$$

In these equations, D is the oxygen diffusion coefficient, MM is the Michaelis-Menten coefficient, OCR is the rate of oxygen consumption, and C is the concentration of oxygen. The diffusion coefficient was obtained from literature with the assumption that the fluid has the same properties as water to equal $2.6 \times 10^{-9} \text{ m}^2/\text{s}$ [87]. The MM was also obtained from an analysis of literature to find an average value of $0.0046 \text{ mol}/\text{m}^3$ [88]. The OCR of a single cell was found to be $1.40 \times 10^{-17} \text{ mol}/\text{cell}\cdot\text{s}$ [89]. The model can build off of the OCR value if the scaffold is assumed to be a perfect cylinder with a volume of 5.66 mm^3 and 1×10^6 cells seeded consistently throughout. The final OCR value for modelling was calculated to be $2.48 \times 10^{-}$

$\text{mol/m}^3 \cdot \text{s}$. The concentration at the inlet of the device was assumed to be 0.20 mol/m^3 to represent complete oxygen saturation in the liquid.

The fluid flow was assumed to be laminar after evaluating the geometry and flow rate of the chamber. The inlet velocity reflected a flow rate of 2 mL/min with a constant velocity since there are no geometric changes in the system and the flow rate is constant. The entire length of the model spans the length of 75 cm to reflect the length of a microscope slide. Scaffold stacks were placed 10 mm away from the exit, and each center point of the scaffold stacks are 10 mm apart from their respective center points. A full protocol for designing our COMSOL model can be seen in **Appendix G**.

Figure 27 describes the model that the team has designed for preliminary testing. The two-dimensional model captures a cross section through the center of one of the stacking sequences on a chip. Each chip has two rows of stacks, so the number of scaffolds represented in the model is doubled in practice. Although the number of scaffolds does not align, both rows of scaffolds should experience similar oxygen consumption gradients to their parallel counterparts. To further examine how oxygen consumption changes with chip design, **Figure 28** and **Figure 29** show how the models vary with increasing stack size and increasing numbers of stacks respectively.

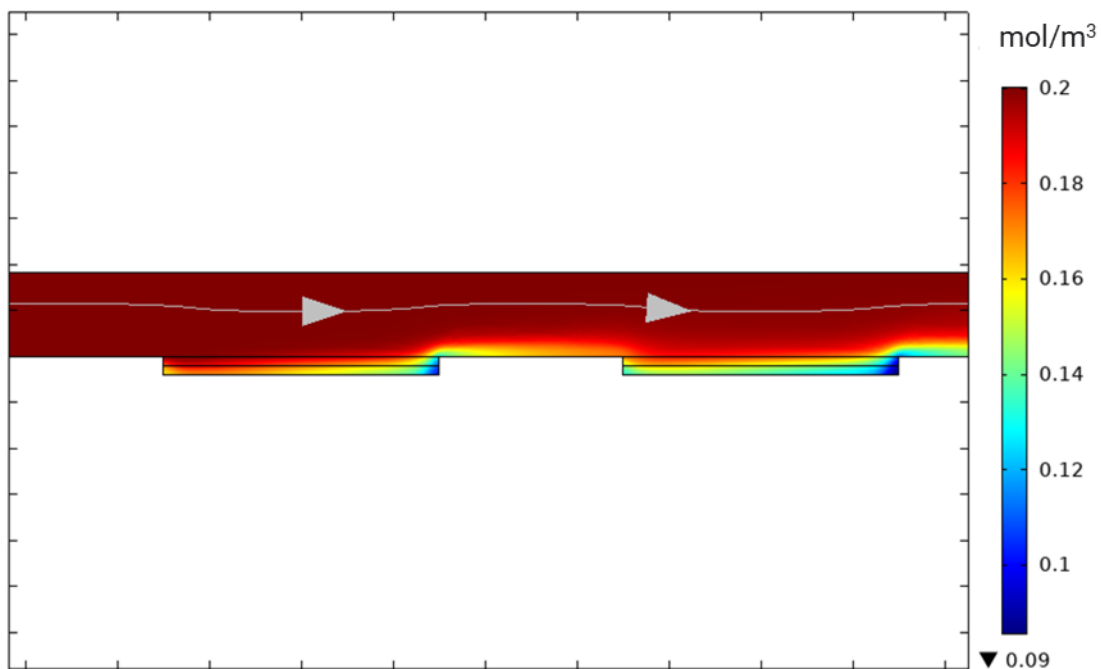


Figure 27. Oxygen Concentration Profile for the Design Validation Study

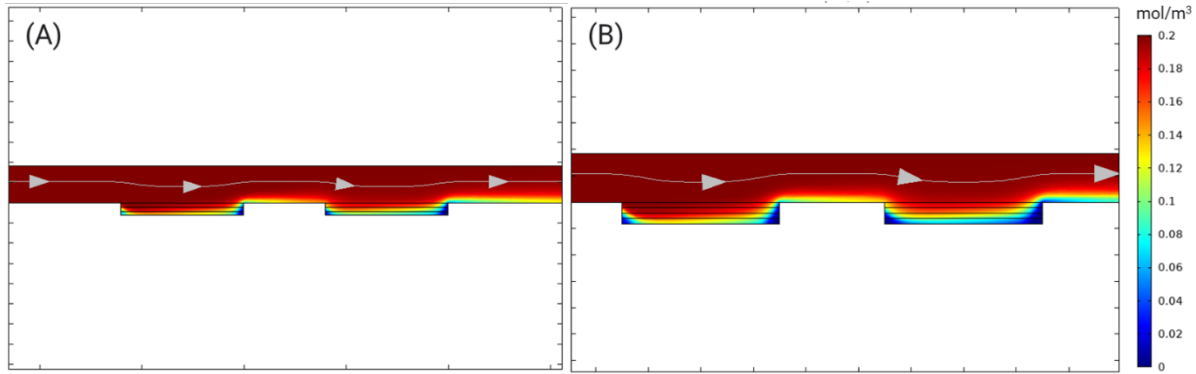


Figure 28. Oxygen Concentration Profile with Stacks of 3 (A) and Stacks of 4 (B)

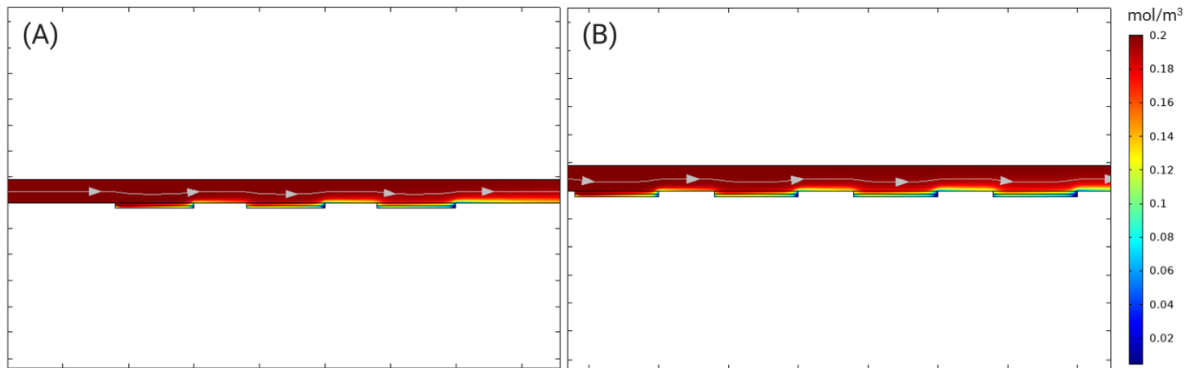


Figure 29. Oxygen Concentration Profile with 3 Stacks (A) and 4 Stacks (B)

6.2.2 DNA Quantification for Assessing Cell Sustainability

To quantify the DNA content in scaffolds, a PicoGreen assay was used. The DNA content is reported in micrograms, and this value correlates to the number of cells alive in a specific culture. Standard two-dimensional culture and cell-seeded scaffolds in a media suspension were used as controls in addition to stacked scaffolds prepared as per the Coburn Lab method. The experimental group consisted of four stacked scaffold models that had two scaffolds in each stack. These experimental stacks were secured in the chip and subjected to a constant flow rate of 2 mL/min for 3 days. Data was acquired and analyzed according to the protocol outlined in **Appendix H**. The average DNA content in each condition can be seen in **Figure 30**. The experimental stacked scaffolds were separated into scaffolds that were on the top layer and scaffolds on the bottom layer for data analysis. The scaffolds cultured according to the Coburn Lab method were separated into outer stacks and inner stacks for consistency. There were 6 replicates of the two-dimensional and three-dimensional controls. The Coburn Lab stacking method had 4 replicates each and the team's proposed method had three replicates each. A one-way ANOVA for comparison of means and the Tukey's Honest Significant Difference test was used to assess statistical significance between groups.

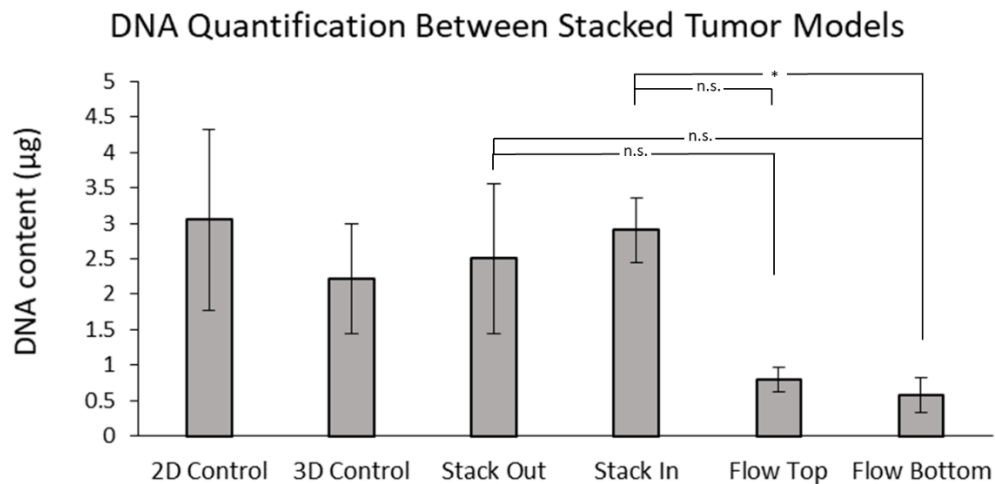


Figure 30. DNA Quantification Between Stacked Tumor Models.
Not Significant (n.s.), p<0.05 (*)

6.2.3 Cell Sustainability Histology

In addition to quantifying cell count, the cell distribution in the scaffolds was also observed. Harris hematoxylin and eosin (H&E) staining was used to stain the silk and the cell nuclei purple. The eosin stains the cytoplasm of cells a light pink. The Coburn lab stacked model with a stack of four scaffolds was observed and compared to the stacked model consisting of two scaffolds exposed to fluid flow in our design. The images can be seen in **Figure 31**. To obtain these images samples were frozen, cryosectioned, and stained according to the protocol in **Appendix I**.

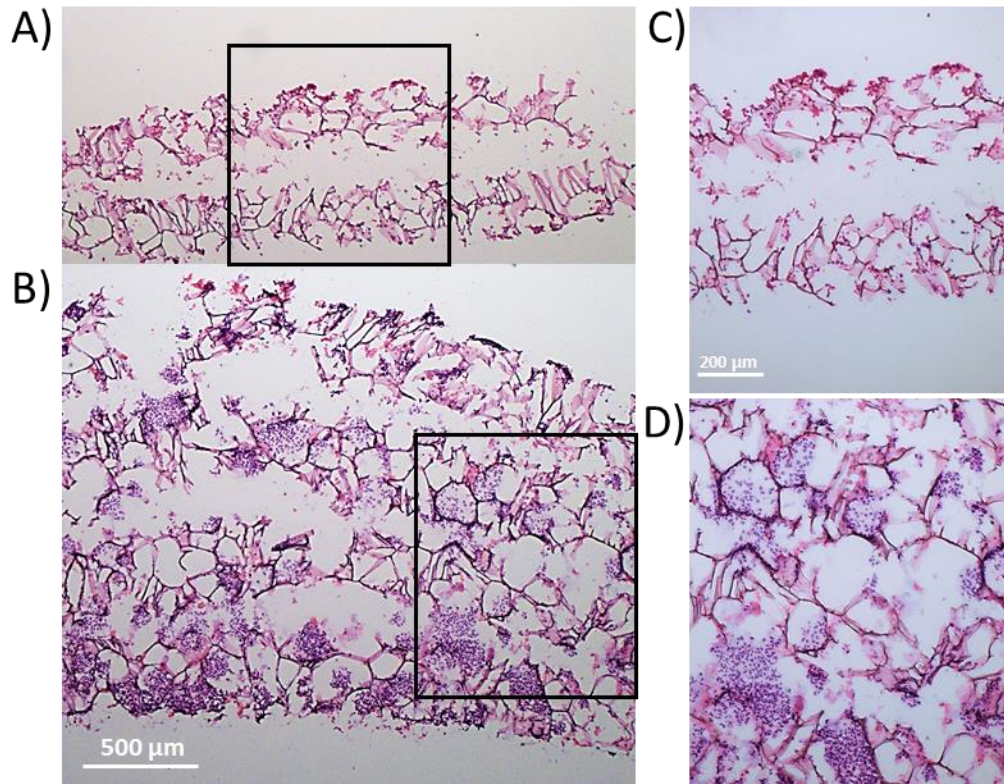


Figure 31. H&E Visualization Our Stacked Model (A) and the Coburn Lab Stacked Model (B). Enlarged Images for Each Stack are Seen in (C) and (D) Respectively

6.3 Industry Standards

The final design of this product took industry standards into account. Section 3.3, Standards and Lab-Specific Protocols describes the relevant standards that the team took into consideration when developing the bioreactor system.

6.4 Project Impact

The team considered how their project will contribute to medical research and the community at large. This subsection provides some analysis on the impact of this project.

6.4.1 Economic Impact

When made in bulk, the bioreactor device can cost about \$130 per device. While the team does not have any data available on the length of time the system can be used for, it is believed that with the amount of media and chemotherapeutics being saved makes it a cost-effective device. Considering the device is a closed system, it is believed that the device can reduce contamination as well, which saves researchers time through reducing failed experiments that need to be re-run. The impact of the tumor on a chip device would have a positive influence on the economy, particularly for those interested in research and drug efficacy testing.

6.4.2 Environmental Impact

While the bioreactor is made out of a thermoplastic, it will be able to be re-used, lessening the negative environmental impact as opposed to a single use device. Furthermore, the device will reduce the exposure harmful chemotherapeutics, which also provides better outcomes for the environment. This project works in conjunction with the metabolism of neuroblastoma to minimize waste products.

6.4.3 Societal Influence

This device will have limited social influence or impact on “ordinary” people; however, it may have impact on researchers or oncologists working to use drug efficacy testing in a scaffold to reduce cost and prevent any living animal or human from undergoing unnecessary testing. This alternative may prove to have many desirable characteristics for users. Production is currently limited to machining but could be scaled up in the future with appropriate resources, at which point more would be done to sell and market the device. Word of mouth and usage in WPI labs would likely help increase the societal influence.

6.4.4 Political Ramifications

The purpose of this device and creation of the device has few political ramifications as the project is not controversial. Assuming the scaffolds could be designed in an anatomically correct fashion, the device would reduce the ethical and cultural concerns of using living organisms for experimental research. The ease of use, the ability to save money, and reuse of the system makes it highly desirable and would contribute positive outcomes to the global market as well as international cultures, especially those which are concerned with scaling up research efforts in a sustainable manner.

6.4.5 Ethical Concerns

This project is an ethical option for drug efficacy testing. By using neuroblastoma cells directly in the device, there is no *in vivo* testing, which comes with many concerns. This device is intended to be high throughput, suggesting that research can be conducted faster and progress in novel treatments multiply. Not only will this project reduce poor outcomes for patients, but it will also increase options for patients with neuroblastoma. This disease presents itself in so many ways and this could serve as a tool to model individualized treatments (in future iterations of the project). This bioreactor was designed to make the scaffold stacking process and scaffold treatment process easier which in turn could expedite research initiatives leading to better and more satisfying lives for those directly impacted by research.

6.4.6 Health and Safety Concerns:

Public health will be influenced by this project by conducting research requiring minimal human contact as handling chemotherapeutics can be dangerous and may increase contamination risk. By containing the media and drugs in closed containers and a closed device, there will still be the possibility for diffusion of oxygen, however there will be less exposure to air. This will make the device safer for humans to touch and increase personal safety. This bioreactor will contribute to the development of more effective treatments for pediatric cancer patients.

6.4.7 Manufacturability

The device was created using PTFE, silicone, metal screw, luer locks, tubing, glass slides, and PDMS (in addition to the necessary pumps). The device is designed using SolidWorks and converted to an ESPRIT file in order to be machined. The team cut out the silicone using an X-Acto knife and the procedures for creating the plasma bonded glass-PDMS slides are outlined in earlier sections of this report. If someone else were to replicate this project, it should be easy to manufacture. All resources and protocols for machining our device is found in **Appendix J**.

6.4.8 Sustainability

Sustainable was not a large consideration when determining the outcome of this project. No renewable energy sources were utilized in the creation of this project, however designing a device that can be reused has a positive outcome for the environment. Currently, manufacturing is taking place in a machine shop which would have better impacts for the environment as opposed to a factory facility.

CHAPTER 7 – DISCUSSION

Three-dimensional tumor models provide a better platform to evaluate the efficacy of chemotherapeutics. However, limitations in throughput and user error negatively impact the current research using silk scaffolded neuroblastoma models. This project was able to successfully address both issues by increasing throughput and mitigating areas of user error. The project team was able to introduce more physiologically accurate conditions by integrating fluid flow. The team was also able to reduce the risk of system contamination by creating an easy-to-use device with larger components and utilizing a peristaltic pump for a closed system. Additionally, the team confirmed that scaffolds cultured in the new bioreactor have both visual cells present and quantifiable levels of DNA. Over the course of the cell study, the conservation of resources was confirmed by the reduction in media usage. These findings show that the team was able to fabricate and validate a functional bioreactor that improves upon the current lab methods for neuroblastoma tumor modeling.

7.1 Device Functionality

The cytotoxicity testing confirmed that the chosen materials for our device would be compatible for longtime exposure to cell culture. Images revealed that the only condition with visual cytotoxic effects was latex. The silicone condition interestingly showed cell growth on the material interface after 48 hours of culture. The quantified metabolic activity in terms of fluorescence also revealed no statistical significance among groups other than latex when compared to the negative control. This experiment provided validation for our materials, but it operates under the assumption that metabolic activity is directly proportional to cell sustainability and proliferative ability. This experiment is also limited on how consistently cells were seeded in each well. The team carefully calculated and concentrated the cell suspension prior to seeding and used microscopy to validate the results obtained from the assay. With the evidence provided, the team can confirm with confidence that the materials used in the device will not have any cytotoxic effects.

The functionality of the device was qualitatively assessed in a variety of conditions and pumping systems. The first functional tests assessed the device's capability to maintain constant flow without leaking with the use of a syringe pump. At first, leaks were present in three main locations being the threaded luer lock space, the connecting port for tubing, and the middle screws. Troubleshooting relieved the issues by ensuring the luer lock screws were tightly secured into the device, the tubing had a compatible inner diameter, and the flow rate did not result in pressures to overcome the seal of the silicone gasket. Once the leaking issues were resolved, a chip with silk scaffolds sandwiched between PDMS and a glass slide were applied to determine the ability to apply flow over the top of a stacked scaffold complex. This method resulted in issues with water penetration between the PDMS and glass slides. The team then looked to plasma bond the glass and PDMS together to avoid the issue of this issue in future iterations.

The plasma bonded PDMS was prepared to avoid the previous complications, and the next method for stacked scaffold placement would be to place scaffolds in cylindrical holes punched in the PDMS. Varying diameters and orientations were evaluated with a syringe pump. The 5 mm diameter was too small for scaffold placement, and the 7 mm diameter resulted in scaffold movement and possible issues with limiting fluid flow to the top surface of the stacks. The 6 mm

diameter condition was the best method, as two scaffolds were able to be secured in the PDMS with a 1 mm height. No leaks were observed in this system, but there was an issue of scaffold security after opening the device. Scaffolds appeared to float to the top of the fluid surface and relocate to different areas outside of the cylindrical holes. No scaffolds were found in other areas of the flow chamber, which gives the team reason to believe that this issue is caused by residual liquid in the system while taking the system apart. A possible solution to avoiding this issue is removing liquid from the scaffold culturing area prior to disassembly. This cannot be accomplished by a syringe pump, thus limiting the pumping system that the team can use.

Testing with a peristaltic pump required some troubleshooting to avoid the issue of dislodged scaffolds. The team concluded that scaffolds would not become dislodged if liquid was pushed to the uncultured side of the chip, and this was able to be accomplished by changing the direction of flow throughout the system. The peristaltic pump's direction was changed to allow for air circulation to push the majority of the media out of the system. This resulted in scaffolds to remain secure in their respective conditions of a chip design with four stacked scaffold complexes each containing two scaffolds for a total of eight. The final functional test in terms of functionality focused on longevity. The team wanted to confirm that all of the observations we had made are sustainable for media circulation lasting for 3 days. After three days there were no leaks reported. However, there was a much tighter seal than before, which complicated the disassembly of the device. This caused liquid movement in the chamber after clearing as much liquid as possible, which resulted in the dislodging of the scaffolds.

Finally, the surfaces of glass slides were evaluated for the presence of a PEG overlay. This was essential to the chip portion of the device to reduce the risk of cell migration and prevent cell adhesion to any material besides the scaffold. The Si:C ratio for the untreated glass compared to the PEGylated glass was significantly higher, which is a strong indicator of a PEG overlay on the surface. This attenuation of the silicon peak showed that a material on the surface (presumably PEG) was inhibiting the normal levels of silicon electrons from leaving the surface of the glass. Not only this, but there was a higher peak area ratio for the PEGylated glass for oxidized carbon: primary carbon. The reaction of PEG on the surface of materials results in an increase in oxidized carbon. This higher peak area ratio indicated that the team's PEGylated glass had elevated levels of oxidized carbon compared to untreated glass, further indicating the presence of PEG. The combination of these two results led to the team to believe that the PEGylation protocol was successful in creating a PEG overlay on the surface of the chip glass.

7.2 Modeling Capabilities

The COMSOL modeling indicated that oxygen gradients were achievable under the assumptions established by the team. Although the oxygen gradients are promising to achieve different oxygen concentrations with different stacking formations, the assumptions may limit the ability to accurately recreate these concentrations in practice. The concentration is assumed to be 0.20 mol/m^3 , which may be reduced if the media is not fully saturated with oxygen or if the surface area of the tubing is not great enough to allow for full gas exchange before the fluid recirculates through the device. Another limitation of this model is that it cannot model the oxygen consumption of parallel stacks since it is only a two-dimensional model. A three-dimensional model with more accurate oxygen diffusion characteristics could offer insight to oxygen

concentration profiles with higher accuracy for even more specific tumor microenvironment modeling.

To build off of the virtual simulation and physically validate our device, DNA quantification and histology was used to both quantitatively and qualitatively examine cell viability. The DNA quantification showed that the only scaffolds that were statistically different were inside stack scaffolds of the current model and the bottom scaffolds of the new system. The difference between the current design and the new system may be attributed to nutrient diffusion issues as a result of simplified models or variances in cell behavior when introduced to fluid flow. The fluid flow appears to have a minor effect on cell distribution, as more cells in the new system appear to be at the surface where fluid flow contacts the scaffolds. This may not be caused by fluid flow, but it does show some differences in the distribution. All conditions were able to show cells distributed throughout the stacks as well as DNA content in each scaffold to confirm that our device was successful in culturing cells for 3 days with fluid flow.

CHAPTER 8 – CONCLUSIONS AND RECOMMENDATIONS

8.1 Conclusions

Overall, the team was able to create a device that successfully secured and cultured cells over the course of three days. This included flow that mimicked in vivo fluid flow, and successful stacking. There was no contamination in the experimental run, and in terms of set up there was a reduction in the contact of various materials and human interaction with the scaffolds. Our device also incorporated larger components and screws, which made it easier to use. The team also reduced the media consumption in the system to conserve resources. Our device houses 4 models and used 17 mL of media in one cell study experimental run. This works out to 4.25 mL of media required per model. The standard protocol requires 8 mL of media for each model, so for four models is a required 32 mL of media. This is a 53% reduction in media. Lastly, since we machined multiple devices and each can house multiple models, the team created a potentially scalable system that has a higher throughput when compared to the standard protocol.

8.2 Recommendations

When conducting cytotoxicity testing, the team recommends using a plate shaker to ensure all the cells in each of the wells has equal contact to the material under test. The team noticed instances where the cells died when they were in direct contact with the material, but the rest of the cells were alive, which could impact fluorescence results.

The team also recommends purchasing stock material that is slightly larger than the actual dimensions necessary. During the machining process material is lost during initial stock cutting, smoothing out material imperfections, and the machine operations. Extra material ensures the device is large enough to evenly place the screws.

In the future, the team would like to improve the project by incorporating more detailed COMSOL modeling into the design. This would provide insight for cell viability given modified parameters such as nutrient or oxygen diffusion given the spacing and number of stacks within each device. Another goal would be to scale up the quantity of replicate studies being conducted in parallel by attaching multiple devices to the pump to speed up data collection. This provides opportunities to expand the scope of therapies and diseases this system could be applied to. Furthermore, altering the depths of the flow channel could allow for stacks with a greater number of scaffold layers to be used or the number of stacks on the chip.

This is beneficial as it would allow for additional stacks of scaffolds to evaluate. Altering these chambers may help to streamline the fabrication process as the current design uses very specific bits and the small wells take a long time to precisely machine. The team recommends finding a more streamlined way to machine the device, while using a durable thermoplastic makes the system readily autoclavable and biocompatible, it is difficult to fabricate given the available resources in the WPI Manufacturing Labs, also known as Washburn Shops. Furthermore, making the device smaller while still maintaining integrity and appropriate dimensions to achieve laminar flow would reduce costs and time to machine.

The team believes that a beneficial modification in future designs would be a way to easily manipulate the depths of the wells. This customization would ensure that the correct number of stacks and scaffolds per stack can be placed given the needs of an experiment. One way to aid in this customization would be to fabricate a mold for the PDMS out of silicone instead of PLA. This would not only help to make the change of depths easy to manipulate but would also aid in the removal of PDMS from the mold as it often sticks to the plastic.

All in all, the team believes the bioreactor device developed here can be used for drug testing to find curative treatments for neuroblastoma with less deleterious, long-term side effects to the patients.

REFERENCES

- [1] E.K. Barr, M.A. Applebaum, Genetic Predisposition to Neuroblastoma, *Children (Basel)* 5(9) (2018) 119.
- [2] A. Coulon, M. Flahaut, A. Mühlethaler-Mottet, R. Meier, J. Liberman, K. Balmas-Bourloud, K. Nardou, P. Yan, S. Tercier, J.-M. Joseph, L. Sommer, N. Gross, Functional Sphere Profiling Reveals the Complexity of Neuroblastoma Tumor-Initiating Cell Model, *Neoplasia (New York, N.Y.)* 13(10) (2011) 991-IN30.
- [3] P. Vinay, M. Sham, Research and Development Spending to Bring a Single Cancer Drug to Market and Revenues After Approval, *Archives of internal medicine (1960)* 177(11) (2017) 1569.
- [4] J. Hoarau-Véchet, A. Rafii, C. Touboul, J. Pasquier, Halfway between 2D and Animal Models: Are 3D Cultures the Ideal Tool to Study Cancer-Microenvironment Interactions?, *International journal of molecular sciences* 19(1) (2018) 181.
- [5] K.J. Ornell, K.S. Mistretta, E. Newman, C.Q. Ralston, J.M. Coburn, Three-Dimensional, Scaffolded Tumor Model to Study Cell-Driven Microenvironment Effects and Therapeutic Responses, *ACS biomaterials science & engineering* 5(12) (2019) 6742-6754.
- [6] A. Abbott, K. Bond, T. Chiba, S. Sims-Lucas, L. Oxburgh, J.M. Coburn, Development of a mechanically matched Silk Scaffolded 3D clear cell renal cell carcinoma model, *Materials Science and Engineering: C* (2021) 112141.
- [7] K.J. Ornell, K.S. Mistretta, C.Q. Ralston, J.M. Coburn, Development of a stacked, porous silk scaffold neuroblastoma model for investigating spatial differences in cell and drug responsiveness, *Biomaterials science* 9(4) (2021) 1272-1290.
- [8] R.L. Siegel, K.D. Miller, A. Jemal, *Cancer statistics, 2018*, CA: a cancer journal for clinicians 68(1) (2018) 7-30.
- [9] T. Teitz, J.J. Stanke, S. Federico, C.L. Bradley, R. Brennan, J. Zhang, M.D. Johnson, J. Sedlacik, M. Inoue, Z.M. Zhang, S. Frase, J.E. Rehg, C.M. Hillenbrand, D. Finkelstein, C. Calabrese, M.A. Dyer, J.M. Lahti, Preclinical models for neuroblastoma: establishing a baseline for treatment, *PloS one* 6(4) (2011) e19133-e19133.
- [10] S.M. Ries, J.G. Gurney, M. Linet, T. Tamra, J.L. Young, G.R. Bunin, *Cancer Incidence and Survival among Children and Adolescents: United States SEER Program 1975-1995*, National Cancer Institute, SEER Program. NIH Pub, Bethesda, MD, 1999.
- [11] C.A. Stiller, D.M. Parkin, International variations in the incidence of neuroblastoma, *International journal of cancer* 52(4) (1992).
- [12] J.M. Maris, M.D. Hogarty, R. Bagatell, S.L. Cohn, Neuroblastoma, *The Lancet (British edition)* 369(9579) (2007) 2106-2120.
- [13] L. Borriello, R.C. Seeger, S. Asgharzadeh, Y.A. DeClerck, More than the genes, the tumor microenvironment in neuroblastoma, *Cancer letters* 380(1) (2015) 304-314.
- [14] G. Courtois, T.D. Gilmore, Mutations in the NF- κ B signaling pathway: implications for human disease, *Oncogene* 25(51) (2006) 6831-6843.
- [15] F.R. Greten, L. Eckmann, T.F. Greten, J.M. Park, Z.W. Li, L.J. Egan, M.F. Kagnoff, M. Karin, IKK β Links Inflammation and Tumorigenesis in a Mouse Model of Colitis-Associated Cancer, *Cell (Cambridge)* 118(3) (2004) 285-296.
- [16] T.L. Whiteside, The tumor microenvironment and its role in promoting tumor growth, *Oncogene* 27(45) (2008) 5904-5912.

- [17] L. de Pontual, V. Raynal, V. Combaret, G. Pierron, J. Amiel, A. Ribeiro, J. Michon, S. Lyonnet, I. Janoueix-Lerosey, L. Brugières, D. Lequin, G. Schleiermacher, O. Delattre, A. Puisieux, D. Valteau-Couanet, T. Frebourg, Somatic and germline activating mutations of the ALK kinase receptor in neuroblastoma, *Nature (London)* 455(7215) (2008) 967-970.
- [18] G.M. Brodeur, Neuroblastoma: biological insights into a clinical enigma, *Nature reviews. Cancer* 3(3) (2003) 203-216.
- [19] G.M. Brodeur, R. Bagatell, Mechanisms of neuroblastoma regression, *Nature reviews. Clinical oncology* 11(12) (2014) 704-713.
- [20] M. Yoshimoto, S.R. Caminada de Toledo, E.M. Monteiro Caran, M.T. de Seixas, M.L. de Martino Lee, S. de Campos Vieira Abib, S.M.R. Vianna, S.T. Schettini, J. Anderson Duffles Andrade, MYCN Gene Amplification, *The American journal of pathology* 155(5) (1999) 1439-1443.
- [21] V.M. Weaver, C.D. Roskelley, Extracellular matrix: the central regulator of cell and tissue homeostasis, *Trends in cell biology* 7(1) (1997) 40-42.
- [22] D.A. Tweddle, A.D.J. Pearson, M. Haber, M.D. Norris, C. Xue, C. Flemming, J. Lunec, The p53 pathway and its inactivation in neuroblastoma, *Cancer Letters* 197(1) (2003) 93-98.
- [23] T. Van Maerken, J. Vandesompele, A. Rihani, A. De Paepe, F. Speleman, Escape from p53-mediated tumor surveillance in neuroblastoma: switching off the p14 -MDM2-p53 axis, *Cell death and differentiation* 16(12) (2009) 1563-1572.
- [24] K. Hiyama, M.A. Piatyszek, J.W. Shay, E. Hiyama, Y. Matsuura, T. Yokoyama, Correlating telomerase activity levels with human neuroblastoma outcomes, *Nature medicine* 1(3) (1995) 249-255.
- [25] K.B. Challagundla, P.M. Wise, P. Neviani, H. Chava, M. Murtadha, T. Xu, R. Kennedy, C. Ivan, X. Zhang, I. Vannini, F. Fanini, D. Amadori, G.A. Calin, M. Hadjidaniel, H. Shimada, A. Jong, R.C. Seeger, S. Asgharzadeh, A. Goldkorn, M. Fabbri, Exosome-mediated transfer of microRNAs within the tumor microenvironment and neuroblastoma resistance to chemotherapy, *JNCI : Journal of the National Cancer Institute* 107(7) (2015).
- [26] A.J. Carlisle, C.A. Lyttle, R.Y. Carlisle, J.M. Maris, CXCR4 expression heterogeneity in neuroblastoma cells due to ligand-independent regulation, *Molecular cancer* 8(1) (2009) 126-126.
- [27] A. Chlenski, S. Liu, S.L. Cohn, The regulation of angiogenesis in neuroblastoma, *Cancer letters* 197(1) (2003) 47-52.
- [28] T. Teitz, J.M. Lahti, V.J. Kidd, Aggressive childhood neuroblastomas do not express caspase-8: an important component of programmed cell death, *Journal of molecular medicine (Berlin, Germany)* 79(8) (2001) 428-436.
- [29] S. Barbero, A. Mielgo, V. Torres, T. Teitz, D.J. Shields, D. Mikolon, M. Bogyo, D. Barilà, J.M. Lahti, D. Schlaepfer, D.G. Stupack, Caspase-8 association with the focal adhesion complex promotes tumor cell migration and metastasis, *Cancer research (Chicago, Ill.)* 69(9) (2009) 3755-3763.
- [30] L.A. Lampson, C.A. Fisher, J.P. Whelan, Striking paucity of HLA-A, B, C and beta 2-microglobulin on human neuroblastoma cell lines, *The Journal of immunology* (1950) 130(5) (1983) 2471.
- [31] J. Navrátilová, T. Hankeová, P. Beneš, J. Smarda, Low-glucose conditions of tumor microenvironment enhance cytotoxicity of tetrathiomolybdate to neuroblastoma cells, *Nutrition and cancer* 65(5) (2013).

- [32] G.V.H. Matthew, C.C. Lewis, B.T. Craig, Understanding the Warburg Effect: The Metabolic Requirements of Cell Proliferation, *Science (American Association for the Advancement of Science)* 324(5930) (2009) 1029-1033.
- [33] B. de Bernardi, V. Mosseri, H. Rubie, V. Castel, A. Foot, R. Ladenstein, G. Laureys, M. Beck-Popovic, A.F. de Lacerda, A.D.J. Pearson, J. de Kraker, P.F. Ambros, Y. de Rycke, M. Conte, P. Bruzzi, J. Michon, Treatment of localised resectable neuroblastoma. Results of the LNESG1 study by the SIOP Europe Neuroblastoma Group, *British journal of cancer* 99(7) (2008) 1027-1033.
- [34] D.L. Baker, M.L. Schmidt, S.L. Cohn, J.M. Maris, W.B. London, A. Buxton, D. Stram, R.P. Castleberry, H. Shimada, A. Sandler, R.C. Shamberger, A.T. Look, C.P. Reynolds, R.C. Seeger, K.K. Matthay, Outcome after Reduced Chemotherapy for Intermediate-Risk Neuroblastoma, *The New England journal of medicine* 363(14) (2010) 1313-1323.
- [35] N.R. Pinto, M.A. Applebaum, S.L. Volchenboum, K.K. Matthay, W.B. London, P.F. Ambros, A. Nakagawara, F. Berthold, G. Schleiermacher, J.R. Park, D. Valteau-Couanet, A.D.J. Pearson, S.L. Cohn, Advances in Risk Classification and Treatment Strategies for Neuroblastoma, *Journal of clinical oncology* 33(27) (2015) 3008-3017.
- [36] M. Clinic, Neuroblastoma - Diagnosis and treatment, 2019.
<https://www.mayoclinic.org/diseases-conditions/neuroblastoma/diagnosis-treatment/drc-20351022>.
- [37] A. Mazloom, C.U. Louis, J. Nuchtern, E. Kim, H. Russell, W. Allen-Rhoades, R. Krance, A.C. Paulino, Radiation Therapy to the Primary and Postinduction Chemotherapy MIBG-Avid Sites in High-Risk Neuroblastoma, *International journal of radiation oncology, biology, physics* 90(4) (2014) 858-862.
- [38] M. Kapałczyńska, T. Kolenda, W. Przybyła, M. Zajączkowska, A. Teresiak, V. Filas, M. Ibbs, R. Bliźniak, Ł. Łuczewski, K. Lamperska, 2D and 3D cell cultures - a comparison of different types of cancer cell cultures, *Archives of medical science* 14(4) (2018) 910-919.
- [39] K.J. Ornell, J.M. Coburn, Developing preclinical models of neuroblastoma: driving therapeutic testing, *BMC biomedical engineering* 1(1) (2019) 33-33.
- [40] O. Hashimoto, M. Yoshida, Y.-i. Koma, T. Yanai, D. Hasegawa, Y. Kosaka, N. Nishimura, H. Yokozaki, Collaboration of cancer-associated fibroblasts and tumour-associated macrophages for neuroblastoma development: The role of non-tumour stromal cells in neuroblastoma progression, *The Journal of pathology* 240(2) (2016) 211-223.
- [41] M. Terme, M. Dorvillius, D. Cochonneau, T. Chaumette, W. Xiao, Chimeric Antibody c.8B6 to O-Acetyl-GD2 Mediates the Same Efficient Anti-Neuroblastoma Effects as Therapeutic ch14.18 Antibody to GD2 without Antibody Induced Allodynia (vol 9, e87210, 2014), *PloS one* 9(7) (2014).
- [42] N. Baek, O.W. Seo, M. Kim, J. Hulme, S.S.A. An, Monitoring the effects of doxorubicin on 3D-spheroid tumor cells in real-time, *OncoTargets and therapy* 9 (2016) 7207-7218.
- [43] H.R. Kumar, X. Zhong, D.J. Hoelz, F.J. Rescorla, R.J. Hickey, L.H. Malkas, J.A. Sandoval, Three-dimensional neuroblastoma cell culture: proteomic analysis between monolayer and multicellular tumor spheroids, *Pediatric surgery international* 24(11) (2008) 1229-1234.
- [44] G.K. Gransbury, P. Kappen, C.J. Glover, J.N. Hughes, A. Levina, P.A. Lay, I.F. Musgrave, H.H. Harris, Comparison of KP1019 and NAMI-A in tumour-mimetic environments, *Metallomics* 8(8) (2016) 762-773.

- [45] M.E. Carnes, G.D. Pins, Etching anisotropic surface topography onto fibrin microthread scaffolds for guiding myoblast alignment, *Journal of biomedical materials research. Part B, Applied biomaterials* 108(5) (2020) 2308-2319.
- [46] S.A. Langhans, Three-dimensional in vitro cell culture models in drug discovery and drug repositioning, *Frontiers in pharmacology* 9 (2018) 6-6.
- [47] K.M. Park, D. Lewis, S. Gerecht, Bioinspired Hydrogels to Engineer Cancer Microenvironments, *Annual review of biomedical engineering* 19(1) (2017) 109-133.
- [48] E. Monferrer, S. Martin-Vano, A. Carretero, A. Garcia-Lizarribar, R. Burgos-Panadero, S. Navarro, J. Samitier, R. Noguera, A three-dimensional bioprinted model to evaluate the effect of stiffness on neuroblastoma cell cluster dynamics and behavior, *Scientific reports* 10(1) (2020) 6370-6370.
- [49] A. Marrella, A. Dondero, M. Aiello, B. Casu, D. Olive, S. Regis, C. Bottino, D. Pende, R. Meazza, G. Caluori, R. Castriconi, S. Scaglione, Cell-Laden Hydrogel as a Clinical-Relevant 3D Model for Analyzing Neuroblastoma Growth, Immunophenotype, and Susceptibility to Therapies, *Frontiers in immunology* 10 (2019) 1876-1876.
- [50] J. Kazantseva, R. Ivanov, M. Gasik, T. Neuman, I. Hussainova, Graphene-Augmented Nanofiber Scaffolds Trigger Gene Expression Switching of Four Cancer Cell Types, *ACS biomaterials science & engineering* 4(5) (2018) 1622-1629.
- [51] M. Mitra, C. Mohanty, A. Harilal, U.K. Maheswari, S.K. Sahoo, S. Krishnakumar, A novel in vitro three-dimensional retinoblastoma model for evaluating chemotherapeutic drugs, *Molecular vision* 18 (2012) 1361-1378.
- [52] G. Vunjak-Novakovic, M. Radisic, Cell Seeding of Polymer Scaffolds, in: A.P. Hollander, P.V. Hatton (Eds.), *Biopolymer Methods in Tissue Engineering*, Humana Press, Totowa, NJ, 2004, pp. 131-145.
- [53] X. Xin, H. Yang, F. Zhang, S.-T. Yang, 3D cell coculture tumor model: A promising approach for future cancer drug discovery, *Process biochemistry* (1991) 78 (2019) 148-160.
- [54] A.R. Murphy, D.L. Kaplan, Biomedical applications of chemically-modified silk fibroin, *Journal of materials chemistry* 19(36) (2009) 6443-6450.
- [55] Y. Qi, H. Wang, K. Wei, Y. Yang, R.-Y. Zheng, I.S. Kim, K.-Q. Zhang, A review of structure construction of silk fibroin biomaterials from single structures to multi-level structures, *International journal of molecular sciences* 18(3) (2017) 237.
- [56] N. Thang Phan, N. Quang Vinh, N. Van-Huy, L. Thu-Ha, H. Vu Quynh Nga, D.-V.N. Vo, T. Quang Thang, S.Y. Kim, L. Quyet Van, Silk Fibroin-Based Biomaterials for Biomedical Applications: A Review, *Polymers* 11(12) (2019) 1933.
- [57] X. Wang, J.A. Kluge, G.G. Leisk, D.L. Kaplan, Sonication-induced gelation of silk fibroin for cell encapsulation, *Biomaterials* 29(8) (2007) 1054-1064.
- [58] E. Dondajewska, W. Juzwa, A. Mackiewicz, H. Dams-Kozłowska, Heterotypic breast cancer model based on a silk fibroin scaffold to study the tumor microenvironment, *Oncotarget* 9(4) (2018) 4935-4950.
- [59] G. Trujillo-de Santiago, B.G. Flores-Garza, J.A. Tavares-Negrete, I.M. Lara-Mayorga, I. González-Gamboa, Y.S. Zhang, A. Rojas-Martínez, R. Ortiz-López, M.M. Álvarez, The Tumor-on-Chip: Recent Advances in the Development of Microfluidic Systems to Recapitulate the Physiology of Solid Tumors, *Materials* 12(18) (2019) 2945.
- [60] J.J. Heys, N. Holyoak, A.M. Calleja, M. Belohlavek, H.P. Chaliki, Revisiting the simplified bernoulli equation, *The open biomedical engineering journal* 4(1) (2010) 123-128.
- [61] O. Ali, Chapter 1 - Fluid Mechanics and Biofluids Principles, Elsevier Inc, 2016, pp. 1-60.

- [62] Elveflow, *Microfluidics and Microfluidic Devices: A Review*, 2021. <https://www.elveflow.com/microfluidic-reviews/general-microfluidics/microfluidics-and-microfluidic-device-a-review/>. (2020).
- [63] C.F. Carlborg, T. Haraldsson, K. Öberg, M. Malkoch, W. Van Der Wijngaart, Beyond PDMS: Off-stoichiometry thiol-ene (OSTE) based soft lithography for rapid prototyping of microfluidic devices, *Lab on a chip* 11(18) (2011) 3136-3147.
- [64] P.J. Hung, P.J. Lee, P. Sabounchi, R. Lin, L.P. Lee, Continuous perfusion microfluidic cell culture array for high-throughput cell-based assays, *Biotechnology and bioengineering* 89(1) (2005) 1-8.
- [65] C.W. Chang, Y.J. Cheng, M. Tu, Y.H. Chen, C.C. Peng, W.H. Liao, Y.C. Tung, A polydimethylsiloxane-polycarbonate hybrid microfluidic device capable of generating perpendicular chemical and oxygen gradients for cell culture studies, *Lab on a chip* 14(19) (2014) 3762-3772.
- [66] C. Matellan, A.E. Del Río Hernández, Cost-effective rapid prototyping and assembly of poly(methyl methacrylate) microfluidic devices, *Scientific reports* 8(1) (2018) 6971-13.
- [67] V. Faustino, S.O. Catarino, R. Lima, G. Minas, Biomedical microfluidic devices by using low-cost fabrication techniques: A review, *Journal of biomechanics* 49(11) (2015) 2280-2292.
- [68] S.B. Campbell, Q. Wu, J. Yazbeck, C. Liu, S. Okhovatian, M. Radisic, Beyond Polydimethylsiloxane: Alternative Materials for Fabrication of Organ-on-a-Chip Devices and Microphysiological Systems, *ACS biomaterials science & engineering* (2020).
- [69] F.M. Veronese, A. Mero, The Impact of PEGylation on Biological Therapies, *BioDrugs : clinical immunotherapeutics, biopharmaceuticals, and gene therapy* 22(5) (2008) 315-329.
- [70] C. Zhang, S. Hekmatfar, A. Ramanathan, N.W. Karuri, PEGylated human plasma fibronectin is proteolytically stable, supports cell adhesion, cell migration, focal adhesion assembly, and fibronectin fibrillogenesis, *Biotechnology progress* 29(2) (2013) 493-504.
- [71] C.F. Buchanan, S.S. Verbridge, P.P. Vlachos, M.N. Rylander, Flow shear stress regulates endothelial barrier function and expression of angiogenic factors in a 3D microfluidic tumor vascular model, *Cell adhesion & migration* 8(5) (2014) 517-524.
- [72] J.A. Tom, B. Alex, D. Alexis, F. Andrea, G. Maggie, H. Seichi, S.M. William, R.P. Jim, R. David, S. Giovanna, T. Esa-Pekka, V. Jos, S.V. Francesco, Scientific basis of ISO standards on biomechanical risk factors, *Scandinavian journal of work, environment & health* 44(3) (2018) 323-329.
- [73] ISO 11737-2:2009, 2009. <https://www.iso.org/standard/44955.html>. (2021).
- [74] ISO 14937:2009, 2020. <https://www.iso.org/standard/44954.html>. (2021).
- [75] ISO 10993-1:2018(en), Biological evaluation of medical devices” Part 1: Evaluation and testing within a risk management process, 2018. <https://www.iso.org/obp/ui#iso:std:iso:10993:-1:ed-5:v2:en>. (2021).
- [76] @US_FDA, How to Determine if Your Product is a Medical Device | FDA, (2021).
- [77] ISO 13485:2016, 2020. <https://www.iso.org/standard/59752.html>. (2021).
- [78] ISO 20069:2019, 2019. <https://www.iso.org/standard/59752.html>. (2021).
- [79] ISO 13408-1:2008, 2017. <https://www.iso.org/cms/render/live/en/sites/isoorg/contents/data/standard/03/78/37842.html>. (2021).
- [80] ISO 24998:2008, 2017. <https://www.iso.org/standard/42736.html>. (2021).
- [81] ISO 20391-2:2019, 2019. <https://www.iso.org/standard/67892.html>. (2021).

- [82] D.N. Rockwood, R.C. Preda, T. Yücel, X. Wang, M.L. Lovett, D.L. Kaplan, Materials fabrication from *Bombyx mori* silk fibroin, *Nature protocols* 6(10) (2011) 1612.
- [83] E. Fröhlich, G. Bonstingl, A. Höfler, C. Meindl, G. Leitinger, T.R. Pieber, E. Roblegg, Comparison of two in vitro systems to assess cellular effects of nanoparticles-containing aerosols, *Toxicology in vitro* 27(1) (2013) 409-417.
- [84] P.M. Hinderliter, K.R. Minard, G. Orr, W.B. Chrisler, B.D. Thrall, J.G. Pounds, J.G. Teeguarden, ISDD: A computational model of particle sedimentation, diffusion and target cell dosimetry for in vitro toxicity studies, *Particle and fibre toxicology* 7(1) (2010) 36-36.
- [85] Y.X. Wang, C. Xiang, B. Liu, Y. Zhu, Y. Luan, S.T. Liu, K.R. Qin, A multi-component parallel-plate flow chamber system for studying the effect of exercise-induced wall shear stress on endothelial cells, *Biomedical engineering online* 15(Suppl 2) (2016) 154-154.
- [86] K. Ziolkowska, E. Jedrych, R. Kwapiszewski, J. Lopacinska, M. Skolimowski, M. Chudy, PDMS/glass microfluidic cell culture system for cytotoxicity tests and cells passage, *Sensors and actuators. B, Chemical* 145(1) (2010) 533-542.
- [87] P. Han, D.M. Bartels, Temperature Dependence of Oxygen Diffusion in H₂O and D₂O, *Journal of physical chemistry* (1952) 100(13) (1996) 5597-5602.
- [88] M. Astolfi, B. Péant, M.A. Lateef, N. Rousset, J. Kendall-Dupont, E. Carmona, F. Monet, F. Saad, D. Provencher, A.M. Mes-Masson, T. Gervais, Micro-dissected tumor tissues on chip: an ex vivo method for drug testing and personalized therapy, *Lab on a chip* 16(2) (2016) 312-325.
- [89] J.J. Casciari, S.V. Sotirchos, R.M. Sutherland, Mathematical modelling of microenvironment and growth in EMT6/Ro multicellular tumour spheroids, *Cell proliferation* 25(1) (1992) 1-22.

APPENDIX

Appendix A: PEGylation Protocol

PEG Coating Protocol

1. Dip glass slides in Piranha Solution (Sulfuric Acid and Hydrogen Peroxide) to remove organic material per lab specific protocol.
 - a. Piranha solution is a 2:1 ratio of concentrated sulfuric acid and concentrated hydrogen peroxide.
2. Rinse slides with DI water and leave to dry overnight.
3. Right before use, prepare 0.5% PEG in Ethanol with 1% Acetic Acid, e.g., 5mg of PEG-Silane in 1mL of Ethanol and 10uL of Acetic Acid.
4. Drop 50uL onto the middle of a slide and take another slide and drop it on top of the drop to spread the PEG solution and coat two pieces at a time.
5. Place the slide/PEG solution sandwich at 70 degrees C for ~30minutes.
6. Immerse the slides/slips in DI water. Separate the glass slides underwater.
7. Rinse 2-3 times with DI water by dipping.
8. Dry and use.

Appendix B: Resazurin Assay Protocol

Schedule:

Day -1: Wednesday (2/17) – 11 am CE
plate cells (~2 hours)

Day 0: Thursday (2/18) – 12 pm CES
image cells and add materials (~2 hours)

Day 1: Friday (2/19) – 10:30 am CES
image cells, create resazurin mixture and add to cells (~2 hours)
~3/4 pm
spectroscopy (~1.5 hours)

Day 2: Saturday (2/20) – 10:30am CES
image cells, create resazurin mixture and add to cells (~2 hrs)
~3/4 pm
spectroscopy (~1.5 hours)

Materials:

- No materials just cells (Just Cells) - 1 row, 3 wells for each timepoint
 - 6 wells
- Standard PDMS (St PDMS) - 1 row, 3 wells for each timepoint
 - 6 wells
- PLA made PDMS (PLA PDMS) - 1 row, 3 wells for each timepoint
 - 6 wells
- PLA (PLA) - 1 row, 3 wells for each timepoint
 - 6 wells
- Silicone (Silicone) - 1 row, 3 wells for each timepoint
 - 6 wells
- Latex (Latex) - 1 row, 3 wells for each timepoint
 - 6 wells

Well-Plate Layout:

24 Hour Time Point: Need 2 well plate total

Just Cells	Standard PDMS	PLA made PDMS	Silicone
Just Cells	Standard PDMS	PLA made PDMS	Silicone
Just Cells	Standard PDMS	PLA made PDMS	Silicone

Latex	PLA	Empty	Empty
Latex	PLA	Empty	Empty
Latex	PLA	Empty	Empty

48 Hour Time Point: Need 2 more well plates

Just Cells	Standard PDMS	PLA made PDMS	Silicone
Just Cells	Standard PDMS	PLA made PDMS	Silicone
Just Cells	Standard PDMS	PLA made PDMS	Silicone

Latex	PLA	Empty	Empty
Latex	PLA	Empty	Empty
Latex	PLA	Empty	Empty

Seeding Cells:

- Cells seeded on day –1
- Four twelve-well plates were prepared with 5.0×10^4 (50k) cells seeded per well and 2 mL of culture medium in each well.
 - Following the plate layouts above

Microscopy:

- Images taken on Day 0, Day 1, and Day 2
- We will image each well on the best objective
 - We will note which objective we use and keep it consistent throughout the experiment
- After analysis, we will use the same objective to image a scalebar and apply scalebars with Image J Analysis

Resazurin:

Assays run on Day 1, and Day 2

1. Make working solution of resazurin (filtered, with PBS to dilute)
 - a. 10x down to 1x in PBS from stock to working
2. Add media to make a media/res stock solution
 - a. This is a 1:5 dilution with working stock to medium
 - b. should have at least 10 mL more than you'll need for all the wells
3. Remove the plate you're doing the assay on from the incubator
4. Aspirate (with a pipette and pipette assist, *NOT the vacuum connect*) the media from the wells
 - a. NOTE: use one pipette for each category (i.e. one to aspirate all of the latex)
5. Add 0.5 mL of the media/res stock solution to each well
6. Save the extra media/res stock solution to use for the analysis
7. Incubate for three hours then remove from the incubator for transfer of analyte on the benchtop
8. Collect 100 μ L four times from each sample and transfer to a blackplate
 - a. The layout can be seen following the protocol
9. Read the fluorescence with the lab protocol
10. Wash and dry the blackplates after use

Black Plate Layout										
Just Cells 1	Just Cells 2	Just Cells 3	StPDMS 1	StPDMS 2	StPDMS 3	PLA PDMS 1	PLA PDMS 2	PLA PDMS 3	Media/Res Stock	Media/Res Stock
Just Cells 1	Just Cells 2	Just Cells 3	StPDMS 1	StPDMS 2	StPDMS 3	PLA PDMS 1	PLA PDMS 2	PLA PDMS 3	Media/Res Stock	Media/Res Stock
Just Cells 1	Just Cells 2	Just Cells 3	StPDMS 1	StPDMS 2	StPDMS 3	PLA PDMS 1	PLA PDMS 2	PLA PDMS 3	Media/Res Stock	Media/Res Stock
Just Cells 1	Just Cells 2	Just Cells 3	StPDMS 1	StPDMS 2	StPDMS 3	PLA PDMS 1	PLA PDMS 2	PLA PDMS 3	Media/Res Stock	Media/Res Stock
Silicone 1	Silicone 2	Silicone 3	Latex 1	Latex 2	Latex 3	PLA 1	PLA 2	PLA 3	Media/Res Stock	Media/Res Stock
Silicone 1	Silicone 2	Silicone 3	Latex 1	Latex 2	Latex 3	PLA 1	PLA 2	PLA 3	Media/Res Stock	Media/Res Stock
Silicone 1	Silicone 2	Silicone 3	Latex 1	Latex 2	Latex 3	PLA 1	PLA 2	PLA 3	Media/Res Stock	Media/Res Stock
Silicone 1	Silicone 2	Silicone 3	Latex 1	Latex 2	Latex 3	PLA 1	PLA 2	PLA 3	Media/Res Stock	Media/Res Stock

Appendix C: Plasma Bonding Protocol

Plasma bonding uses neutral gas and a strong magnetic field to activate the surface hydrophobic materials in order to increase the adhesion potential of the material.

In order to utilize the plasma bonder in Gateway the team first created their PDMS using their PLA mold. Working on a clean surface, the team punched holes on the PDMS with a six-millimeter biopsy punch in the areas where they wanted to place silk scaffold stacks. These small, circular punched holes were then used as a stencil on the glass slide to prevent any plasma treatment from reaching the surface that scaffolds would be placed on. To do this, the cut PDMS was laid on the glass and the holes filled back in. The outer PDMS layer was then removed for treatment. The team then plasma bonded the PDMS (with holes) and a glass slide of the same size that had been thoroughly cleaned with piranha solution and PEGylated. In order to plasma treat the surface, the team used the instructions posted on the machine. The materials were exposed to the plasma treatment for 45 seconds before carefully being removed and stacked, after the PDMS stencil disks had been removed. The tops of each material were put in contact with each other to optimize the bonding potential and light pressure was applied for about a minute. When the chip (glass plus PDMS) was adhered to each other, the team then put the chips in a 60-degree Celsius oven for about 10 min to ensure the seal was held tight.

Appendix D: XPS Analysis

The process of X-ray Photoelectron Spectroscopy starts with an aluminum anode. This anode creates aluminum K-alpha X-rays. The X-rays are then sent to a monochromator, which selectively directs a specific wavelength of X-rays onto the sample. When the rays hit the sample, they interact with the surface of the sample only. This is usually between 5 and 10 nm deep. They also interact with core-level electrons in the atoms on the surface. This excites the electrons enough that photoelectrons from the atoms leave the material. A hemispherical analyzer directs the photoelectrons towards a detector, which then measures the kinetic energy and location of the photoelectron. This kinetic energy and location can be directly translated to the binding energy of the electron to the atom, which tells us what atoms are present on the surface. Researchers are able to make the distinction on which atom is present based on known binding energies, often already established in a reference. The Grimm laboratory website offered a detailed catalog of reference spectra at <http://grimmgroup.net/research/xps/referencespectra/> . More detailed background can be found at the Grimm lab website: <http://grimmgroup.net/research/xps/background/>

Once the raw data is collected from the XPS, the team utilized CasaXPS in order to conduct baseline and peak fitting. This allowed for peak area ratios to be calculated so that the team could quantify differences in the treated versus untreated glass.

Appendix E: Sterilization Techniques

Component	Sterilization Technique
PTFE Flow Chamber	Autoclave
Silicone Gasket	Autoclave
Screws	Autoclave
Washers	Autoclave
Allen Wrench	Autoclave
Forceps	Autoclave
Media Reservoir	Autoclave
Media Reservoir Cap	Autoclave
Chip	Autoclave
Peristaltic Pump Tubing	70% Ethylene Oxide
Silicone Tubing	70% Ethylene Oxide
Tubing Connectors	70% Ethylene Oxide
Luer Locks	70% Ethylene Oxide

Appendix F: Device User Manual

<i>Worcester Polytechnic Institute</i>	
<i>Biomedical Engineering Department - Coburn Lab</i>	
<i>Standard Operating Procedure No. 1</i>	
Title: Set-up of Fluidic Bioreactor for Neuroblastoma Tumor Models	

1. Purpose

1.1 The purpose of this procedure is to set up the fluidic bioreactor to prepare it for a cell study.

2. Responsibility

2.1 Operators:

- 2.1.1 Follow this document as written.
- 2.1.2 Record all information in the proper forms.

3. Equipment and Materials

- 3.1 PTFE Fluid Chamber
- 3.2 Silicone Gasket
- 3.3 (6X) ¼-20 inch screws
- 3.4 (6X) ¼ inch washers
- 3.5 Chip component
- 3.6 (2X) Forceps
- 3.7 20 mL glass vial
- 3.8 Silicone vial stopper with two ⅛ inch holes punched in the top
- 3.9 Watson Marlow pump specific tubing section
- 3.10 (2X) 1 ft 1/16 in ID silicone tubing
- 3.11 (2X) Female luer to ¼-28 screw tubing adaptor
- 3.12 (2X) Male luer to 1/16 inch barb tubing adaptor
- 3.13 ⅛ in ID to 1/16 inch ID tubing adaptor
- 3.14 Allen Wrench
- 3.15 (8X) 6mm diameter silk fibroin scaffolds seeded with SK-N-AS cells
- 3.16 Watson Marlow peristaltic pump
- 3.17 Sharpie or hydrophobic pen
- 3.18 100 mL beaker
- 3.19 17 mL SK-N-AS cell media
- 3.20 25 mL pipette
- 3.21 Pipette assist device

4. Definitions

4.1 N/A

5. Safety / Caution Statements

5.1 N/A

6. Procedures

6.1 Place every material except for the peristaltic pump and 6mm diameter silk fibroin scaffolds seeded with SK-N-AS cells into a clean biosafety cabinet.

6.1.1 NOTE: All of these materials should be appropriately sterilized prior to experiment.

6.2 Assemble tubing and connections.

6.2.1 Place one end of the Watson Marlow pump tubing section into one hole of the silicone vial stopper and pull 1.5 inches through. A pair of forceps may be needed to assist in placing the tubing.

(Reference Image in Attachment 1)

6.2.2 At the other end of the Watson Marlow pump tubing, insert the 1/8 inch end of the 1/8 in ID to 1/16 inch ID tubing adaptor.

6.2.3 Attach one of the 1 ft 1/16 in ID silicone tubing sections to the open end of the 1/8 in ID to 1/16 inch ID tubing adaptor.

6.2.4 To the open end of the 1/16 in ID silicone tubing section, insert the barb of the male luer to 1/16 inch barb tubing adaptor

6.2.5 To the open male luer lock, attach the corresponding female side of the female luer to 1/4-28 screw tubing adaptor.

6.2.6 Place one end of the other 1 ft 1/16 inch ID silicone tubing into the remaining hole of the silicone vial stopper and pull 1/2 inches through.

6.2.7 To the open end of the 1/16 inch ID silicone tubing section, insert the barb of the second male luer to 1/16 inch barb tubing adapter.

6.2.8 To the open male luer lock, attach the second corresponding female side of the female luer to 1/4-28 screw tubing adapter.

(Reference Image in Attachment 2)

6.3 Assemble media reservoir.

6.3.1 Take the 20mL glass vial and place it underneath the bottom silicone vial stopper.

6.3.1.1 Using forceps readjust the length of the tubing so that the section that is pulled 1.5 inches down from the silicone vial stopper hovers just above the bottom of the glass vial.

6.3.2 Using the 25mL pipette and the pipette assist device, aliquot 17mL of SK-N-AS cell media into the glass vial.

6.3.3 Place the vial stopper back on the top of the glass vial and fold the edges of the vial stopper to create a seal around the top of the glass vial.

(Reference Image in Attachment 3)

- 6.3.4 Place the glass vial in a 100 mL beaker to keep it upright.
- 6.4 Place scaffolds in chip component
 - 6.4.1 Remove the culturing 6mm diameter silk fibroin scaffolds seeded with SK-N-AS cells from an incubator and place in the biosafety cabinet.
 - 6.4.2 Using a pair of forceps, place two silk scaffolds stacked on top of each other into each of the 4 wells in the chip component. The scaffolds should line up with each other and fit snugly into the wells.
(Reference Image in Attachment 4)
- 6.5 Secure chip component into device.
 - 6.5.1 Place the chip component with the scaffolds into the bottom section of the flow chamber.
 - 6.5.2 Place the silicone gasket on top of the bottom section of the flow chamber.
(Reference Image in Attachment 5)
 - 6.5.3 Place the top section of the flow chamber on top of the silicone gasket so that all of the screw holes match up with the bottom section of the flow chamber.
 - 6.5.4 Place one washer over the top of each screw hole.
 - 6.5.5 Insert (but do not tighten yet) the screws into each screw hole.
(Reference Image in Attachment 6)
 - 6.5.6 Using the Allen Wrench, slowly tighten the screws in small iterations to prevent material deformation. Tighten in a star pattern around the device to equally distribute pressure.
 - 6.5.6.1 Once each screw is about finger tight, use the Allen Wrench to do an additional quarter turn to ensure the device is secure.
(Reference Image in Attachment 7)
 - 6.5.7 Mark the outside edge of the device on the side that contains the scaffolds with a sharpie or hydrophobic marker.
- 6.6 Attach device to tubing.
 - 6.6.1 Identify the section of tubing connected to the media reservoir that is shortest.
 - 6.6.2 Take the ¼-28 screw tubing adapter attached to the end of the shortest tubing section and screw into the top hole of the device on the side that is marked with the marker.
 - 6.6.2.1 Once it is finger-tight, tighten an additional ½ rotation to secure the screw.
 - 6.6.3 Take the ¼-28 screw tubing adapter attached to the end of the longest tubing section and screw into the top hole of the device on the side that is NOT marked with the marker.
 - 6.6.3.1 Once it is finger-tight, tighten an additional ½ rotation to secure the screw.

(Reference Image in Attachment 8)

- 6.7 Place the peristaltic pump into the back of an incubator.
- 6.7.1 Open one cassette for tubing insertion.
- 6.8 Using one hand to pick up the bioreactor and the other to pick up the media reservoir, place the system in front of the peristaltic pump in the incubator. The media reservoir should be on the right side of the pump.
- 6.9 Insert the section of the Watson Marlow pump specific tubing into the cassette of the peristaltic pump so that the purple and white notches are outside of the cassette. Tighten and secure the cassette.
- 6.10 Set the direction of flow to counter-clockwise, and insert the appropriate flow rate by adjusting on the home screen of the peristaltic pump.
- 6.11 Turn on the pump and observe the process as the media primes the system.
- 6.12 Look for signs of leakage. If none have occurred by the time the system is fully primed, the experimental run can continue.

(Reference Image in Attachment 9)

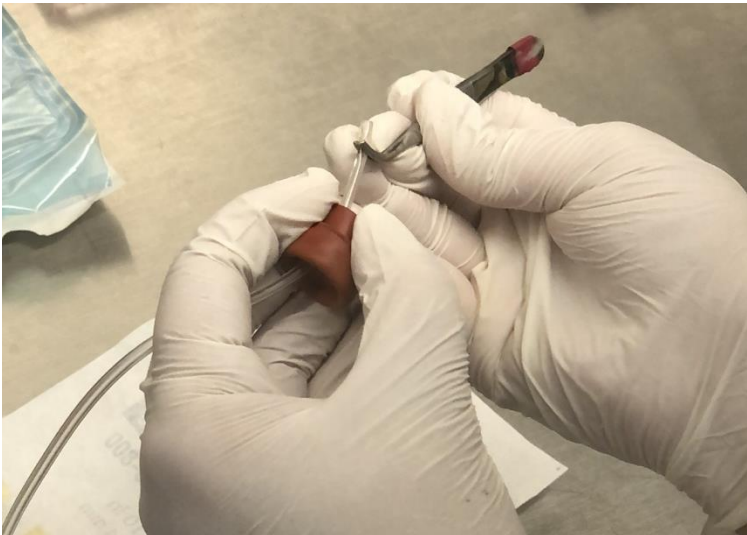
- 6.13 Close the incubator, and ensure the temperature is set to 37 degrees Celsius and the CO2 level is set to 5%.

7. Appendices

7.1. N/A

8. Attachments

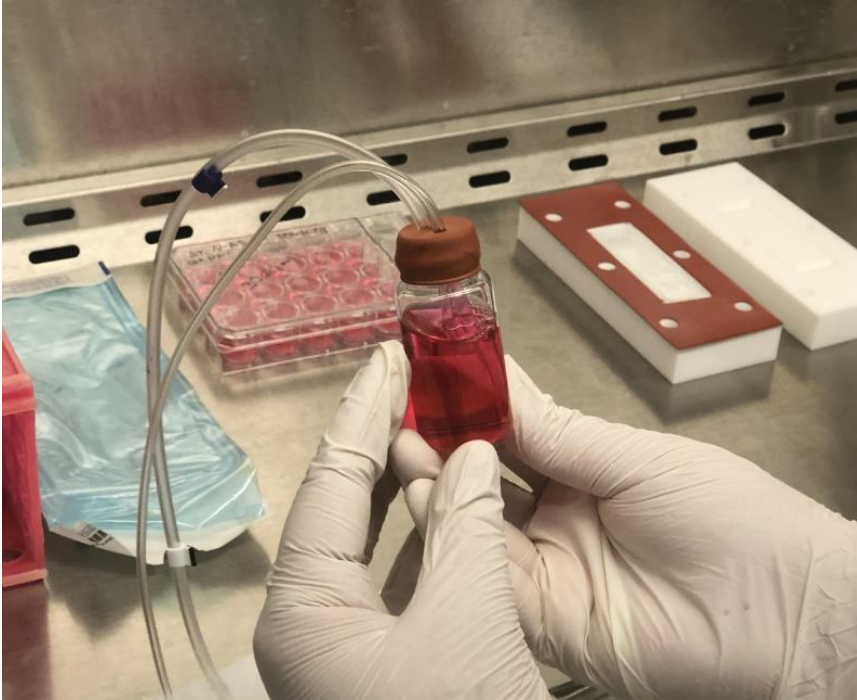
8.1. Attachment 1: Tubing through Rubber Stopper



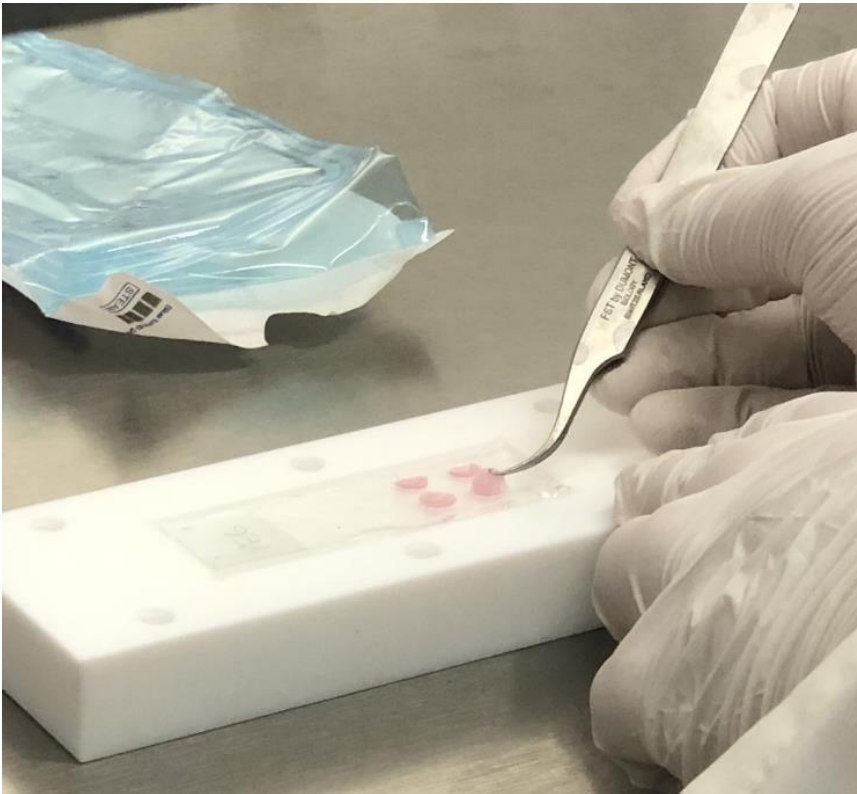
8.2. Attachment 2: Tubing Connections



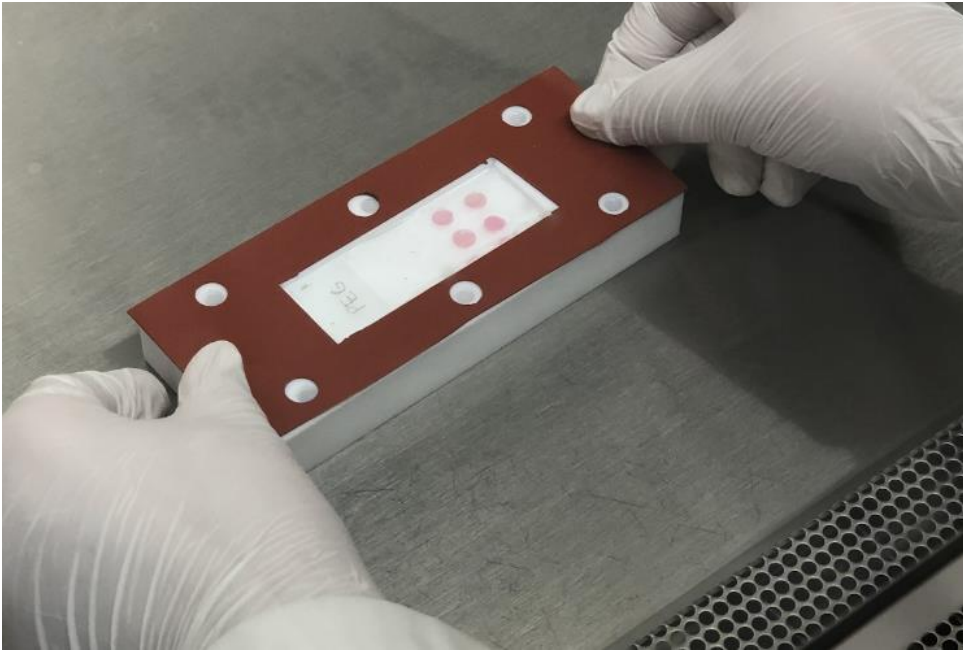
8.3. Attachment 3: Media Reservoir



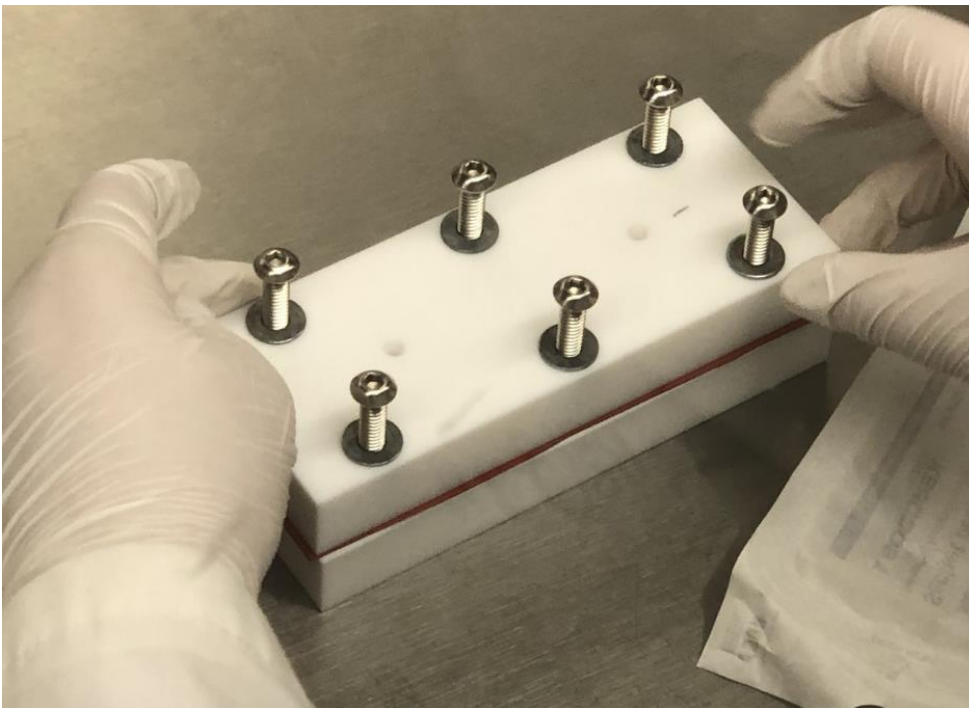
8.4. Attachment 4: Scaffold Placement



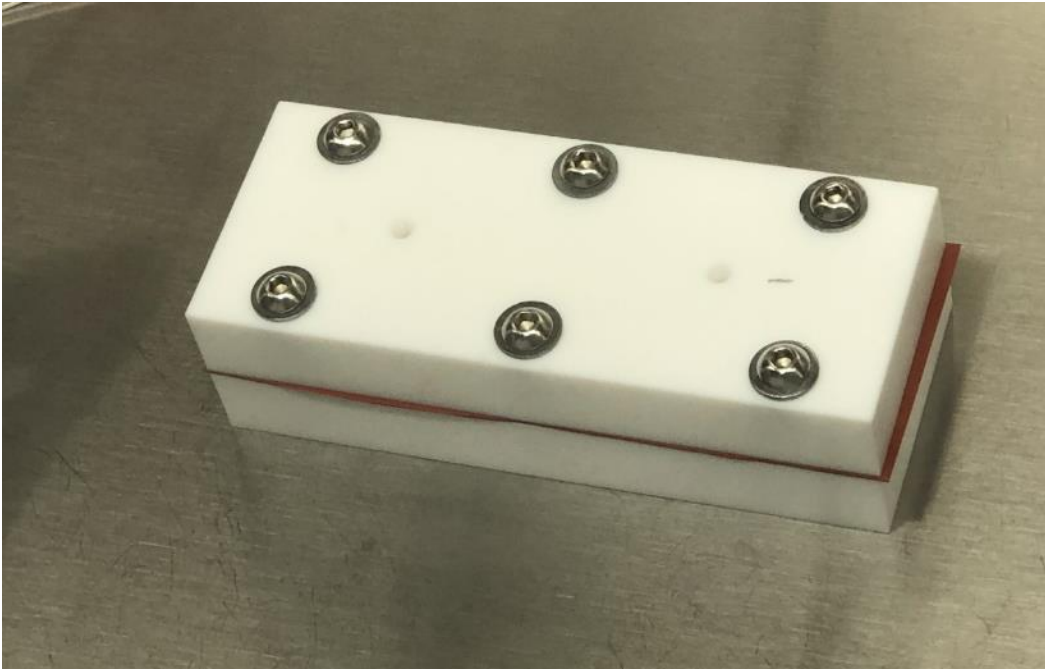
8.5. Attachment 5: Silicone Gasket Alignment



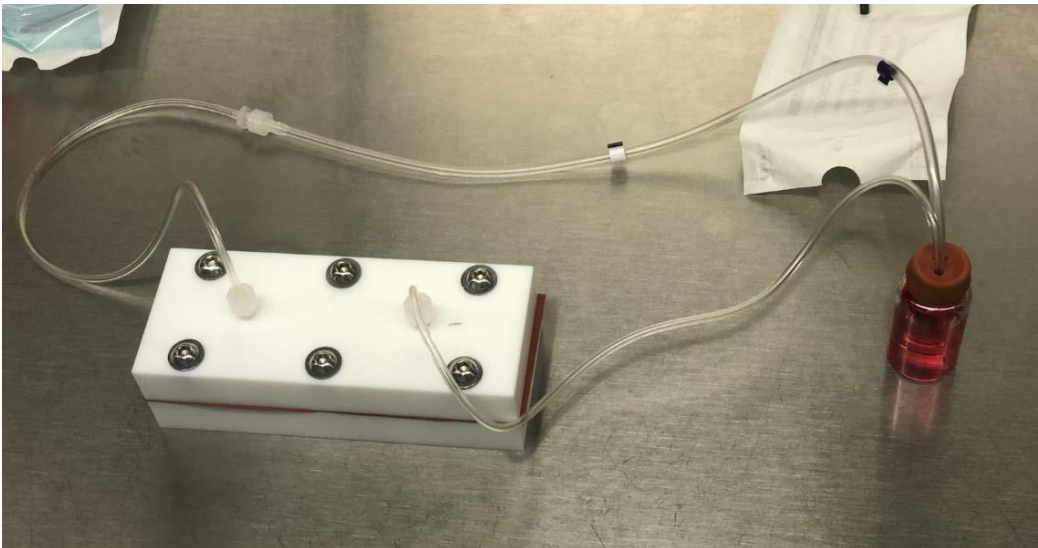
8.6. Attachment 6: Screw Placement



8.7. Attachment 7: Fully Secured Flow Chamber



8.8. Attachment 8: Flow Chamber Attached to Media Reservoir



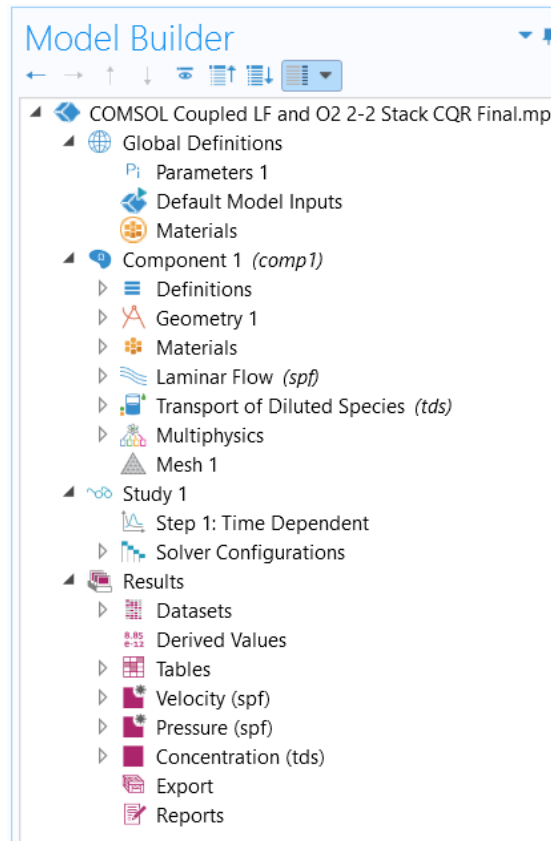
8.9. Attachment 9: Final System



Appendix G: COMSOL User Manual

The COMSOL software is available over remote desktop on arclab servers at WPI. To begin, start by opening the program and choosing a new model. The new model should be created with the specifications that the user aims to look at including the dimensionality of the model, the physics the model aims to incorporate, and the time dependence of the study.

Once created, the user will see the following box titled “Model Builder” in the left of the program. This box can be used to navigate between the parameters, the geometry, the physics, and the study.



If the user has set parameters needed for later equations, they can define them in the parameter tab. An example of how the parameter tab is set up can be seen in the following image.

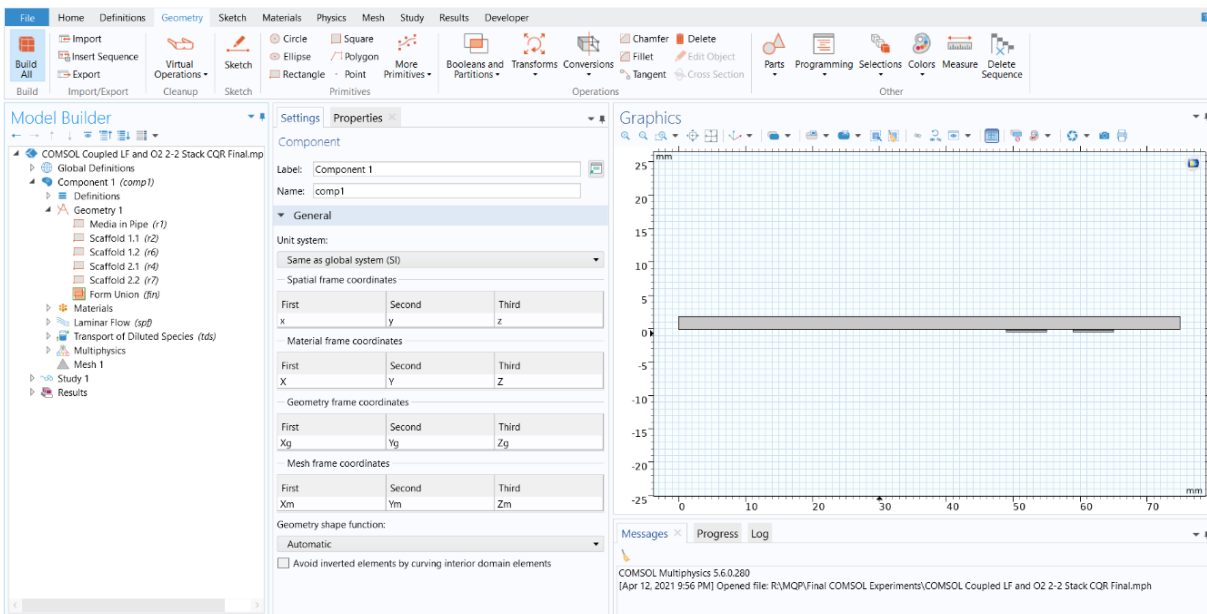
Parameters

Label: Parameters 1

▼ Parameters

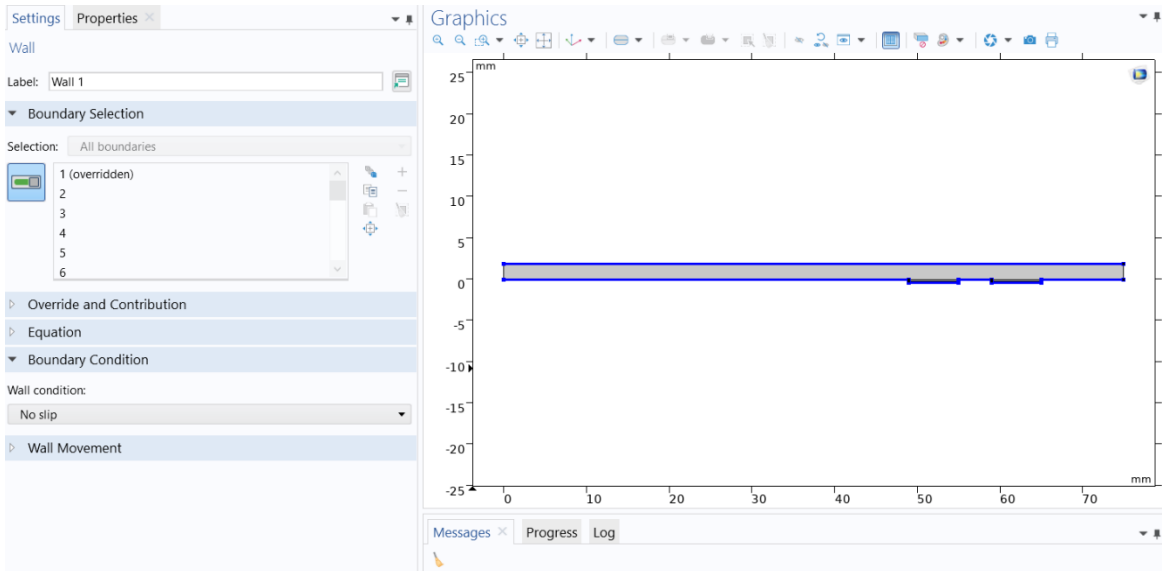
Name	Expression	Value	Description
Diff	0.000026[cm^2...	2.6E-9 m ² /s	
OCR	0.00248[mol/m...	0.00248 mol/(...	
o_initial	0.20[mol/m^3]	0.2 mol/m ³	
MM	0.00000463[mol...	0.00463 mol/...	
o_liquid	0.178[mol/m^3]	0.178 mol/m ³	

Next, the model's geometry can be built with the desired dimensions of the area the user is attempting to simulate. Note that the geometry should be constructed as the space it occupies and not the space around the model. To ensure that a model is fully combined, use the "Form Union" tab to form a union with all of the parts that make up the desired geometry. An example geometry can be seen in the picture below.

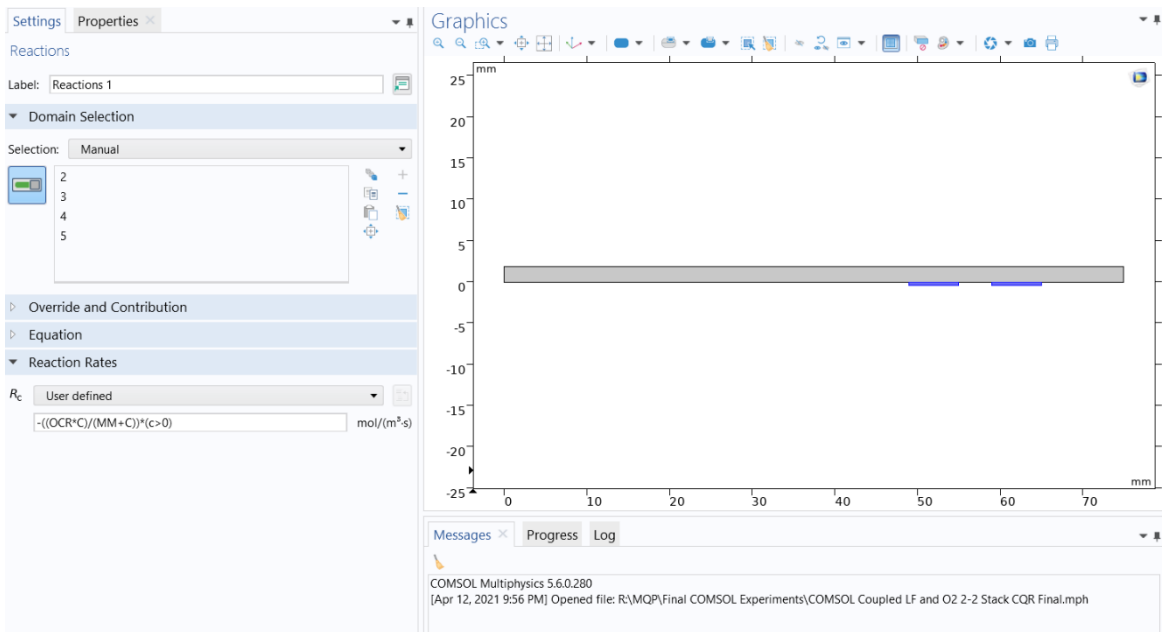


Once the geometry is set and grouped, then the material can be set. For fluid flow, assuming the system is water is a safe assumption, but other fluids can be chosen according to the reference list in COMSOL. The materials can be modified by the user as well for more accurate approximations if the user chooses to do so.

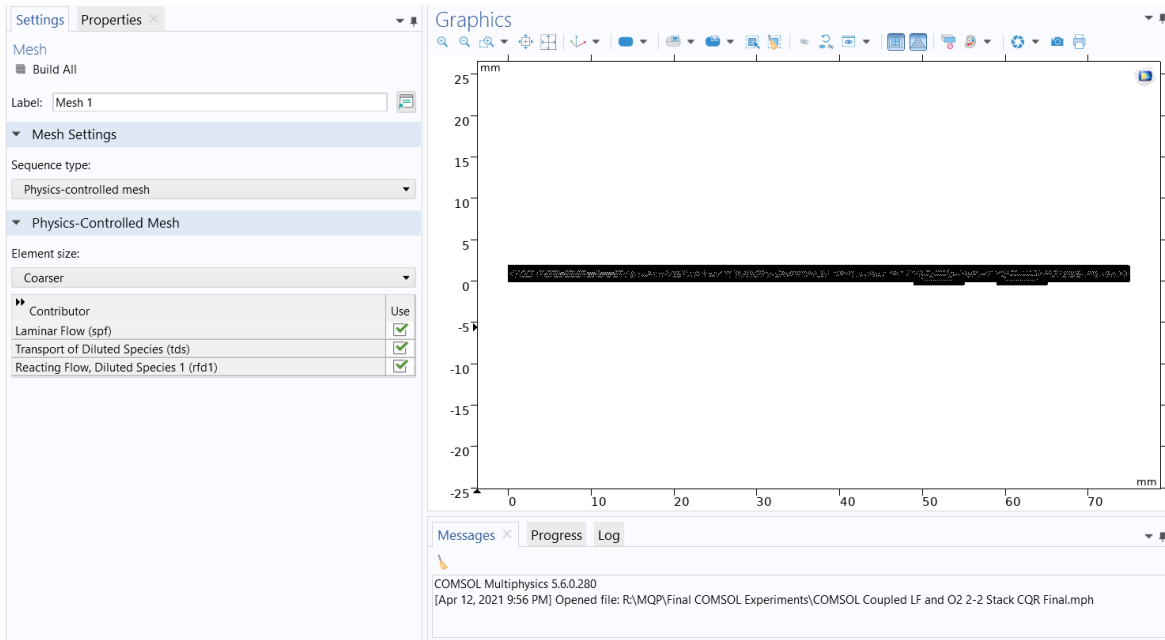
If using fluid flow, the boundaries of the model must be set as well as appropriate inlets and outlets. The flowing image shows the boundaries being set with the inlet being the line on the vertical left and the outlet being the vertical line on the right. The inlet velocity was set to a value equal to the constant flow rate in the designed geometry, and the outlet values were set accordingly.



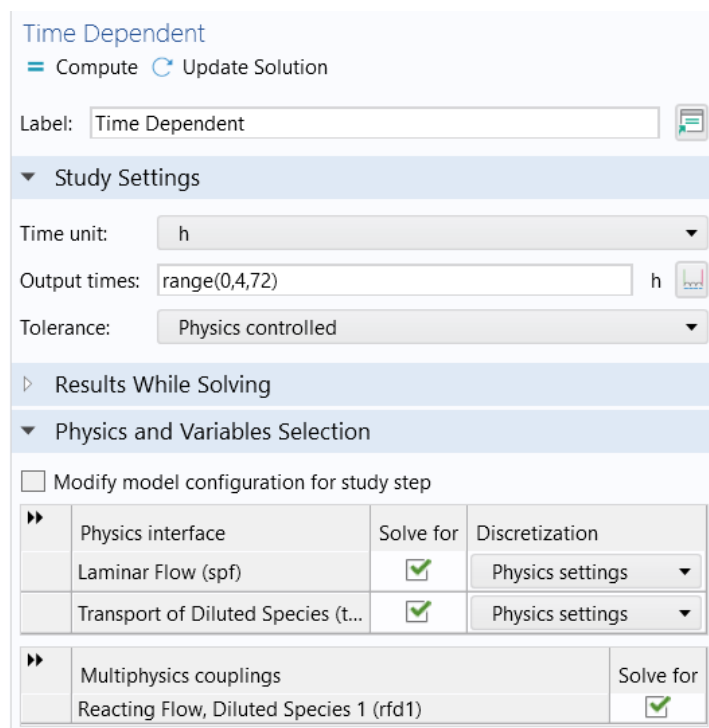
After establishing the specifications for fluid flow, a transport of diluted species module can be coupled using multiphysics analysis. The transport of diluted species used the equation shown in the image below to approximate reaction rates in the areas of interest. The areas of interest in this specific example are cell-seeded scaffolds and their oxygen consumption rates. Additionally, initial concentrations were applied to an inlet as well as the initial concentration of the overall device at the initial time point.



After the physics modules have been established, then the model will then begin preparation for the virtual simulation. The “Mesh” tab is where the user can set the “element size” of the model. The complexity of the model increases as the mesh becomes finer. If the user would like to have a quicker but less comprehensive study, then a coarse mesh will suffice. The image below shows a “coarser” mesh used to run a time dependent study.



Finally, the study’s time points can be altered according to the following image. The “output times” can be adjusted with the first number being the initial time point, the second number being the step size, and the final number being the end time point. The units can also be adjusted to the appropriate unit of time.



Appendix H: PicoGreen Protocol

- Quanti-iT PicoGreen dsDNA Reagent and Kit
 - 20X TE Buffer
 - Lambda DNA Standard
 - PicoGreen dsDNA reagent
- Black Plate (brand new – this is because it is believed that PicoGreen stains plates)
- Calculate how much working PicoGreen solution you need based on your number of samples and standards (50 μ L per).

1. Make fresh 1 x TE buffer **if necessary**. (1.25 mL 22 x buffer into 23.75 mL filtered milliQ water). Left over buffer can be stored in the fridge 4C.
2. Dilute all the sample supernatant as described with 1X TE buffer using labeled new tubes, so that the final concentration of Triton is 0.1% (ex 80 ul of 1x TE + 20 ul of sample in 0.5% TE buffer)
3. Prepare DNA standard (found in kit in fridge). In 1x TE + 0.1% Triton

Standard	How to Prep
S1 -2 ug	5 μ L DNA standard & 245 μ L 1X TE Buffer
S2- 0.667 ug	75 μ L S1 & 150 μ L of 1X TE Buffer
S3-0.222 ug	75 μ L S2 & 150 μ L of 1X TE Buffer
S4-0.074 ug	75 μ L S3 & 150 μ L of 1X TE Buffer
S5-0.025 ug	75 μ L S4 & 150 μ L of 1X TE Buffer
S6-0.008 ug	75 μ L S5 & 150 μ L of 1X TE Buffer
S7-0.0027 ug	75 μ L S6 & 150 μ L of 1X TE Buffer

S8 Blank	200 μ L of 1X TE Buffer
----------	-----------------------------

	1	2	3	4	5	6
A	S1	S1	Stack Out	Flow Top	2D	3D
B	S2	S2	Stack Out	Flow Top	2D	3D
C	S3	S3	Stack Out	Flow Top	2D	3D
D	S4	S4	Stack Out	Flow Bot.	2D	3D
E	S5	S5	Stack In	Flow Bot.	2D	3D
F	S6	S6	Stack In	Flow Bot.	2D	3D
G	S7	S7	Stack In			
H	Blank	Blank	Stack In			

4. Prepare pico green reagent diluting in 5 μL per 995 μL of 1X TE Buffer (12.5 μL in 2.488 mL).
5. Turn off the lights in work area.
6. Grab a black plate and, to the unused wells, add 50 μL of PicoGreen to each well and then add 50 μL of sample/standard to the respective wells. Mix thoroughly. Plate duplicates of standard.
7. Let incubate in a drawer for 5 minutes.
8. Read on gel/doc plate reader using the appropriate PicoGreen protocol (we typically read the plate three times, to confirm readings). Record and save data for later analysis.
9. Vacuum out liquid from plate. Tape over wells used to prevent accidental re-use of those wells. Discard of PicoGreen reagent and samples.

Appendix I: H&E Staining Protocol

After collecting samples, place the stacks in blocks of OCT and place them in a freezer set to -80°C. After freezing, the stacks will be sectioned at a thickness of 20 µm in a cryostat and transferred onto positively charged microscope slides. Slides will then be stored in a freezer until staining.

The H&E staining protocol follows the following protocol:

1. Prepare cold 100% and 25% (4°C) methanol
2. Take slides from freezer and put them in 100% methanol for 5 minutes
3. 25% methanol for 5 minutes
4. 1x PBS for 10 minutes
5. Harris Hematoxylin (3 minutes)
6. Place under flowing water gently running from tap (dump the water once the histology box is a deep purple)
7. Repeat until the purple tint in the surrounding liquid is faint or totally removed
8. 3 dips in acid alcohol
9. Water for 1 minute (not running)
10. Ammonia (3 dips)
11. 95% ethanol (1 minute)
12. Eosin (30 seconds)
13. 95% ethanol (1 minute)
14. 95% ethanol (1 minute) in a new histology box
15. 100% ethanol (1 minute)
16. 100% ethanol (1 minute) in a new histology box
17. Xylene (2 minutes)
18. Xylene (5 minutes)
19. Cytoseal 60 nonaqueous mounting media used to mount coverslips onto the slides (Place drops on the scaffolds and gently place the coverslips to avoid bubbles)
20. Dry overnight

Appendix J: Machining

After shopping around at various sites for the most cost-effective PTFE, the team purchased from US Plastics (options: US plastics, Interstate plastics, Grainger, McMaster-Carr, or K-mac Plastics).

In order to use the machine shop on campus, the team had to convert their SolidWorks prototype into a working ESPRIT file. ESPRIT is a computer aided manufacturing software that is compatible with the equipment in the shop. In order to convert these files, the team worked with the Manufacturing Lab staff. James Loiselle was a huge help during this process. By the end of this process, there were four files; both the top and bottom plates had top part and bottom part (called operation 1 and 2 or OP1 or 2 respectively).

The team then scheduled machine shop time with a lab monitor who could work closely with us while creating the device iterations. Before using the PTFE, the team practiced machining using a piece of aluminum as it is less expensive and easier to work with. The first step when using the PTFE was to cut the stock material using a bandsaw in order to divide the one square foot of material into eight equal pieces. The edges were rough and were smoothed using a file and a specific MiniMill operation.

Considering that PTFE and plastics in general are rarely used in the machine shop, there was an intensive cleaning process as the beginning and end of each session. The team had to thoroughly clean the machine and rake any metal debris out before using the machine and rake all of the plastic pieces at the end; any contamination makes it incredibly challenging for the lab to recycle the metal.

The team worked with the lab monitor to collect the appropriate bits such as the 1/8 ball end mill, #21 drill bit, and 1/4-20 tap. The necessary bits were indicated within the final ESPRIT file. From there, the team used the Haas MiniMill, with the bits placed in their proper collet and loaded into the machine. The lab monitor had to convert the ESPRIT file into a g code, a numerical control programming language. This instructed to the machine to make specific cuts using a coordinate system. The team learned how to load the device into the system, how to adjust the coolant when changing operations, and how to modify some features of the system in order to achieve the desired cuts.

The aforementioned files can be found in the Coburn Lab Research Drive.

Below is a table of tools used for each operation of the device machining:

Tool	Operation
Face Mill	Bottom Operation 1
CM .375 Drill Mill	Bottom Operation 1
#7 Drill	Bottom Operation 1
1/4-20 Tap	Bottom Operation 1
3/8 End Mill	Bottom Operation 1
1/16 End Mill	Bottom Operation 1
3/8 End Mill	Bottom Operation 2
Face Mill	Bottom Operation 2
CM .375 Drill Mill	Bottom Operation 2
Face Mill	Top Operation 1
3/8 End Mill	Top Operation 1
CM .375 Drill Mill	Top Operation 1
F Drill – Screw Machine Length	Top Operation 1
#21 Drill	Top Operation 1
1/8 End Mill	Top Operation 1
1/8 Ball End Mill	Top Operation 1
3/8 End Mill	Top Operation 2
Face Mill	Top Operation 2
CM .375 Drill Mill	Top Operation 2